

1-16-2014 12:00 AM

## Numerical Simulation of Liquid-Solid Circulating Fluidized Beds

Abbas Dadashi, *The University of Western Ontario*

Supervisor: Dr. Chao Zhang, *The University of Western Ontario*

Joint Supervisor: Dr. Jesse Zhu, *The University of Western Ontario*

A thesis submitted in partial fulfillment of the requirements for the Master of Science degree in  
Mechanical and Materials Engineering

© Abbas Dadashi 2014

Follow this and additional works at: <https://ir.lib.uwo.ca/etd>



Part of the [Computational Engineering Commons](#)

---

### Recommended Citation

Dadashi, Abbas, "Numerical Simulation of Liquid-Solid Circulating Fluidized Beds" (2014). *Electronic Thesis and Dissertation Repository*. 1874.

<https://ir.lib.uwo.ca/etd/1874>

This Dissertation/Thesis is brought to you for free and open access by Scholarship@Western. It has been accepted for inclusion in Electronic Thesis and Dissertation Repository by an authorized administrator of Scholarship@Western. For more information, please contact [wlsadmin@uwo.ca](mailto:wlsadmin@uwo.ca).

# **Numerical Simulation of Liquid-Solid Circulating Fluidized Beds**

(Thesis format: Integrated-Article)

**By**

**Abbas Dadashi**

**Graduate Program**

**In**

**Engineering Science**

**Department of Mechanical & Materials Engineering**

**A thesis submitted in partial fulfilment  
of the requirements for the degree of  
Master of Science**

**The School of Graduate and Postdoctoral Studies  
The University of Western Ontario  
London, Ontario**

## Abstract

Liquid-solid circulating fluidized bed (LSCFB) reactors are obtaining extensive attraction in the extraction process of functional proteins from industrial broth. A typical LSCFB is comprised of a riser, a downcomer, a liquid-solid separator, a top solids-return pipe and a bottom solids-return pipe. In light of the literature review conducted in this research, a detailed modeling of the protein extraction using an LSCFB ion-exchange system requires a microscopic study including hydrodynamic field, mass transfer and kinetics reactions.

A computational fluid dynamics (CFD) model was developed to simulate the hydrodynamics of the two phase flow in an LSCFB riser. The model is based on Eulerian–Eulerian (E-E) approach incorporating the kinetic theory of granular flow. The predicted flow characteristics agree well with our earlier experimental data. Furthermore, the model can predict the residence time of both liquid and solid phases in the riser using a pulse technique.

A numerical model was developed to predict the protein extraction process using an LSCFB ion exchange system. The model for the riser is an extension of the previous CFD hydrodynamic model for the riser incorporating the kinetics reaction. The model for the downcomer includes a one-dimensional mathematical model using the adsorption kinetics correlations. The numerical predictions were compared favorably with the experimental data from a lab-scale system. The model was used to investigate the effects of operating condition on the protein production rate and the system efficiency.

For further study on the hydrodynamics in the downcomer of an LSCFB, the CFD technique was used to simulate the counter-current two phase flow in the downcomer. The model is based on E-E approach incorporating the kinetic theory of granular flow. The predicted results agree well with our earlier experimental data. Furthermore, it is shown that the bed expansion of the particles in the downcomer is directly affected by the superficial liquid velocity in downcomer and solids circulation rate.

As results, it is demonstrated that the developed CFD model can be adapted to simulate and control the other applications of the LSCFB, such as wastewater treatment, petroleum and metallurgical industries.

## Keywords

Numerical Simulation, Computational Fluid Dynamics (CFD), Liquid-Solid Circulating Fluidized Bed, Risers, Downcomer, Protein Extraction Process, Turbulence Model, Optimization

## Co-Authorship Statement

Chapters 2, 3 and 4 of this thesis have been submitted for publishing in journals.

All papers are drafted by Abbas Dadashi and modified under the supervision of Dr. Chao Zhang and Dr. Jesse Zhu. The numerical results are validated by the experimental data which have been obtained by Dr. Jesse Zhu's research group.

## Acknowledgments

I would like to express my sincere gratitude to Professors Chao Zhang and Jesse Zhu for their guidance throughout this research. As my supervisors, their advice, encouragement, patience, and financial support were the driving force for me to conduct and complete the work.

I would also like to thank the Natural Sciences and Engineering Research Council of Canada (NSERC) for their financial support through the NSERC Discovery Grants to Profs. Zhu and Zhang and the NSERC Engage Grant sponsored by Renix Inc.

I would also like to thank all the members from Prof. Zhang and Prof. Zhu's research groups, especially Mehran Andalib, Rajeev Kumar, Lei Kong, Amin Jaberli and Rajib Saha for their help and friendship through these years.

Finally, I would like to thank my parents. Their encouragement and support have given me a bright lamp in my study and life. I also thank my brothers for their kind supports.

# Table of Contents

Abstract.....	ii
Co-Authorship Statement.....	iv
Acknowledgments.....	v
Table of Contents.....	vi
List of Tables.....	x
List of Figures.....	xi
Nomenclature.....	xiv
Chapter 1.....	1
1 General introduction.....	1
1.1 Background.....	1
1.2 Literature review.....	5
1.2.1 Hydrodynamic characterization of LSCFB.....	5
1.2.2 CFD models.....	9
1.2.3 Protein extraction from biological broth using an LSCFB ion exchange system.....	13
1.3 Objectives and thesis structure .....	17
References.....	19
Chapter 2.....	22

2	A Computational Fluid Dynamics Study on the Flow Field in a Liquid-Solid Circulating Fluidized Bed Riser .....	22
2.1	Introduction.....	22
2.2	Experimental setup of the LSCFB system .....	24
2.3	Mathematical modeling .....	25
2.3.1	Governing equations .....	26
2.3.2	Boundary conditions .....	28
2.4	Numerical methodology .....	32
2.5	Results and Discussion .....	32
2.5.1	The effect of turbulence models.....	33
2.5.2	Effect of liquid superficial velocity.....	35
2.5.3	Effect of solids circulation rate.....	36
2.5.4	Residence time distribution.....	37
2.6	Conclusions.....	40
	References.....	42
	Chapter 3.....	44
3	CFD modeling of continuous protein extraction process using liquid-solid circulating fluidized beds.....	44
3.1	Introduction .....	44
3.2	Experimental setup of the LSCFB system.....	46
3.2.1	Apparatus.....	46



3.2.2	Materials.....	49
3.2.3	Kinetics of Ion Exchange mechanism in the LSCFB System.....	49
3.3	Mathematical modeling.....	50
3.3.1	CFD modeling of flow field and mass transfer in the Riser.....	50
3.3.2	Hydrodynamics and mass transfer simulation in downcomer.....	51
3.3.3	Parameters of modeling.....	55
3.3.4	Numerical methodology.....	56
3.4	Results and Discussion.....	58
3.4.1	Validation of the numerical model.....	59
3.4.2	Effect of the liquid velocity in the downcomer.....	63
3.4.3	Effect of the liquid velocity in the riser.....	64
3.4.4	Effect of the feed concentration.....	64
3.4.5	Evaluation of the system efficiency and protein production rate.....	66
3.5	Conclusions.....	67
	References.....	68
	Chapter 4.....	72
4	Numerical Simulation of Counter-Current Flow Field in the Downcomer of a Liquid-Solid Circulating Fluidized Bed.....	72
4.1	Introduction.....	72
4.2	Configuration of the LSCFB ion-exchange system.....	72
4.3	Mathematical modeling.....	74

4.3.1	Governing equations.....	75
4.3.2	Boundary conditions.....	75
4.4	Numerical methodology.....	78
4.5	Results and Discussion.....	78
4.5.1	Validations of the numerical model.....	80
4.5.2	Effect of superficial liquid velocity on solids holdup.....	81
4.5.3	Effect of solids circulation rate on solids holdup.....	82
4.5.4	Radial distribution of the solids holdup.....	83
4.5.5	Effect of superficial liquid velocity on the dispersion of the solid particles.....	84
4.6	Conclusions.....	85
	Reference.....	87
Chapter 5.....		89
5	Conclusions.....	89
	Curriculum Vitae.....	91

## List of Tables

Table 2.1:	The constitutive correlations for closure of the transport equations	30
Table 3.1:	Properties of Diaion HPA25 ion-exchange particles (Lan et al. 2002)	49
Table 3.2:	Governing equations for liquid-solid flows in the riser	52
Table 3.3:	Model parameters (Lan et al., 2000)	56
Table 3.4:	Protein production rate and system efficiency under different operating conditions	66
Table 4.1:	Governing equations for liquid-solid flows	76

## List of Figures

Figure 1.1:	Schematic diagram of the liquid–solid circulating fluidized bed (LSCFB) reactor	2
Figure 1.2:	The axial solid holdup distribution along the upper dilute zone of LSCFB riser for glass beads and steel shots, under different liquid velocity (Zheng et al., 1999)	7
Figure 1.3:	Radial profiles of solids holdup at the level $H = 0.8\text{m}$ (a) for different solids flow rates (b) for different superficial liquid velocities. (Zheng et al. 2001)	8
Figure 1.4:	The radial distribution of the liquid velocity under $G_s = 5 \text{ kg/m}^2\text{s}$ and different liquid velocities for glass beads (Zheng et al. 2002)	9
Figure 2.1:	Schematic diagram of the liquid-solid circulating fluidized bed (Zheng et al., 2003)	25
Figure 2.2:	The computational domain in the LSCFB riser	31
Figure 2.3:	Comparison of the liquid velocity profile using three types of the $k-\varepsilon$ multi-phase turbulence models (Experimental data by Zheng et al. (2003))	33
Figure 2.4:	Comparison of the solids holdup profile using three types of $k-\varepsilon$ multiphase turbulence models (Experimental data by Zheng et al. (2002))	34
Figure 2.5:	Comparison of the radial distributions of the liquid velocity under different liquid superficial velocities (Experimental data by Zheng et al. (2003))	35
Figure 2.6:	Comparison of the radial distributions of the solid holdup under different liquid superficial velocities (Experimental data by Zheng et al. (2002))	36
Figure 2.7:	The radial distributions of the solid holdup under different solids circulation rates (Experimental data by Zheng et al. (2002))	37

Figure 2.8:	The residence time distributions of (a) the liquid phase and (b) the solids phase at $G_s=5 \text{ kg/m}^2\text{sec}$ and $U_l=10 \text{ cm/s}$	39
Figure 2.9:	The residence time distributions of (a) the liquid phase and (b) the solid phase at $G_s=5 \text{ kg/m}^2\text{sec}$ and $U_l=15 \text{ cm/s}$	40
Figure 3.1:	Schematic diagram of the LSCFB ion-exchange system Lan et al. (2000)	48
Figure 3.2:	Computational domain of in the downcomer and riser of the LSCFB. (a) Downcomer and (b) Riser	58
Figure 3.3:	Comparison of the liquid protein concentration along the downcomer at different superficial liquid velocities ( $U_{ld}$ ) in the downcomer at $C_{od}=2 \text{ kg/m}^3$ , $G_s=1.24 \text{ kg/m}^2/\text{s}$ , $U_{lr}=0.0113 \text{ m/s}$ (Experimental data by Lan et al. (2000, 2002a))	60
Figure 3.4:	Comparison of the liquid protein concentration along the riser at different superficial liquid velocities ( $U_{lr}$ ) in the riser at $C_{od}=2 \text{ kg/m}^3$ , $G_s=1.24 \text{ kg/m}^2/\text{s}$ , $U_{ld}=0.006 \text{ m/s}$ (Experimental data by Lan et al. (2000, 2002a))	61
Figure 3.5:	Contour of the protein concentration of the liquid n the riser, $C_r$ ( $\text{kg/m}^3$ )	62
Figure 3.6:	Variation of the liquid protein concentration along the riser at different superficial liquid velocity in downcomer, $U_{ld}$ ( $C_{od}=2 \text{ kg/m}^3$ , $G_s=1.24 \text{ kg/m}^2/\text{s}$ , $U_{lr}=0.0113 \text{ m/s}$ )	63
Figure 3.7:	Influence of the feed protein concentration ( $C_{od}$ ) on the protein concentration of the liquid phase at $G_s=1.24 \text{ kg/m}^2/\text{s}$ , $U_{ld}=0.0006 \text{ m/s}$ , and $U_{lr}=0.0113 \text{ m/s}$ . (a) downcomer, (b) riser	65
Figure 4.1:	Schematic diagram of the LSCFB ion-exchange system Lan et al. (2000)	73
Figure 4.2:	Schematic diagram of the computational domain to simulate the liquid-solid flow in the downcomer of the LSCFB	77

Figure 4.3:	Predicted solids holdup distribution in the downcomer at $U_{ld} = 0.55$ mm/sec and $G_s = 0.05$ kg/m <sup>2</sup> sec	79
Figure 4.4:	Comparison of numerical and experimental results for the average solids holdup in the dense zone of the downcomer (Experimental data by Lan et al. (2000))	81
Figure 4.5:	Variation of the solids holdup in the dense zone of the downcomer ( $\alpha_{sd}$ ) at different superficial liquid velocity	82
Figure 4.6:	Variation of the solids holdup in the dense zone of the downcomer ( $\alpha_{sd}$ ) at different solids circulation rates	83
Figure 4.7:	Radial distribution of the solids holdup in the dense zone of the downcomer at $G_s = 0.05$ kg/m <sup>2</sup> sec and $x = 1.5$ m	84
Figure 4.8:	The residence time distributions of the solid phase at $G_s = 0.05$ kg/m <sup>2</sup> sec and (a) $U_{ld} = 0.55$ mm/sec, (b) $U_{ld} = 0.65$ mm/sec	86

# Nomenclature

## Notation

$a$	Specific surface area of the ion-exchange resin ( $A_p/V_p$ ) ( $m^2/m^3$ )
$C$	Protein concentration in liquid phase ( $kg/m^3$ )
$C_{1\epsilon}$	Constants
$C_{2\epsilon}$	Constants
$C_D$	Drag coefficient, dimensionless
$d_p$	Mean particle diameter, m
$D$	Riser diameter, m
$e$	Restitution coefficient for interparticle collisions, dimensionless
$e_w$	Restitution coefficient for particle-wall collisions, dimensionless
$g$	Acceleration due to gravity, $m/s^2$
$g_0$	Radial distribution function, dimensionless
$G_s$	Solids circulation rate, $kg/(m^2 s)$
$k$	Turbulent kinetic energy, $m^2/s^2$
$k_f$	Film mass transfer coefficient ( $m/s$ )
$K_d$	Dissociation constant ( $kg/m^3$ )
$K_L$	Lumped mass transfer rate coefficient ( $m/s$ )
$K_{sl}$	Interphase Momentum exchange coefficient, $kg/(m^3 s)$
$k_r$	Desorption rate constant ( $s^{-1}$ )
$n$	Bed expansion index
$p_s$	Solids pressure, Pa

## Greek letters

$\alpha_s$	Local solids volume fraction, dimensionless
$\bar{\alpha}_s$	Mean solids volume fraction at certain cross-section, dimensionless
$\alpha_{sd}$	solids volume fraction in the dense zone of the downcomer
$\epsilon$	Turbulent energy dissipation rate, $m^2/s^3$
$k_{\Theta s}$	Granular conductivity, $kg/m^3 s$
$\gamma_{\Theta}$	Collisional energy dissipation rate, $kg/(m s^3)$
$\Phi_{ls}$	Interphase Energy exchange, $kg/(m s^3)$
$\alpha_s$	Local solids fraction, dimensionless
$\epsilon_s$	Solid holdup
$\epsilon_l$	Bed voidage
$\theta$	Granular temperature, $m^2/s^2$
$\lambda$	Solids bulk viscosity, $kg m/s$
$\mu$	Viscosity, $kg m/s$
$\nu$	Kinematic viscosity, $m^2/s$
$\rho$	Density, $kg/m^3$
$\sigma_k$	Constants
$\sigma_\epsilon$	Constants
$\tau$	Shear stress, $kg m/s^2$
$k_{\Theta s}$	Granular conductivity, $kg/(m^3 s)$
$\Psi$	Constant factor which indicates the effect of inter-particle diffusion

$P$	Fluid pressure, Pa	<b>Subscripts</b>	
$Re$	Reynolds number, dimensionless	$l$	liquid phase
$t$	Time (s)	$s$	solid phase
$U_t$	Particle terminal velocity, m/s	$f$	fluid
$U$	Superficial liquid velocity, m/s	$a$	auxiliary
$v$	Velocity, m/s	$eq$	Equilibrium
$z$	Distance from bottom of downcomer, m	$d$	Downcomer
		$t$	turbulence



## Chapter 1

### 1 General introduction

#### 1.1 Background

Fluidization is characterized as a phenomenon which a bed of particles gains properties of fluid and is converted from solid state to fluid state. Fluidization occurs when fluid flow is introduced in the bottom of a bed of solids particles at such a velocity that the buoyed weight of the particles is completely supported by the drag force imposed by the fluid. As a result, the particles are able to move in the bed. The term “fluidization” reflects this state of fluid-like properties onto the solid particles, as the term liquefaction is used to denote the act of making liquid properties.

Fluidized-bed includes gas–solid, liquid–solid and gas–liquid–solid fluidized-beds in terms of the fluid–particulate systems. With respect to bed scheme and operation, there are the stationary fluidized beds (SFB) or fixed fluidized beds (FFB), where the particles essentially stay in the fluidized bed and the circulating fluidized beds (CFB), where particles are mostly entrained out of the fluidized beds but at the same time recirculated back to or fresh particles added to the same fluidized beds. SFB are often called conventional fluidized beds since they were the first to be used in various industrial applications. In liquid–solid systems, the SFB basically has only one operating regime, the particulate fluidization regime, where the particles are uniformly distributed in the upflowing liquid.

In CFB, the fluidizing gas or liquid (or the two combined) velocity is high enough to entrain all particles out of the bed; and in order to keep a continuous operation in fluidized bed, particles (either recycled or fresh) need to be fed into the bottom of the fluidized bed. In CFB, there are also different regimes: the fast fluidization regime, the pneumatic transport regime, and the dense suspension upflow or dense-phase transport regime for high suspension density and high particle flux operations (Grace et al., 1999). The schematic of the liquid-solid circulating fluidized bed (LSCFB) reactor is shown in

Figure 1.1. The major components of an LSCFB include a riser, a down-comer, a liquid-solid separator, a top solids-return pipe and a bottom solids-return pipe.

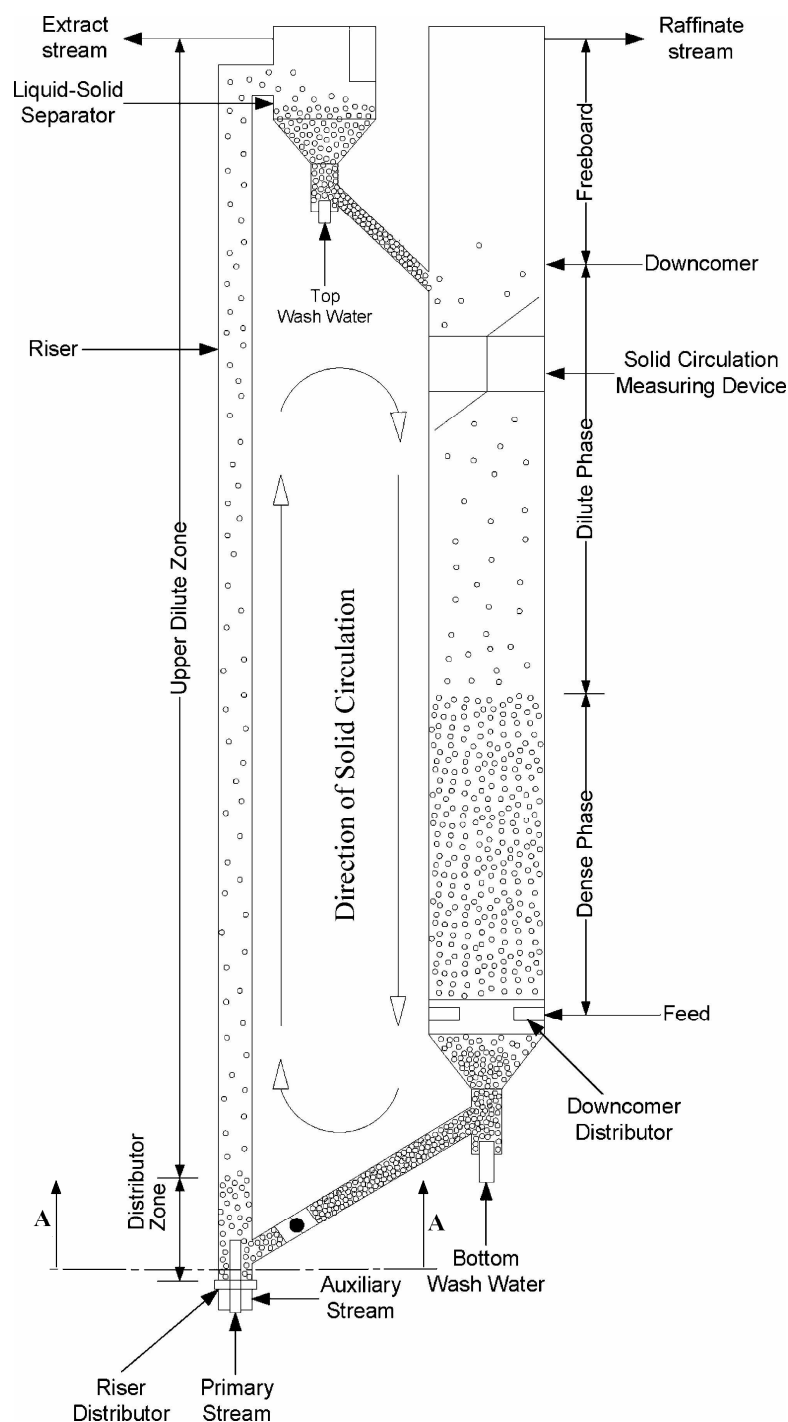


**Figure 1.1: Schematic diagram of the liquid–solid circulating fluidized bed (LSCFB) reactor.**

The first modern application of a fluidized-bed reactor was a stationary, dense-phase gas–solid fluidized-bed reactor (Winkler, 1922) operated for coal gasification in Germany to produce synthesis fuel from coal. It started with gas-solid fluidization and then extended to liquid-solid and gas-liquid-three-phase fluidization. The first type of CFB reactor was gas-solid CFB reactor which was proposed in the late 1960's. They have been used in many different kinds of industries during last 30 years.

In comparison to gas-solid system, the LSCFB and the gas-liquid-solid circulating fluidized bed (GLSCFB) have received too many attentions until recent years. The CFB has some advantages over conventional fluidized bed such as high gas/liquid velocity, low backmixing, larger processing capability, better interphase contact and good heat and mass transfer capabilities (Yang et al., 1993). On the other hand, solid particles or catalysts are very expensive and need to be continuously regenerated and also, most of the bio-processes and gasifiers prefer continuous mode of operation. In those cases, the deactivated catalysts, bio-media, ion exchange resins, or adsorbents can be regenerated continuously by CFB reactors (Zhu, 2000). Because of these advantages, LSCFBs have applied in a wide range of chemical processes including wastewater treatment, continuous protein recovery from cheese whey and so on.

The interest in recovery of various functional proteins from large volume of industrial broths and biological wastewater streams has increased in recent years, due to the advancement in genetic engineering and concerns about recycling limited resources (Lan, 2001). Lan et al. (2002) developed an LSCFB ion-exchange system for the continuous recovery of protein from unclarified broth. LSCFB ion-exchange system was used as an integrated reactor and regenerator system; two different operations (adsorption and desorption) were carried out simultaneously in two separate columns (down-comer and riser, respectively) with continuous circulation of ion exchange particles between the two columns. Proper understanding of the hydrodynamics, mass transfer and kinetics of adsorption and desorption of protein in the LSCFB ion-exchange system is fundamental and crucial to design, scale up of the LSCFB system, and optimize the operating parameters.

A number of models have been developed to describe the protein adsorption and desorption behavior in different kinds of fluidized beds considering various types of approximation to physical reality (Wright and Galsser, 2001; Ping et al., 2005 and Gaikwad et al. 2008). However, detailed hydrodynamics of the LSCFB was not included in their models and they assumed that the distribution of solid holdup ( $\varepsilon_s$ ), solid velocity ( $u_s$ ) and liquid velocity ( $u_l$ ) are uniform along the riser and downer.

On the other hand, some comprehensive experimental studies on the hydrodynamics of LSCFBs have been reported (Liang and Zhu, 1997; Liang et al., 1996 and 1997; Zheng et al., 1999 and 2002 and Zheng and Zhu, 2003). In particular, the radial flow structure in the riser of an LSCFB was investigated by Liang et al. (1996) and Zheng et al (2001). They pointed out that unlike the conventional liquid–solids fluidized bed, the radial distribution of bed voidage ( $\varepsilon_l$ ) is not uniform for glass beads in the liquid–solids circulating fluidization regime. In fact, the core-annulus structure mechanisms were observed, so solid holdup was high near the wall and low at the central part of riser. Zheng et al. (1999) have studied the axial hydrodynamic behavior of an LSCFB using three different particles of nearly same size. They have observed that because of the arrangement of the riser distributor, two distinct zones (based on their solid holdup) were established along the riser named as a dense zone at the bottom of riser and as a dilute zone at the upper part of riser.

Experimental data demonstrate that axial and radial hydrodynamic properties are not uniform along the riser of an LSCFB and a complete modeling of the protein extraction using an LSCFB ion-exchange system requires a microscopic study on the nature of this system including hydrodynamic field, mass transfer and kinetics reactions. It is of fundamental importance for designing and scaling up LSCFB ion-exchange systems and optimizing operating parameters.

The literature review of the work done on this field over the last two decades is given in next section to identify the gaps and discrepancies and, thus to come up with the objectives and road map of the present research work.

## 1.2 Literature review

The literature review is conducted in three areas, (1) experimental studies on hydrodynamic characteristics of LSCFB, (2) the review of relevant computational fluid dynamics (CFD) models on two-phase flow and (3) investigation of protein extraction process based on ion exchange system.

### 1.2.1 Hydrodynamic characterization of LSCFB

Many Experimental studies have been carried out about conventional liquid-solid fluidization in the 1950s. Their results confirm that almost all liquid-solid systems fluidized at liquid velocities below the particle terminal velocity are indeed homogenous and axial and radial distributions of particles are uniform (Richardson and Zaki, (1954)). In 1954, Richardson and Zaki made a significant contribution to this field by proposing a simple relationship between the operating liquid velocity and the bed voidage. Later, Kwauk (1963) suggested that the concept developed by Richardson and Zaki (1954) could also be used to identify co-current and countercurrent liquid-solid flow.

Few works have been done on the fluidization of liquid-solid system under high liquid velocity. Since particle entrain out from the bed when the liquid fluidizing velocity is higher than the particle terminal velocity, it would be necessary to feed new particles into the bottom of the bed or to separate the entrained particles from the top and recirculate them back to the bottom of the bed. That need has caused to design an LSCFB. Aside from two reports on applications of LSCFBs to binary solids mixing (Felice et al., 1989) and fermentation (Pirozzi et al., 1989), most hydrodynamics studies on the riser of LSCFB were carried out at Tsinghua University (Liang et.al., 1993, 1995 and 1996; Liang and Zhu, 1997; Yang et al., 1993 ) and more recently at the University of Western Ontario (Zheng et al., 1999; Zheng and Zhu, 1999 and 2000). Roy and et al (2001) also conducted experimental investigations on CFB riser for alkylation process with new solid acid catalysts. In this section, a critical review of the key results from those studies is provided.

When the liquid velocity of riser is higher than the critical transition velocity, particles start circulating between two columns (riser and down-comer). Zheng et al. (1999) illustrated the variation of the solid circulation rate,  $G_s$ , with respect to superficial liquid velocity in riser. They observed two different types of the circulating fluidization regime for a given auxiliary liquid flow: (1) above particle terminal velocity, the initial circulating fluidization regime in which solid circulation rate increases quickly with increase in liquid flow rate and (2) with further increase in the liquid velocity, the developed circulating fluidization regime where solid circulation rate increases insignificantly with increase in liquid flow rate.

Zheng et al. (1999) worked on the axial flow structure in the riser of LSCFB under different operating condition. They have found out two distinct zones (based on their solid holdup) along the riser, namely a dense zone at the bottom of riser and an upper dilute zone. Solid holdup in the distributor zone is much higher and can be considered to be operated as conventional fluidization. The upper dilute zone is operated in circulating fluidization regime. Also, Both Liang et al. (1997) and Zheng et al. (1999) investigated the influence of particle properties on axial flow structure. They showed that under the initial circulating fluidization regime, the axial profiles of solid holdup for the glass beads (light particles) are uniform in the upper dilute zone of riser (Figure 1.2). However, the behavior of the steel shots is different from that of the lighter particles under the initial circulating fluidization regime. As shown in Figure 1.2, the axial distribution of solid holdups for the steel shot is not uniform under initial circulating fluidization regime; moreover, Further increasing the liquid velocity, the system enters the developed circulating fluidization regime where the solid holdup distribution becomes uniform in the riser for two different types of particles, as it's shown in Figure 1.2.

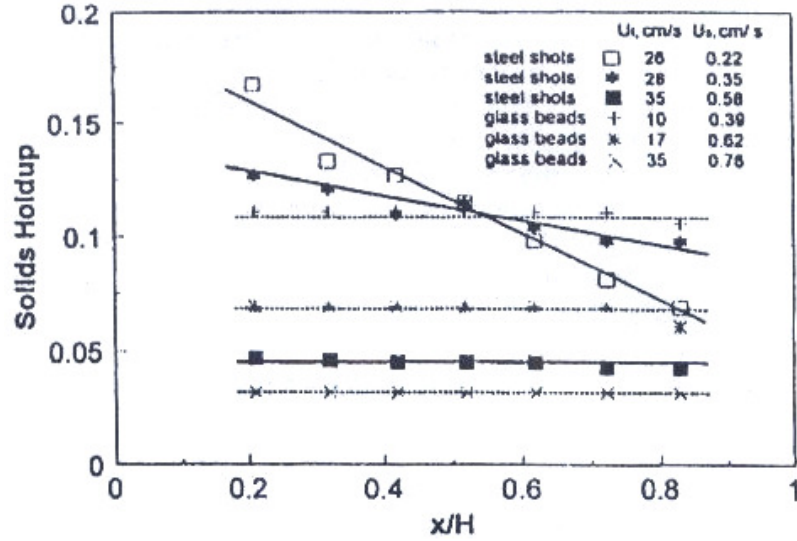


**Figure 1.2: The axial solid holdup distribution along the upper dilute zone of LSCFB riser for glass beads and steel shots, under different liquid velocity (Zheng et al., 1999)**

The radial flow structure in the liquid–solids circulating fluidization regime has been examined by Liang et al. (1996). They pointed out that unlike the conventional liquid–solids fluidized bed, the radial distribution of bed voidage is not uniform for glass beads, in the liquid–solids circulating fluidization regime. However, this work was carried out with only one type of particles under limited operating conditions.

Zheng et al (2001) presented solids holdup distribution in a lab-scale LSCFB by means of a fiber-optical probe. They claimed that the flow structure was affected significantly by operating conditions and physical properties of particles. Typical radial distributions of solid holdup plotted in Figure 1.3 shows that the radial flow is not completely uniform, but has higher solids concentrations near the wall. These results agree with the earlier reports by Liang et al. (1996) and Roy et al. (1997).

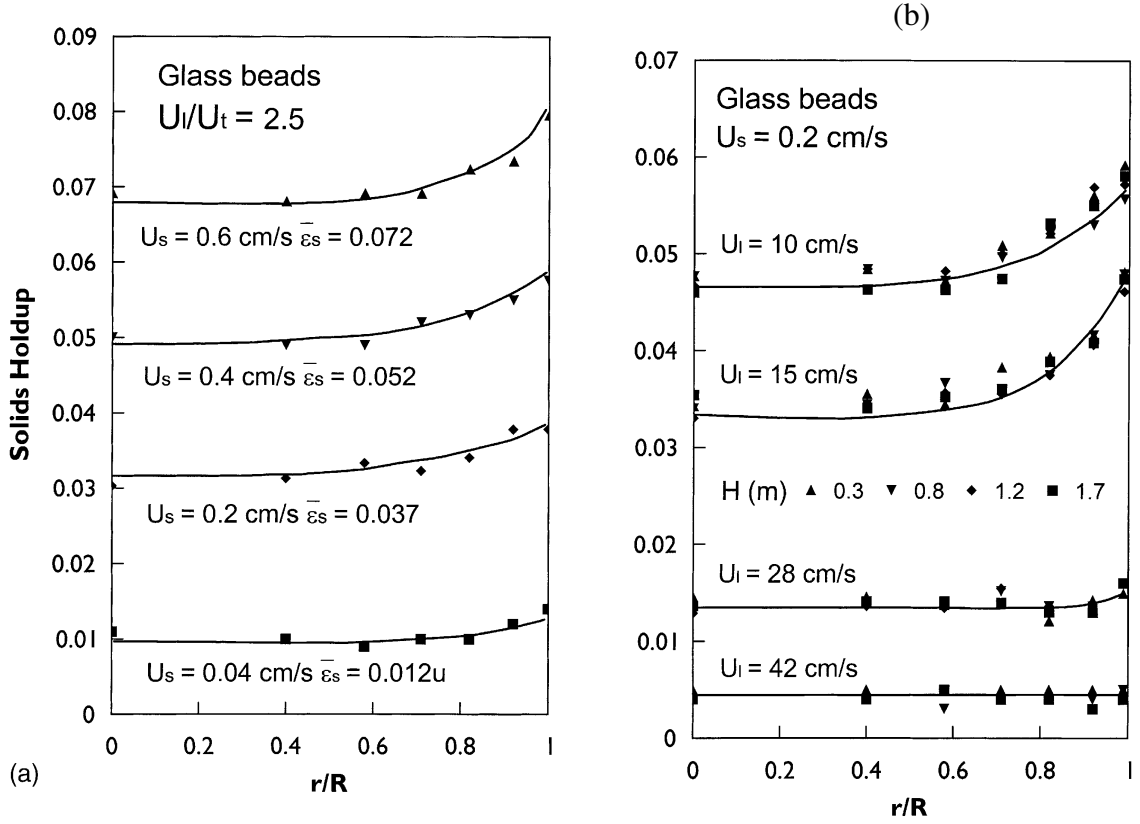


**Figure 1.3: Radial profiles of solids holdup at the level  $H = 0.8$ m (a) for different solids flow rates (b) for different superficial liquid velocities. (Zheng et al. 2001)**

Liang et al. (1996) and Zheng et al. (2002) have conducted a study on the local liquid velocity distributions and reported that a non-uniform distribution of liquid velocity also exists in the LSCFB. It is seen that liquid velocity are higher at the axis of the riser and lower near the wall. In Figure 1.4, the radial non-uniformity is seen to increase with increasing superficial liquid velocity. On further increasing the liquid velocity, the radial non-uniformity of local liquid velocity distribution decreases due to the transition from the circulating fluidization regime to the dilute liquid transport regime (Liang et al., 1996).

Roy et al (1997) measured the radial distribution of particle velocity in the riser of LSCFB. Experiments were performed using the CARPT method (computer-automated radioactive particle tracking) to track fairly large particles. It is interesting to note that the radial profiles of particle velocity are less uniform than those of liquid velocity and particles come down close to the wall in the most of operating conditions. Their results



demonstrate that the increase in the liquid superficial velocity steepens the radial profiles of particle velocity in the operating range of their study. They also found that the radial profiles of particle velocity do not change significantly with the axial position.

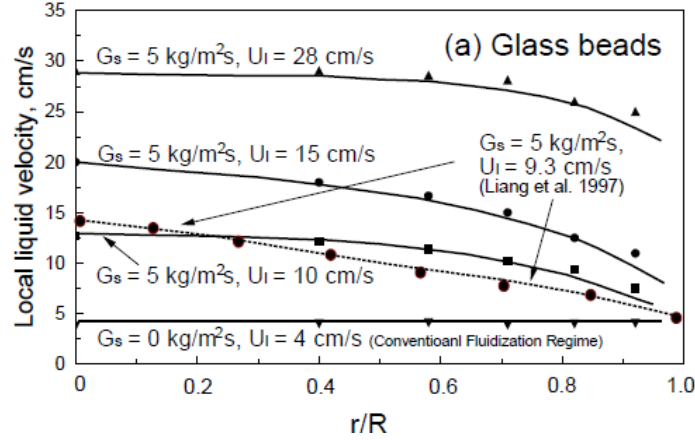


**Figure 1.4: The radial distribution of the liquid velocity under  $G_s = 5 \text{ kg/m}^2\text{s}$  and different liquid velocities for glass beads (Zheng et al. 2002).**

### 1.2.2 CFD models

In recent decades, CFD techniques have received a lot of attentions in simulating the transport phenomena in two-phase fluidized beds. CFD simulations are able to give very detailed information about the local values of solid hold-up ( $\epsilon_s$ ), liquid phase flow patterns and the intermixing levels of the individual phases especially in the regions where measurements are either difficult or impossible to obtain. Such information can be useful in the understanding of the transport phenomena in fluidized beds.

Generally, there are two approaches to solve two-phase flow: Eulerian-Lagrangian (E-L) approach and Eulerian-Eulerian (E-E) approach. In the E-L approach, the gas phase is considered as a continuous phase and Navier–Stokes (N-S) equations are solved for the gas phase. The solid phase is treated as a discrete phase and each solid particle is tracked by solving Lagrangian force balance equation. By averaging the movement parameters of a great number of particles tracked, the solid phase flow and concentration distribution can be estimated. This method has many advantages, such as clear and simple physical mechanism. However, its biggest drawback is that the high computational cost is required

to solve dense two-phase flow which has a large number of particles. Therefore, at present, this method can only be applied to some engineering cases which two-phase flow is dilute enough.

In the Eulerian-Eulerian approach, also well known as two fluid model, each phase is treated as an interpenetrating continuum and the concept of phasic volume fraction is introduced. The conservation equations of mass, momentum, and energy for both the particulate and the fluid phases are derived which have similar structure for all phases. In order to close pseudo N-S equation for solids phase, some constitutive correlations are required for solid-phase viscosity, pressure and stresses. So far, some researches have developed various assumptions to derive these correlations.

In the case of two-phase flow in the fluidized beds where the number of solids particles is huge, The E-E approach is the more attractive and practical method. That's why it has been widely used for simulations of two-phase flows in fluidized beds. Two fluid model was originally developed by Jackson (1963), Soo (1967), Garg and Pritchett (1979) to simulate the flow structure of bubbling fluidized beds. Their models were based on the assumptions of zero gas and solids viscosities. They were able mainly to predict the behavior of bubbling beds. Another heavily simplified model was constant-viscosity model introduced by Tsuo and Gidaspow (1990) to the simulation of riser column. They assumed that the particle viscosity is 200 times of the gas viscosity. Although this treatment was greatly approximated and highly empirical, their model was claimed to predict some flow patterns in the riser of circulating fluidized bed. However, these models are not quantitative enough to give accurate results close to experimental data.

In 1980s, kinetic theory of granular phase (KTGP) was presented to model the solid viscosity and solid stresses; Moreover, In the case of particulate flows, kinetic theory of granular flow has been widely applied in the literature (Sinclair and Jackson, 1989; Gidaspow, 1994 and Enwald et al., 1996). It is based on the kinetic theory of dense gases, as presented by Chapman and Cowling (1970). It assumes that the random motion of particles arising from particle-particle collisions is analogous to the thermal motion of gas molecules. Also, a granular temperature ( $\theta$ ) proportional to the mean square of the

random particle velocity is then defined. In this Theory, the usual thermal temperature is replaced by a granular temperature for which a differential equation is derived using the methods of kinetic theory. Thus the solid viscosity and the solid stress are a function of this granular temperature, which varies with time and position in a fluidized bed.

Though the published works on CFD modeling of fluidized beds are mostly on the gas-solid fluidized beds, a few CFD studies are available on the liquid-solid fluidized beds. Liquid-fluidized beds should, at least in principle, be simpler to model than gas-fluidized beds, since the hydrodynamics are more homogeneous, turbulence is much less of a factor, and the density difference between the two phases is reduced. Inter-particle collisions are also greatly attenuated, or even absent (Gidaspow and Lu, 1998) due to the liquid film separating particles as they approach each other.

Roy et al (2001) presented a two-fluid model based on the KTGP to simulate the LSCFB riser for alkylation process. The drag force correlation of Wen and Yu was applied to model momentum exchange between two phases. The liquid-phase turbulence was modeled using the standard  $k-\varepsilon$  model. No-slip condition was used at the wall for the liquid (continuous) phase. Johnson and Jackson boundary conditions were applied for velocity and granular temperature of solid phase on the wall. At the inlet, the boundary conditions were set to impose a uniform solids-liquid distribution. The purely convective flow was assumed as the outlet boundary conditions and also the symmetry conditions were imposed at the central axis of the column. Sensitivity to restitution coefficients ( $e$ ) was examined and the predicted profiles were found not very sensitive to the restitution coefficient in the vicinity of  $e=1.0$ . The computed solid velocity vectors indicated solids rising in the middle and flowing down near the walls; moreover, they were in a qualitative agreement with experimentally observed flow patterns. They achieved a typical set of residence time distribution (RTD) curves for the solids and liquid evaluated from solving the scalar transport equations for each phase which were in agreement with experimental data.

Doroodchi et al. (2005) have applied a CFD model to investigate the influence of the inclined plates on the expansion behavior of the fluidized suspensions. This model was

based on Eulerian–Eulerian approach to simulate the laminar regime in the mono-dispersed and binary-dispersed suspensions. For the solid phase, the viscous stress term was neglected. The Richardson and Zaki correlation was used for the drag coefficient. The no-slip condition was imposed on the fluid velocity at the wall while particles were allowed to slip freely at all walls. A maximum possible particle volume fraction of 0.58 was enforced. The numerical results illustrated the effect of the fluidization superficial velocity on the average volume fraction. The CFD models successfully predicted the general trends in the experimental data. They indicated that some CFD model limitations have contributed to the observed deviations between the experimental results and CFD predictions. First, the modified fluidized bed was simulated with a two-dimensional model to reduce computational time, although the suspension is three-dimensional phenomenon. Second, the particle size distribution and the interaction between the solid phases for the binary system of particles were ignored and a laminar flow regime was assumed throughout the vessel.

Lettieri et al. (2006) used the CFD modelling based on Eulerian–Eulerian approach to simulate a liquid fluidized bed of lead shot in slugging mode. The granular kinetic theory was applied to describe the solids pressure and the solid phase stress tensor. The radial distribution function ( $g_o$ ) given by Ding and Gidaspow (1990) was used in their work. The inter-phase momentum exchange was modeled by an equation presented by Gidaspow and Ihme (1994). No-slip boundary conditions were applied for both phases on the wall. The uniform gas inlet velocity was employed as a boundary condition at the bottom of the riser. Pressure boundary conditions were employed at the top of the riser. This implies Dirichlet boundary conditions on pressure and all flow quantities were of zero normal gradient. Results from simulations were analyzed in terms of voidage profiles, bed expansion, pressure drop and pressure fluctuations. The CFD results showed an agreement with the experimental data at low liquid velocities. However, modeling was not able to predict flow structure at high liquid velocity, reasonably.

Cornelissen et al. (2007) presented a CFD model based on multi-fluid Eulerian approach to simulate a liquid–solid fluidized bed. A no-slip boundary condition and pressure outlet condition were imposed on the wall and outlet face, respectively. The case studies have

demonstrated that the mesh size, time step and convergence criteria are three inter-related parameters. They've shown that the Courant number ( $u\Delta t/\Delta x$ ) in the range  $0.03 < \text{Courant No.} < 0.3$  gives the best results which are independent of mesh, time step, and convergence criterion. Also, they have applied both uniform and non-uniform (discrete-hole) distributor at the inlet and flow characteristics was compared between the two distributors. The non-uniform distributor caused a slight decrease in overall bed voidage compared to a perfectly uniform distributor. Also, the perfectly uniform distributor resulted in fewer swirls than the non-uniform distributor. It was also shown that particles near the distributor ascend near the wall and descend in the core, while this pattern reverses in the upper part of the column which is in agreement with the experimental data. The difference between the upward and downward velocities may be caused by a non-uniform radial distribution of voidage, with lower voidage in the downflow region than in the upflow region. The CFD and experimental results were also compared with the predictions from the well-known Richardson and Zaki (1954) equation. The CFD model consistently underpredicts the voidage, but, except at the highest superficial liquid velocities, the predictions are better than those from the Richardson and Zaki equation and within 5% of the experimental data.

### 1.2.3 Protein extraction from biological broth using an LSCFB ion exchange system

One of the common separation methods which are used to extract the protein from biological broth is the ion exchange mechanism. In this section, the principles of ion exchange particle are discussed first and then it's followed by an emphasis on its application in protein recovery.

An anion exchanger can be represented as  $\text{Resin-F}^+ E^-$  which  $\text{Resin-F}^+$  denotes the inert matrix containing the positive fixed ion (functional group) and  $E^-$  indicates the counter-ion. When an anion exchange particle is submerged in a solution containing a different anion,  $A^-$ , the ion exchange will process as following:



When an ion exchanger particle is placed in an aqueous solution, the pores will fill with solution and a sufficient concentration of counter-ions to maintain the overall electric balance in the particle. The counter-ion can move through the matrix by diffusion or under the influence of an electric field. These counter-ions are thus exchanged with ions of the same charge from the bulk solution and this step is the base of the ion exchange process.

The continuous ion exchange processes using different types of fluidized beds were extensively investigated (Byers et al., 1997; Gordon et al., 1990; Higgins, 1969; and Himsley, 1981). The application of conventional fluidized beds for ion exchange process has some benefits such as the low and stable bed pressure drop and the direct application of unclarified whole broth feed. As reviewed by Zhu et al. (2000), compared with conventional fluidized beds, circulating fluidized beds have many advantages including continuous operation with adsorption and desorption carried out simultaneously, high throughput due to high liquid velocity in the riser, highly efficient liquid-solid contact, favorable mass and heat transfer, maintaining the nearly plug flow condition in the riser which reduced back-mixing of phases and integrated reactor and smaller processing volumes. (Felice, 1995; Fan, 1989; and Lan et al., 2000).

The schematic of the LSCFB ion exchange system used by Lan et al. (2000) for continuous protein extraction is shown in Figure 1.1. The major components of the LSCFB extractor include a riser, a downcomer, a liquid-solid separator, a top solids-return pipe, a bottom solids-return pipe, a top washing section, a bottom washing section, a riser distributor and a downcomer distributor. The riser is 3.0 m in height and 0.038 m in diameter, and the downcomer is 2.5 m in height and 0.120 m in diameter.

Two different types of liquid streams are used to fluidize the particles in the riser and downcomer. The liquid velocity in the riser is higher than the terminal velocity of the particles; therefore, the particles can be entrained up along the riser. However, the liquid velocity in the downcomer is less than the terminal velocity of the particles, so particles

can flow down from the top of downcomer. As a result, the particles are able to circulate between the two columns.

The distributor for the downcomer is a tubular ring that is carefully designed in order to have a uniform liquid distribution while allowing the solids to flow down. The riser distributor divides the incoming stream into two streams: the primary and auxiliary streams. The primary stream enters through a tubing of 1.1 cm in ID extending 5.1 cm into the riser. The outlet of the primary stream was located above the solids entrance at the bottom of the riser. Also, the auxiliary stream is introduced through a perforated plate at the bottom of the riser. The particles at the bottom are mobilized by the auxiliary stream, and then the particles are entrained up along the riser by the combination of the primary and auxiliary streams.

The dynamic seals between the riser and downcomer are achieved by maintaining the two solids return pipes in the moving packed-bed regime. The top wash section and the bottom wash section clean the particles before they entering the solids return pipes to avoid penetrating liquid solution from one column to another. The solids circulation rate is controlled by a butterfly valve installed on the bottom solids return pipe. The solids circulation rate was measured by a device which is installed at the top of the downcomer and made of a central vertical plate and two half butterfly valves.

Bovine serum albumin (BSA) was used as model protein and continuous recovery of BSA solution in the LSCFB ion exchange system was conducted with the BSA solution as feed in the downcomer and 0.4 M NaCl solution as the extracting buffer in the riser. Diaion HPA25 particles were used as ion-exchange particles for all BSA adsorption-desorption studies.

The downcomer is assigned for protein adsorption and the riser is designed as a stripper to desorb the protein and to regenerate the particles. Proteins are thus adsorbed onto the adsorbents in the downcomer and the loaded-adsorbents are regenerated simultaneously in the riser in a continuous mode. One of the unique features of the LSCFB extractor is that the downcomer operates as an expanded bed with the adsorbent particles falling down and the liquid phase moving up. The space between particles in the downcomer can

be kept up large enough to allow the passage of the colloids in the feed without clogging the bed. In other words, an unclarified broth containing colloids can be treated directly by an LSCFB extractor without preclarification. This will significantly simplify the overall purification scheme.

Numerical modeling of an LSCFB ion exchange system for protein extract from biological broth is the topic of this thesis. A number of models have been developed to describe the protein adsorption and desorption behaviors in packed beds, expanded beds and circulating fluidized beds considering various types of approximation to physical reality. Several steps are involved in the process of adsorption of proteins onto the adsorbent particles: (1) convective and diffusion mass transfer from the liquid phase to the adsorbent surface, (2) diffusion through the pore of the ion exchange particles and (3) the surface reactions. The surface adsorption process is sufficiently rapid compared to the first two steps and is not usually considered as a limiting step. Veeraraghavan et al. (1989) developed a model for adsorption of phenol onto granular activated carbon in a liquid–solid fluidized bed considering liquid and solid phase axial dispersion, film mass transfer resistance and homogeneous diffusion model for pore diffusion. Wright and Galsser (2001) developed a similar model for the adsorption of proteins in the fluidized bed and studied the effect of operating parameters on the adsorption performance. Later on, Ping et al. (2005) and Junxian et al. (2005) modeled the protein adsorption in expanded bed and in addition to Wright and Galsser (2001), they considered axial distribution of particles size and axial variations of bed voidage. Lan et al. (2000) developed a model for continuous protein recovery in LSCFB ion-exchange systems assuming the process is not surface reaction limited. However, detailed hydrodynamics of the LSCFB was not included in their model. Recently, Gaikwad et al. (2008) developed another model on adsorption in an LSCFB considering the film mass transfer resistance as the limiting step. Their model covered only the adsorption in the down comer whereas the protein desorption process was not considered in the riser.



### 1.3 Objectives and thesis structure

In light of the literature review presented in the previous sections, it is seen that a number of CFD modeling has been done on the hydrodynamics of LSCFBs. Some kinetic models have also been developed to describe the protein adsorption and desorption behaviors in different kinds of fluidized beds considering various types of simplifications to physical reality (Wright and Galsser, 2001; Ping et al., 2005; and Gaikwad et al., 2008). However, detailed hydrodynamics of the LSCFB was not included in their kinetic models and they assumed that the distribution of solid holdup ( $\epsilon_s$ ), solid velocity ( $U_s$ ) and liquid velocity ( $U_l$ ) are uniform throughout the riser and downcomer. In contrast, experimental data have demonstrated that both axial and radial distributions of hydrodynamics properties are not uniform along the riser of an LSCFB.

As a result, a complete modeling of the protein extraction using an LSCFB ion-exchange system requires a microscopic study on the nature of this system including hydrodynamics field, mass transfer and kinetics reactions. It is of fundamental importance for designing and scaling up LSCFB ion-exchange systems and optimizing operating conditions.

At this research work, first, the hydrodynamics field of an LSCFB riser will be simulated by Eulerian-Eulerian model based on the kinetics theory of granular flow. Then, the influence of operating conditions such as liquid superficial velocity and solids holdup on the flow structure will be investigated. And next, in order to simulate the protein extraction process using the LSCFB ion-exchange system, the mass transfer model of the protein species will be coupled to the initial CFD model for the hydrodynamics. Finally, a CFD model is developed to capture the hydrodynamic characteristics of the counter-current flow in the downcomer of the LSCFB. Therefore, the thesis structure is as follows:

Chapter 1 gives an introduction and comprehensive review to the experimental studies on the hydrodynamics characterization of the LSCFB, the CFD modeling of the liquid-solid two phase flow and the protein extraction process from biological broth using LSCFB ion exchange systems.

Chapter 2 reports a numerical investigation on the hydrodynamics of the LSCFB riser using a CFD model based on Eulerian-Eulerian approach and incorporating the granular kinetics theory.

Chapter 3 presents a sophisticated numerical model to simulate the protein extraction process using the LSCFB ion-exchange system. This model will take into account a more accurate study on the nature of this system including hydrodynamics, mass transfer and kinetics. A axisymmetric CFD model is developed to capture the detailed information about the local values of volume fraction, velocity and protein concentration of both the liquid stream and the solid particles in the riser. In addition, the adsorption process in the LSCFB downcomer is simulated by a one-dimensional mathematical model using the adsorption kinetics correlations.

Chapter 4 reports a CFD model to simulate the hydrodynamics of the counter-current two phase flow in the downcomer of the LSCFB. The model is based on Eulerian-Eulerian (E-E) approach incorporating the kinetic theory of granular flow. Furthermore, the effect of operating condition on hydrodynamic characteristic is examined.

Chapter 5 summarizes the key results from all above studies and recommends the future work.

Therefore, the results of this research would expand our knowledge on:

- (1) Nature of hydrodynamics of the two phase flow in an LSCFB riser.
- (2) Detailed simulation of the protein extraction process from industrial broth using an LSCFB ion-exchange system
- (3) Optimization of the protein extraction process from industrial broth using an LSCFB ion-exchange system.
- (4) Hydrodynamic characteristics of the counter-current two phase flow in the downcomer of an LSCFB.

## References

- Byers, C. H., Sisson, W. G., Snyder, T. S., Beleski, R. J., Nayak, U. P., & Francis, T. L. (1997). *Zirconium and hafnium separation in sulfate solution using continuous ion exchange chromatography*. U.S. Patent No. 5,618,502.
- Chapman, S., & Cowling, T. G. (1970). *The Mathematical Theory of Non-Uniform Gases*. 3rd ed.. Cambridge Univ. Press.
- Gaikwad, A., Kale, S., & Lali, (2008). A. Modeling of counter-current adsorption in continuous liquid-solid circulating fluidized bed adsorption chromatography. *Chem Eng Sci.*, 63, 1062–1071.
- Garg, S. K., & Pritchett, J. W. (1975). Dynamics of Gas-Fluidized Beds. *J. Appl. Phys.*, 46, 4493.
- Gidaspow, D. (1994). *Multiphase Flow and Fluidization: Continuum and Kinetic Theory Descriptions*. Boston: Academic Press.
- Gidaspow, D., & Lu, H. (1998). A comparison of gas–solid and liquid–solid fluidization using kinetic theory and statistical mechanics. In: Fan, L. S., Knowlton, T. M. (Eds.), *Fluidization IX. Engineering Foundation*, New York, 661–668.
- Gordon, N. F., Tsujimura, H., & Cooney, C. L. (1990). Optimization and simulation of continuous affinity recycle extraction. *Bioseparation*, 1, 9–21.
- Grace, J. R., Issangya, A. S., Bai, D., Bi, H. T., & Zhu, J. Z. (1999). Situating the high-density circulating fluidized bed. *AIChE J.*, 45, 2108.
- Higgins, I. R. (1969). Continuous ion exchange of process water. *Chemical Engineering Progress*, 65, 59–62.
- Himsley, A. (1981). Continuous countercurrent ion exchange process. U.S. Patent No. 4,279,755.

- Jackson, R. (1963). The Mechanics of Fluidized Beds. *Trans. Inst. Chem. Eng.*, 41.
- Junxian, Y., Dong, Q. L., Shan, J. Y. (2005). Predictive modeling of protein adsorption along the bed height by taking into account the axial nonuniform liquid dispersion and particle classification in expanded beds. *J Chromatogr A*, 1095, 16–26.
- Lan, Q. D. (2001). *Development of Continuous Liquid-Solid Circulating Fluidized Bed Ion Exchange System and its Application in Protein Purification* (Ph.D. dissertation). University of Western Ontario.
- Liang, W. G., & Zhu, J. X. (1997). A core-annulus model for the radial flowstructure in a liquid-solid circulating fluidized bed (LSCFB). *Chem Eng J.*, 68, 51–62.
- Liang, W. G., Zhang, S. L., Zhu, J. X., Yu, Z. Q., Jin, Y., & Wang, Z. W. (1997). Flow characteristics of the liquid-solid circulating fluidized bed. *Powder Tech.*, 90, 95–102.
- Liang, W. G., Zhu, J. X., Jin, Y., Yu, Z., Wang, Z. W., & Zhou, J. (1996). Radial Non-uniformity of flow structure in a liquid solid circulating fluidized bed. *Chemical Engineering Science*, 50, 2001-2010.
- Ping, L., Guohua, X., & Alirio, E. R. (2005). Experimental and modeling study of protein adsorption in expanded bed. *AIChE J.*, 51, 2965–2977.
- Roy, S., & Dudukovic, M. P. (2001). Flow Mapping and Modeling of Liquid-Solid Risers. *Ind. Eng. Chem. Res.*, 40, 5440-5454.
- Sinclair, J. L., & Jackson, R. (1989). Gas-particle flow in a vertical pipe with particle-particle interactions. *AIChE J.*, 35, 1473.
- SOO, S. L. (1967). *Fluid Dynamics of Multiphase System*. Waltham, MA: Blaisdell.
- Veeraraghavan, S., Fan, L. T., & Mathews, A. P. (1989). Modeling adsorption in liquid-solid fluidized beds. *Chem Eng Sci*, 44, 2333–2344.
- Wen, C. Y., & Yu, Y. H. (1966). Mechanics of fluidization. *Chemical Engineering Progress Symposium Series*, 62, 100–111.

Winkler, F. (1922). German Patent 437, 970.

Wright, P. R., & Galsser, B. J. (2001). Modelling mass transfer and hydrodynamics in fluidized-bed adsorption of proteins. *AIChE J.*, 47, 474–488.

Yang, Y. L., Jin, Y., Yu, Z. Q., Zhu, J. X., & Bi, H. T. (1993). Local slip behaviors in the circulating fluidized bed. *AIChE Symp. Ser.*, 89, 8190.

Zheng, Y., & Zhu, J. X. (2003). Studies on liquid velocity in a liquid-solid circulating fluidized bed. *Int J Chem Reactor Eng*, 1, 1–7.

Zheng, Y., Zhu, J. X., Marwaha, N., & Bassi, A. S. (2002). Radial solid flow structure in a liquid-solid circulating fluidized bed. *Chem Eng J.*, 88, 141–150.

Zheng, Y., Zhu, J. X., Wen, J. Z., Bassi, A. S., & Margaritis, A. (1999). The axial hydrodynamic behavior in a liquid-solid circulating fluidized bed. *Can J Chem Eng.*, 77, 284–290.

Zhu, J. X., Zheng, Y., Karamanev, D. G., & Bassi, A. S. (2000). (Gas-) Liquid-Solid Circulating Fluidized Beds and Their Potential Applications to Bioreactor Engineering. *Can. J. Chem. Eng.*, 78, 82–94.

## Chapter 2

# 2 A Computational Fluid Dynamics Study on the Flow Field in a Liquid-Solid Circulating Fluidized Bed Riser\*

## 2.1 Introduction

Liquid-solid circulating fluidized bed (LSCFB) reactors are obtaining extensive attraction in diverse fields of industrial processes, such as many new processes in biochemical technology, wastewater treatment, petroleum and metallurgical industries (Atta et al., 2009). This is because this new type of liquid-solids contacting equipment has a large number of unique features, such as effective liquid-solids contacts, short and narrow residence time for both phases and independent control of solids holdup by varying the mass flow rate of particles (Zheng et al., 2002&2003).

A typical LSCFB is comprised of a riser, a downcomer, a liquid-solid separator, a top solids-return pipe and a bottom solids-return pipe. Particles are entrained up by the liquid stream along the riser under a co-current pattern, then separated at the riser top (separator), and finally recirculated back through a particle storage vessel or downcomer to the bottom of the riser (Zheng et al., 2002; Razzak et al., 2009). A proper selection of the reactor is crucial to minimize the costs of the plant and also the negative impact of the reaction products on environment. The reactor modeling approach that illustrates the key features of the multiphase flow pattern and predicts the relevant physical quantities can be a reliable technique to gain the aim. However, a kinetics model describing the reaction chemistry can predict the reactor performance meaningfully, only when the comprehensive flow field information in the reactor is known (Roy et al., 2001).

In recent decades, computational fluid dynamics (CFD) techniques have received many attentions in simulating the flow field in two phase flow. Generally, two different types of the CFD models can be used to simulate two phase flow: Eulerian-Lagrangian (E-L)

---

\* This manuscript has been submitted to Powder Technology Journal for publication

approach and Eulerian-Eulerian (E-E) approach. In the E-L approach, the carrier phase is considered as a continuous phase and the solid phase is treated as a discrete phase and each solid particle is tracked by solving the Lagrangian force balance equation. In the E-E approach, also well known as the two-fluid model, each phase is treated as an interpenetrating continuum. In order to estimate the solids viscosity and solids stresses, the kinetic theory of granular phase (KTGP) is incorporated into the two-fluid model (Sinclair and Jackson, 1989; Gidaspow, 1994; and Ding et al., 1990).

In the case of two-phase flow in the fluidized beds where the number of solid particles is huge, the E-E approach is the more attractive and practical method. The prior CFD studies on this area mostly focused on the gas-solid fluidized bed; and less attention has been dedicated to the CFD modeling of the liquid-solid fluidized bed. Roy et al. (2001) presented a two-fluid model based on the KTGP to simulate the LSCFB riser for alkylation process. The liquid-phase turbulence was modeled using the standard  $k-\varepsilon$  model. They found out that the predicted flow field was not very sensitive to the restitution coefficient in the vicinity of  $e=1.0$ . Doroodchi et al. (2005) applied the E-E approach to investigate the influence of the inclined plates on the expansion behavior of the liquid-solid fluidized bed. The viscous stress of the solids was neglected in the simulation. The CFD models successfully predicted the general trends in the experimental data.

Lettieri et al. (2006) used the E-E approach to simulate a liquid fluidized bed of lead shot in slugging mode. The granular kinetic theory was applied to describe the solids pressure and the solid phase stress tensor. The CFD results showed an agreement with the experimental data at low liquid velocities. However, modeling was not able to accurately predict the flow structure at high liquid velocity. Cheng and Zhu (2005) developed a two-fluid model to simulate the turbulent liquid-solid flow in an LSCFB riser. KTGP was incorporated into the model. The model predictions agreed well with the experimental data in the literature and it was also found that increase in particles size and bed diameter result in more non-uniform distributions of hydrodynamic parameters in the radial direction. Shi et al. (2010) developed a three-dimensional E-E model to describe the

liquid-solid flow in a tubular loop propylene polymerization reactor. The predicted pressure gradients showed a good agreement with the classical calculated data.

In this work, an axisymmetric CFD model is proposed to describe the flow field in LSCFB risers. The model is based on Eulerian–Eulerian approach incorporating the kinetic theory of granular flow. The CFD model is applied to capture the detailed information about the local values of volume fraction and velocity, as well as the residence time of both the liquid stream and the solid particles in the riser with a Pulse technique.

## 2.2 Experimental setup of the LSCFB system

In our earlier works, Zheng et al. (1999, 2002 and 2003) conducted an experimental study on the structure of the solids and liquid flows in an LSCFB which was designed and manufactured in a lab scale. A schematic diagram of the experimental apparatus is shown in Fig. 2.1. The main components of the system are the vertical Plexiglass riser column of 76 mm I.D. and 3.0 m in height, a liquid-solids separator, a liquid stream distributor, a dual flipping valve for measuring solids circulation rate and a solids storage vessel. The distributor divides the incoming liquid stream into two substreams: the primary and auxiliary streams. The primary stream enters through 7 stainless steel tubes (1.27 cm I.D.), occupying 19.5% of the total bed area and extending 0.2 m into the bed. Also, the auxiliary stream is introduced through a perforated plate with 4% opening area at the bottom of the riser. The particles at the bottom are mobilized by the auxiliary stream, and then the particles are entrained up along the riser by the combination of the primary and auxiliary streams. All experiments were carried out at ambient temperature. Tap water was used as carrier liquid phase and glass beads as solid particles ( $d_p=508\ \mu\text{m}$ ,  $\rho_p=2490\ \text{kg/m}^3$  and  $U_t=5.9\ \text{cm/s}$ ).



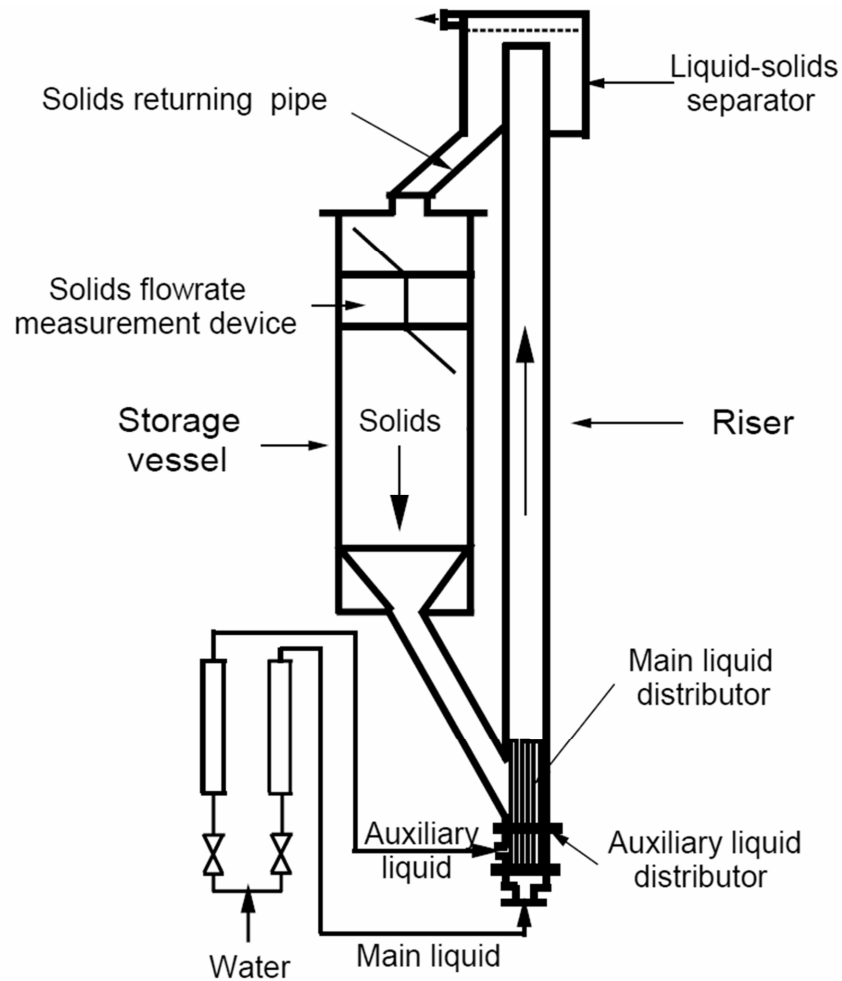


**Figure 2.1: Schematic diagram of the liquid-solid circulating fluidized bed (Zheng et al., 2003).**

## 2.3 Mathematical modeling

Since the liquid phase velocity in the riser is higher than the terminal velocity ( $U_t$ ) of the solid particles, the riser is operated under the circulating fluidization regime (Liang et al., 1997). A CFD axisymmetric model is used to simulate the turbulent flow field in the LSCFB riser. The CFD model is based on Eulerian–Eulerian approach. Thus, the governing equations for the solid phase have similar structure to those for the liquid phase. Furthermore, in order to close the conservation equations for the solid phase, the viscosity, pressure and stresses of the solid phase are modeled by the kinetic theory of granular phase (KTGP). In this theory, the mean square of the random particle velocity is

defined as the granular temperature ( $\Theta$ ). Thus the solids viscosity and the solids stress are correlated by a function of the granular temperature.

The  $k$ - $\varepsilon$  turbulence model is used to incorporate the influence of turbulence on the liquid-solid flow. Three different types of the  $k$ ,  $\varepsilon$  turbulence models are examined to find the most computationally efficient and accurate model.

### 2.3.1 Governing equations

Continuity equation for the phase  $q$  ( $q=l$  for the liquid phase and  $q=s$  for the solid phase) are given as:

$$\frac{\partial}{\partial t}(\alpha_q \rho_q) + \nabla \cdot (\alpha_q \rho_q \vec{v}_q) = 0, \quad \sum_q \alpha_q = 1. \quad (1)$$

Where  $\alpha_q$  is the volume fraction of phase  $q$ . Momentum equations for the liquid phase and the solid phase are written as:

$$\frac{\partial}{\partial t}(\alpha_l \rho_l \vec{v}_l) + \nabla \cdot (\alpha_l \rho_l \vec{v}_l^2) = -\alpha_l \nabla p + \nabla \cdot \bar{\bar{\tau}}_l + \alpha_l \rho_l \vec{g} + K_{sl} (\vec{v}_s - \vec{v}_l), \quad (2)$$

$$\bar{\bar{\tau}}_l = \alpha_l \mu_l (\nabla \cdot \vec{v}_l + \nabla \cdot \vec{v}_l^T). \quad (3)$$

$$\frac{\partial}{\partial t}(\alpha_s \rho_s \vec{v}_s) + \nabla \cdot (\alpha_s \rho_s \vec{v}_s^2) = -\alpha_s \nabla p + \nabla p_s + \nabla \cdot \bar{\bar{\tau}}_s + \alpha_s \rho_s \vec{g} + K_{ls} (\vec{v}_l - \vec{v}_s), \quad (4)$$

$$\bar{\bar{\tau}}_s = \alpha_s \mu_s (\nabla \cdot \vec{v}_s + \nabla \cdot \vec{v}_s^T) + \alpha_s \left( \lambda_s - \frac{2}{3} \mu_s \right) \nabla \cdot \vec{v}_s \bar{\bar{I}}. \quad (5)$$

where the granular bulk viscosity,  $\lambda_s$ , describes the resistance of an emulsion to compression or expansion. Furthermore,  $\mu_s$ ,  $p_s$  and  $K_{sl}$  are the solids viscosity, solids pressure and the coefficient of the momentum exchange between two phases, respectively. External body, lift and virtual mass forces are neglected in the momentum equations. The coefficient of the momentum exchange between the liquid and solid phases ( $K_{sl}$ ) is described by the empirical drag correlation of Wen and Yu (1966):

$$K_{sl} = \frac{3}{4} C_D \frac{\alpha_s \alpha_l \rho_l |\vec{v}_s - \vec{v}_l|}{d_s} \alpha_l^{-2.65},$$

$$C_D = \frac{24}{\alpha_l \text{Re}_s} \left[ 1 + 0.15 (\alpha_l \text{Re}_s)^{0.687} \right], \quad \text{Re}_s = \frac{\rho_l d_s |\vec{v}_s - \vec{v}_l|}{\mu_l}. \quad (7)$$

The granular temperature, which is representing the solid phase velocity fluctuation, is defined as (Roy and Dudukovic, 2001):

$$\theta_s = \frac{2}{3} k_s \quad (8)$$

where  $k_s$  is the kinetic energy due to solids velocity fluctuation. The transport equation of the granular temperature can be written as:

$$\frac{3}{2} \left[ \frac{\partial}{\partial t} (\rho_s \alpha_s \Theta_s) + \nabla \cdot (\rho_s \alpha_s \bar{v}_s \Theta_s) \right] = (-p_s \bar{I} + \bar{\tau}_s) : \nabla \bar{v}_s + \nabla \cdot (k_{\Theta s} \nabla \Theta_s) - \gamma_{\Theta s} - 3K_{ls} \Theta_s \quad (9)$$

where  $(k_{\Theta s})$  and  $(\gamma_{\Theta s})$  are the granular conductivity and the collisional dissipation of energy, respectively.

In this study, three different types of the  $k$ - $\varepsilon$  multiphase turbulence models are used, the mixture turbulence model, dispersed turbulence model and per-phase turbulence model. The mixture turbulence model represents the first extension of the single-phase  $k$ - $\varepsilon$  model. It uses the mixture properties and mixture velocities to capture important features of the turbulent flow. This model is given as:

$$\frac{\partial}{\partial t} (\rho_m k) + \nabla \cdot (\rho_m \bar{v}_m k) = \nabla \cdot \left( \frac{\mu_{t,m}}{\sigma_k} \nabla k \right) + G_{k,m} - \rho_m \varepsilon.$$

$$\frac{\partial}{\partial t} (\rho_m \varepsilon) + \nabla \cdot (\rho_m \bar{v}_m \varepsilon) = \nabla \cdot \left( \frac{\mu_{t,m}}{\sigma_\varepsilon} \nabla \varepsilon \right) + \frac{\varepsilon}{k} (C_{1\varepsilon} G_{k,m} - C_{2\varepsilon} \rho_m \varepsilon). \quad (10)$$

Where  $\rho_m$ ,  $\bar{v}_m$  and  $G_{k,m}$  are the mixture density, mixture velocity and the production of turbulence kinetic energy, respectively.

The  $k$ - $\varepsilon$  dispersed turbulence model uses the standard  $k$ - $\varepsilon$  model supplemented with extra terms that include the interphase turbulent momentum transfer. The dispersed turbulence model is given as:

$$\begin{aligned} \frac{\partial}{\partial t}(\alpha_l \rho_l k_l) + \nabla \cdot (\alpha_l \rho_l \bar{v}_l k_l) &= \nabla \cdot \left( \alpha_l \frac{\mu_{t,l}}{\sigma_k} \nabla k_l \right) + \alpha_l G_{k,q} - \alpha_l \rho_l \varepsilon_l - K_{sl} (2k_l - \sqrt{2k_l} \sqrt{3\Theta_s}), \\ \frac{\partial}{\partial t}(\alpha_l \rho_l \varepsilon_l) + \nabla \cdot (\alpha_l \rho_l \bar{v}_l \varepsilon_l) &= \nabla \cdot \left( \alpha_l \frac{\mu_{t,l}}{\sigma_\varepsilon} \nabla \varepsilon_l \right) + \alpha_l \frac{\varepsilon_l}{k_l} (C_{1\varepsilon} G_{k,l} - C_{2\varepsilon} \rho_l \varepsilon_l) \\ &\quad - C_{2\varepsilon} \frac{\varepsilon_l}{k_l} K_{ls} (2k_l - \sqrt{2k_l} \sqrt{3\Theta_s}), \end{aligned} \quad (11)$$

The per-phase turbulence model includes a set of  $k$ - $\varepsilon$  transport equations for each phase. Since two additional transport equations are solved for the solid phase, the per-phase turbulence model is more computationally expensive than the dispersed turbulence model. The transport equations are closed by the constitutive correlations derived from the kinetic theory of granular flow. They are summarized in table 2.1.

### 2.3.2 Boundary conditions

The computational domain of the riser is shown in Fig. 2.2. As it is seen, the uniform boundary conditions are imposed on the inlet of the riser for both solids and liquid streams. Therefore, the quantities of both phases are distributed uniformly at the entire inlet cross section. The no-slip and free-slip boundary conditions are used on the wall for liquid and solid phases, respectively. Johnson and Jackson (1987) developed the boundary conditions for the slip velocity of solid phase near the wall:

$$\frac{\mathbf{u}_{sl} \cdot (\boldsymbol{\sigma}_c + \boldsymbol{\sigma}_f) \cdot \mathbf{n}}{|\mathbf{u}_{sl}|} + \frac{\phi \sqrt{3\Theta} \tau_p \alpha_p |\mathbf{u}_{sl}|}{6\alpha_{p,\max} [1 - (\alpha_p / \alpha_{p,\max})^{1/3}]} + N_f \tan \delta = 0 \quad (12)$$

The first term on the left side of Eq. (12) denotes the stress within the solids flow approaching the wall. Here,  $u_{sl}$  is the slip velocity between the particles and the wall,  $\sigma_c$  and  $\sigma_f$  are collisional and frictional stress tensors, respectively, and  $n$  is the unit normal vector of the wall. The second term stands for the rate of tangential momentum transfer to the wall by particle-wall collisions, which is the product of the collision frequency for each particle,  $\sqrt{3}\Theta/s$ , the average tangential momentum transferred per collision,  $\phi\rho_p\pi d_p^3 u_{sl}/6$ , and the number of particles adjacent to unit area of the wall,  $1/a_c$ . Here,  $s$  denotes the average distance between the wall and an adjacent particle, estimated by  $s = d_p \left[ (\alpha_{p,\max} / \alpha_p)^{1/3} - 1 \right]$ ,  $a_c$  is the average boundary area per particle read as  $a_c = d_p^2 (\alpha_{p,\max} / \alpha_p)^{2/3}$ , and  $\phi$  is the specularity coefficient.  $\rho_p$  is the density of the solid material,  $d_p$  is the particle diameter,  $\Theta$  is the granular temperature,  $\alpha_p$  is the solids volume fraction, and  $\alpha_{p,\max}$  is the solids volume fraction at a closely random packing state. The third term on the left side of Eq. (12) is the stress due to sliding particles, which is obtained by applying Coulomb's law of friction to the particles sliding over the surface.

**Table 2.1. The constitutive correlations for closure of the transport equations**

Solids pressure	$P_s = \alpha_s \rho_s \Theta_s + 2\rho_s (1 + e_{ss}) \alpha_s^2 g_{O,ss} \Theta_s$	(Lun et al., 1984)
Radial distribution function	$g_{O,ss} = \left[ 1 - \left( \frac{\alpha_s}{\alpha_{s,max}} \right)^{1/3} \right]^{-1}$	(Ding and Gidaspow, 1990)
Solids shear stress	$\mu_s = \mu_{s,col} + \mu_{s,kin} + \mu_{s,fr}$	
Collisional viscosity	$\mu_{s,col} = \frac{4}{5} \alpha_s \rho_s d_s g_{O,ss} (1 + e_{ss}) \sqrt{\frac{\Theta_s}{\pi}}$	(Gidaspow et al., 1994)
Kinetic viscosity	$\mu_{s,kin} = \frac{\alpha_s \rho_s d_s \sqrt{\Theta_s \pi}}{6(3 + e_{ss})} \left[ 1 + \frac{2}{5} (1 + e_{ss}) (3e_{ss} - 1) \alpha_s g_{O,ss} \right]$	(Syamlal et al., 1993)
Frictional viscosity	$\mu_{s,fr} = \frac{p_s \sin \phi}{2\sqrt{I_{2D}}}$	(Schaeffer, 1987)
Bulk viscosity	$\lambda_s = \frac{4}{3} \alpha_s^2 \rho_s d_s g_{O,ss} (1 + e_{ss}) \sqrt{\frac{\Theta_s}{\pi}}$	(Lun et al., 1984)
Granular conductivity	$k_{\Theta_s} = \frac{15d_s \rho_s \alpha_s \sqrt{\Theta_s \pi}}{4(41 - 33\eta)} \left[ 1 + \frac{12}{5} \eta^2 (4\eta - 3) \alpha_s g_{O,ss} + \frac{16}{15\pi} (41 - 33\eta) \eta \alpha_s g_{O,ss} \right]$	(Syamlal et al., 1993)
	$\eta = \frac{1}{2} (1 + e_{ss})$	
Collisional dissipation of energy	$\gamma_{\Theta_s} = \frac{12(1 - e_{ss}^2) g_{O,ss}}{d_s \sqrt{\pi}} \rho_s \alpha_s^2 \Theta_s^{3/2}$	(Lun et al., 1984)

The granular temperature of the solid phase near the wall is calculated based on the correlation by Johnson and Jackson (1987):

$$q_{w,\theta_s} + \frac{\pi\rho_p u_{slip}^2 \psi \sqrt{\theta_s}}{2\sqrt{3} \left( \frac{\alpha_{s,max}}{\alpha_s} - \frac{\alpha_{s,max}^{2/3}}{\alpha_s^{2/3}} \right)} - \frac{\sqrt{3}\pi\rho_p (1-e_{sw}^2) \theta_s^{3/2}}{4 \left( \frac{\alpha_{s,max}}{\alpha_s} - \frac{\alpha_{s,max}^{2/3}}{\alpha_s^{2/3}} \right)} = 0. \quad (13)$$

where  $u_{slip}$  and  $q_{w,\theta_s}$  are the slip velocity and the flux of fluctuation energy within the solids flow approaching the wall.

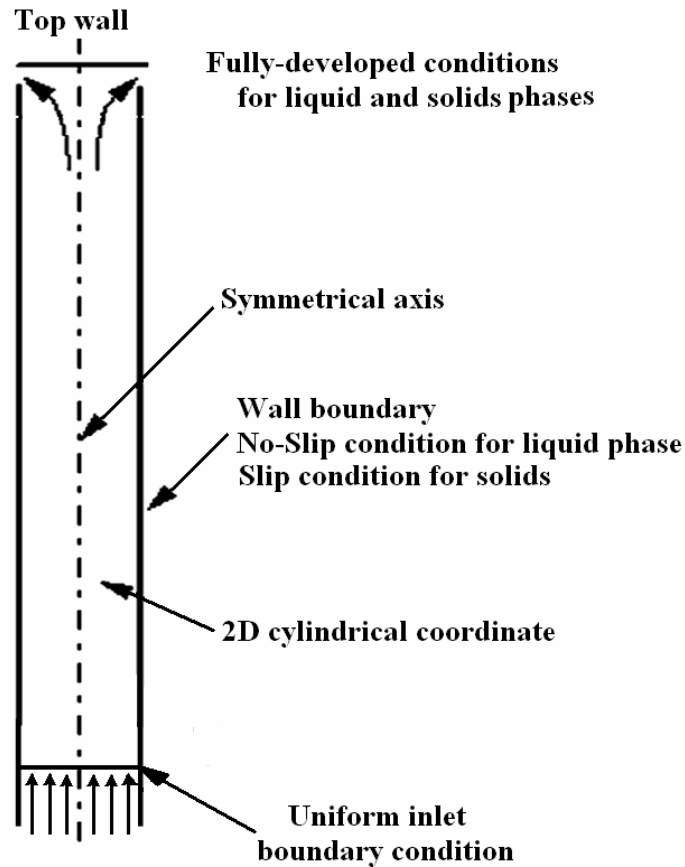


Figure 2.2: The computational domain in the LSCFB riser.

The standard  $k-\varepsilon$  model used for the liquid phase or mixture is only applicable for high Reynolds flow. Therefore, the viscosity-affected near-wall region at which Re number is low is resolved by a near-wall model. In this study, the two-layer approach is used as a near-wall model to calculate the velocity, turbulence energy dissipation and the turbulent viscosity of the liquid phase or mixture in the near-wall region. Fully-developed flow condition is used for all flow quantities at the outlet of the riser. The flow is assumed to be axisymmetric to reduce computational cost.

## 2.4 Numerical methodology

The commercial software, ICEM CFD, Ansys 13.0, is used to create the riser geometry and then generate the mesh. The governing equations are then solved by the commercial CFD code FLUENT, Ansys 13.0. The convection terms and gradients in all transport equations are discretized by the second order upwind method and green-gauss cell based method, respectively. The SIMPLE algorithm using a segregated solution technique is used to solve the pressure field and velocity field. The mesh independence is examined using three different grids,  $25 \times 2500$ ,  $30 \times 3000$  and  $35 \times 3500$ . The radial distributions of the solid holdup at the height of 2.5 m obtained by these three grids are compared. The result from  $30 \times 3000$  grid deviates less than 0.5% from the one using the finer mesh. Therefore, this mesh is used in the rest of simulations in this study. The time step independence test shows that the time step of 0.005 sec can satisfy the time step independency. The specular coefficient ( $\phi$ ), restitution coefficient of interparticle collisions and restitution coefficient of particle-wall collisions are 0.0001, 0.99 and 0.99, respectively.

## 2.5 Results and Discussion

The numerical model presented in this study is used to predict the flow field in the LSCFB riser. The effect of turbulence models on the numerical simulation of the liquid-solid turbulent flow is examined by comparing the numerical results with available experimental data (Zheng et al., 2002 and 2003). Also, the effects of the liquid superficial velocity ( $U_l$ ) and solids circulation rate ( $G_s$ ) on the hydrodynamic characteristics of the



LSCFB riser are investigated. In addition, the residence time distributions (RTD) of both liquid and solid phases are determined under one of the operating conditions.

### 2.5.1 The effect of turbulence models

In order to investigate the influence of turbulence models on the numerical results of the turbulent liquid-solid flow in an LSCFB, simulations are performed using three different types of  $k-\varepsilon$  multiphase turbulence models, the mixture turbulence model, dispersed turbulence model and per-phase turbulence model. The comparison between the numerical results using three different turbulence models and experimental data for the radial liquid velocity profiles is shown in Fig. 2.3 under  $U_l=0.1$  m/sec and  $G_s=5$  kg/m<sup>2</sup>sec at  $H=0.8$  m above the inlet distributor of the riser.

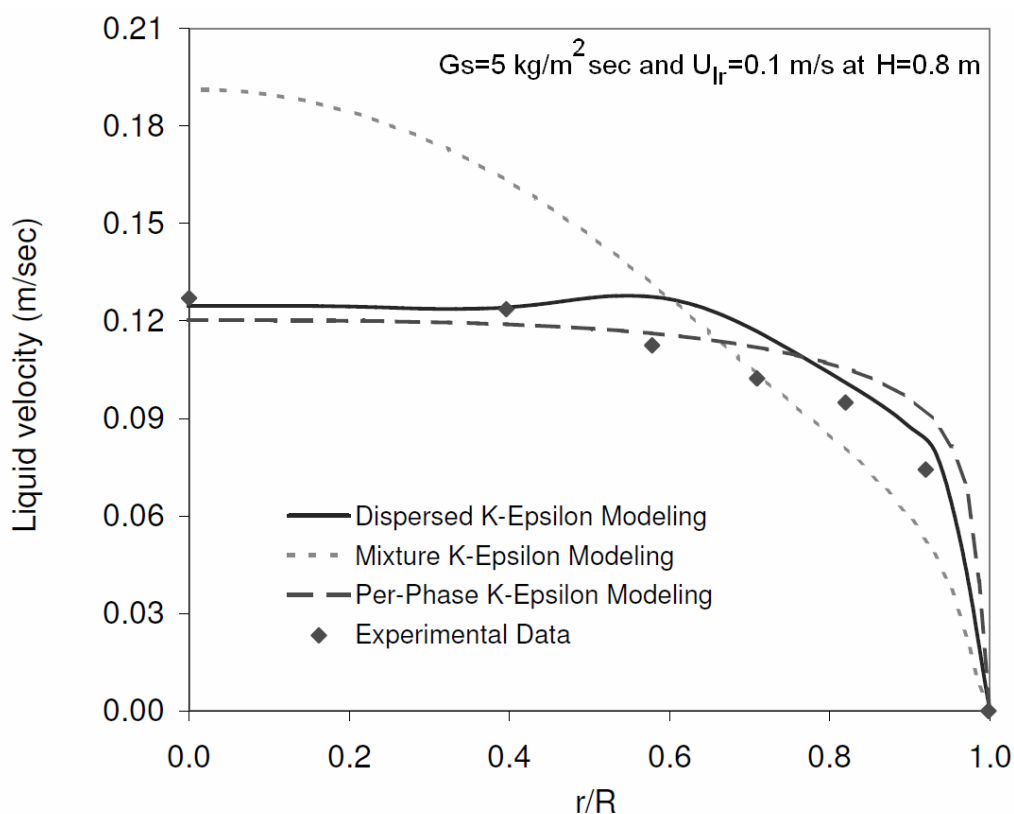


**Figure 2.3: Comparison of the liquid velocity profile using three types of the  $k-\varepsilon$  multiphase turbulence models (Experimental data by Zheng et al. (2003)).**

It can be seen that the predictions using the dispersed and per-phase  $k-\varepsilon$  models are in good agreements with the experimental data obtained by Zheng et al. (2003). In contrast, the mixture  $k-\varepsilon$  model is not an appropriate model for the turbulent two phase flow in a LSCFB, when the density ratio between the two phases is much higher than 1.

The comparison of the numerical prediction for the radial solids holdup profiles with the experimental data is shown in Fig. 2.4. It is seen that there is a slight difference among the solids holdup predictions using three different  $k-\varepsilon$  multiphase models.

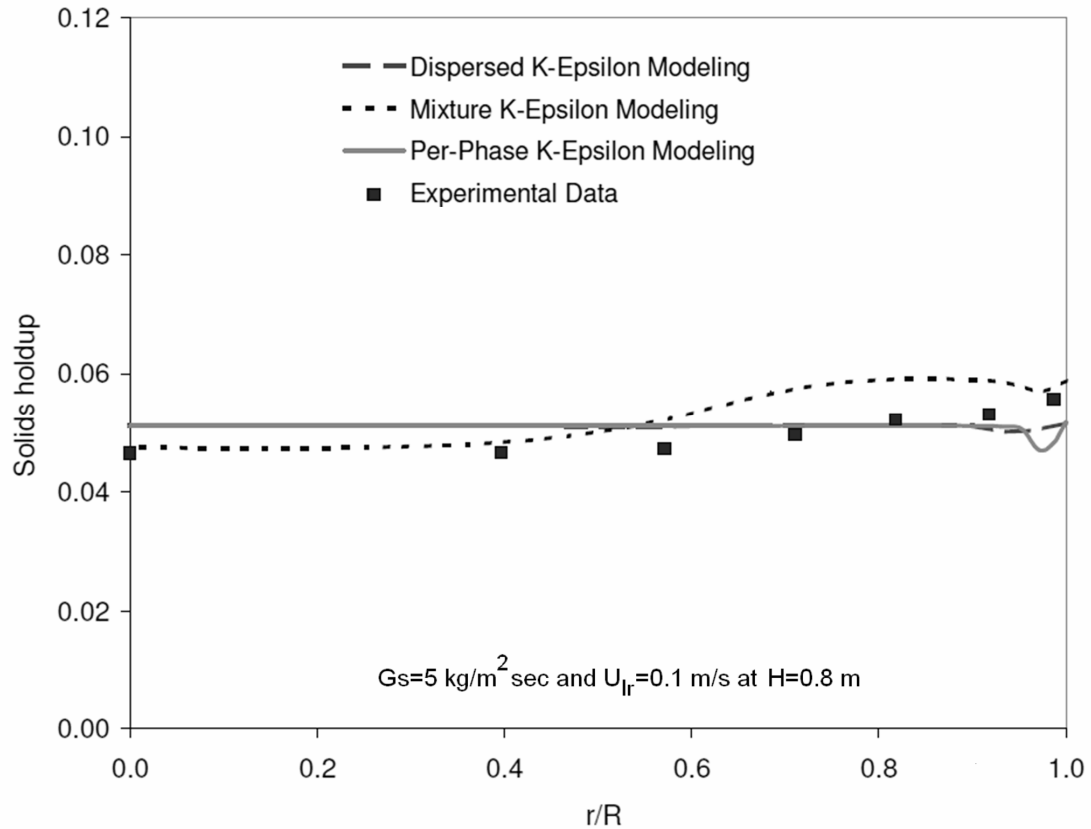


**Figure 2.4: Comparison of the solids holdup profile using three types of  $k-\varepsilon$  multiphase turbulence models (Experimental data by Zheng et al. (2002)).**

Since the dispersed  $k-\varepsilon$  model is computationally less expensive and predicted hydrodynamic quantities equally well as the per-phase turbulence model, it is used for the rest of the simulations in this work.

## 2.5.2 Effect of liquid superficial velocity

In Fig. 2.5, the predicted liquid velocities for  $G_s = 5 \text{ kg/m}^2\text{sec}$  are compared with the experimental data under different liquid superficial velocities.

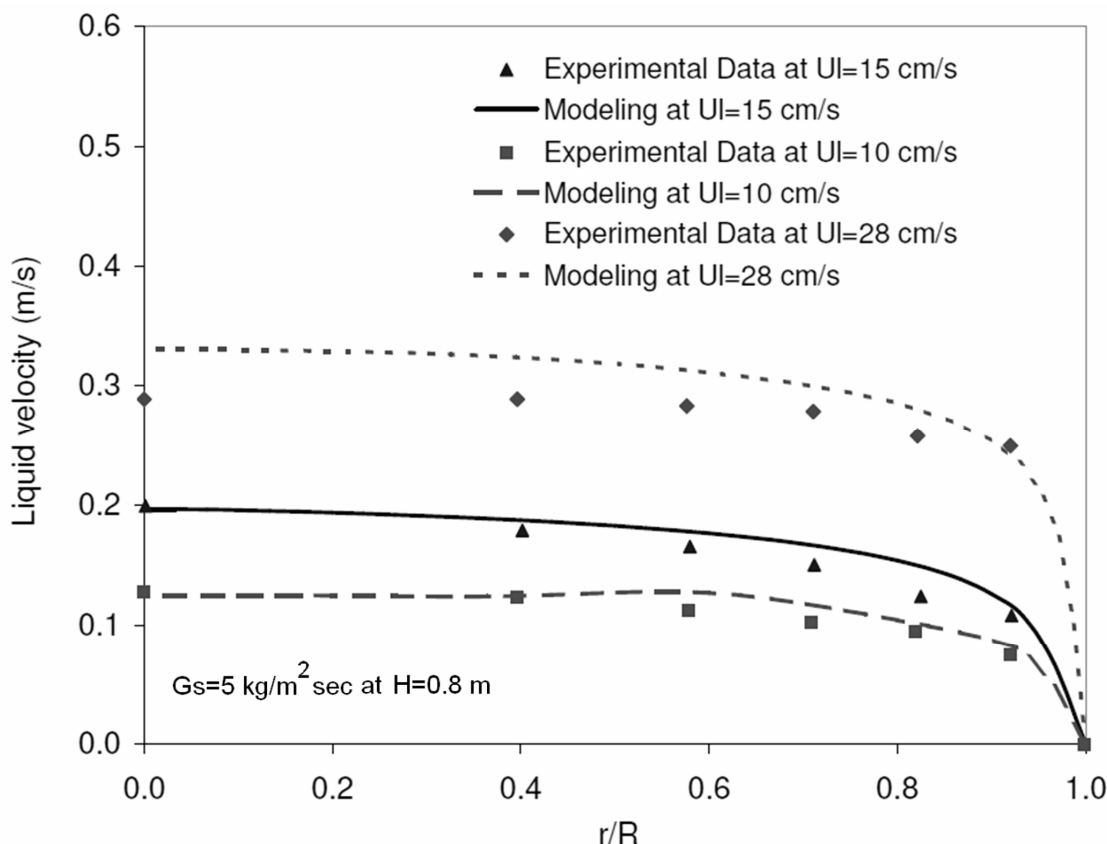


**Figure 2.5: Comparison of the radial distributions of the liquid velocity under different liquid superficial velocities (Experimental data by Zheng et al. (2003)).**

It is illustrated that the numerical predictions for the liquid velocity agree favorably with the experimental data. The difference between the CFD results and the experimental data is below 8.5 %. Also, the radial non-uniformity for the liquid velocity is seen, especially at  $U_l = 15 \text{ cm/s}$ . However, the radial distribution of the liquid velocity in a conventional fluidized bed system is fully-uniform (Zheng et al., 2003).

Fig. 2.6 shows the comparison of the numerical results with the experimental data for the radial distributions of the solids holdup for  $G_s = 5 \text{ kg/m}^2\text{sec}$  under different liquid

velocities. It is shown that the simulation predictions are in an acceptable agreement with the experimental data by Zheng et al. (2002). Furthermore, it is seen that the increase in the liquid superficial velocity decreases the average cross-sectional solids holdup under the same solids circulation rate. That is because the slip velocity between the two phases increases with the increase in the liquid superficial velocity, which results in an increase in the drag force. Therefore, solids particle velocity increases and solids holdup decreases.

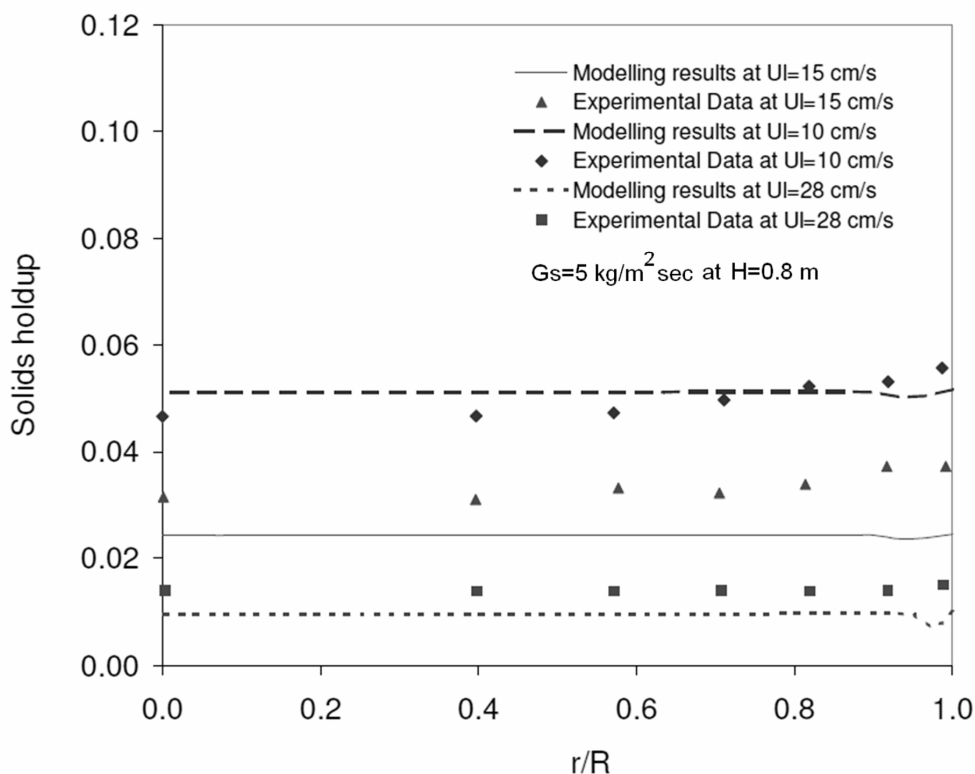


**Figure 2.6: Comparison of the radial distributions of the solid holdup under different liquid superficial velocities (Experimental data by Zheng et al. (2002)).**

### 2.5.3 Effect of solids circulation rate

The comparison of the numerical predictions and experimental data for the radial distributions of the solids holdup in the LSCFB under different solids circulation rates at  $H=0.8$  m above the distributor is plotted in Fig. 2.7. It shows that the CFD predictions favorably agree with the experimental data by Zheng et al. (2002). It is clearly seen that

the increase in the solids circulation rate results in an increase in the average solids holdup for the same liquid superficial velocity since the increase in the solids circulation rate (in terms of the superficial solids velocity) increases the amount of solid particles fed into the system. Therefore, the average solids holdup increases in the riser.

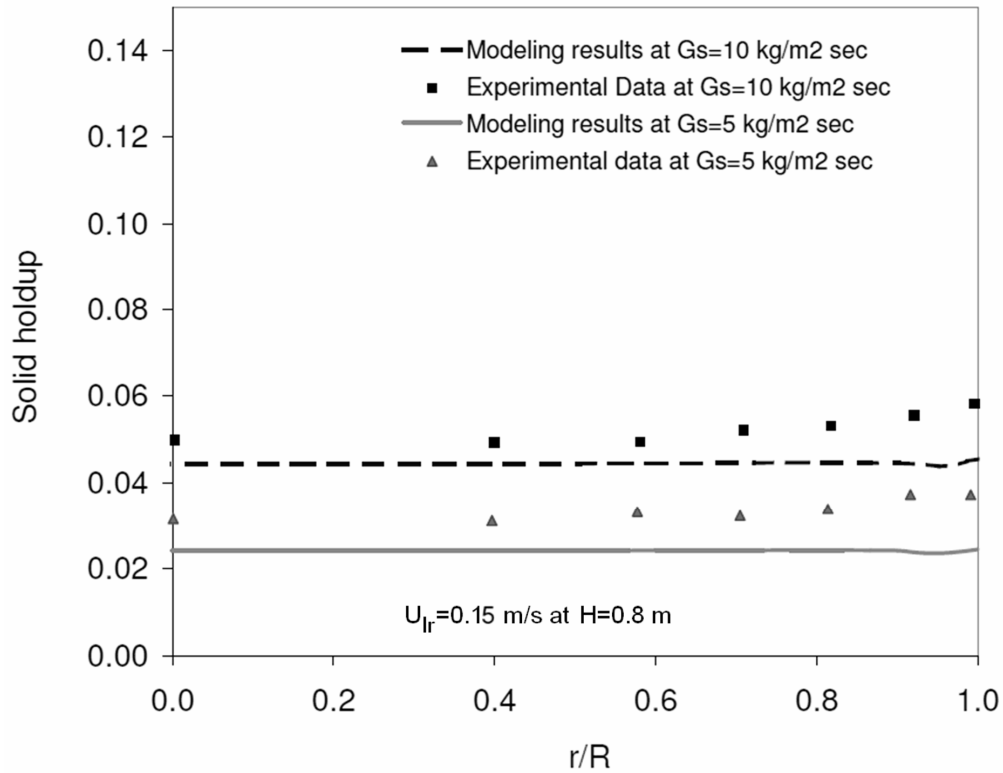


**Figure 2.7: The radial distributions of the solid holdup under different solids circulation rates (Experimental data by Zheng et al. (2002)).**

#### 2.5.4 Residence time distribution

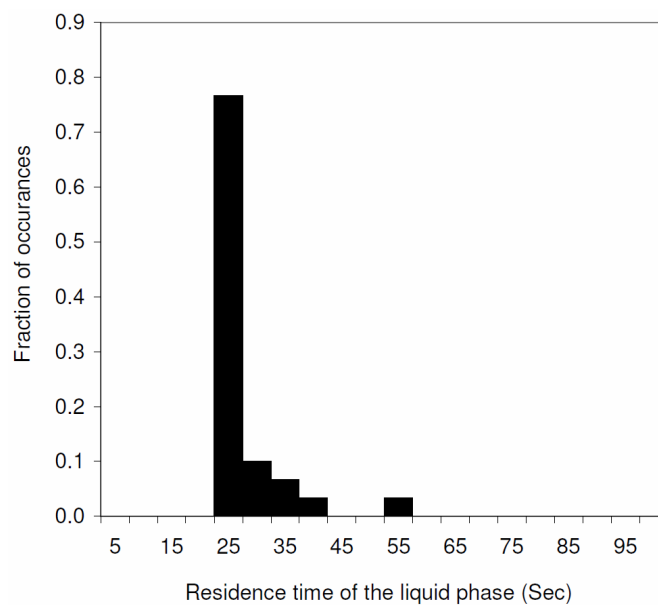
The global dispersion and the residence time distributions (RTDs) for both phases can be estimated using the CFD results and applying the pulse technique (FLUENT User's Guide, 2013). Since the transient CFD simulation reached an invariant state, the final steady-state field is utilized for the calculation of the phasic RTDs. With the pulse technique, tracers with the same physical properties as the solid particles are defined and injected at the inlet boundary of the flow field. After the calculations of the momentum equations are turned off, by solving the Lagrangian equations for each tracer, their

location versus time and the RTD of solid phase can be predicted. However, because only the final steady-state flow field has been used, the micro-mixing effects are neglected in this mathematical method. To obtain the RTD of liquid phase by the pulse technique, massless particles are injected at the inlet boundary of the riser and then particle positions are computed in the entire computational domain by generating pathlines.

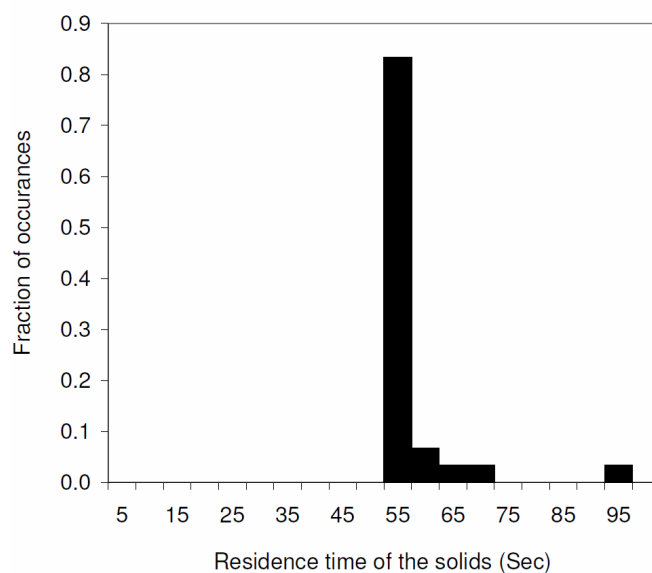
Fig. 2.8 shows the predicted RTD curves for the solids and liquid phases at  $U_l = 10$  cm/s and  $G_s = 5$  kg/m<sup>2</sup>s. Clearly, the liquid and solids flow patterns are very close to the plug flow. Moreover, the average residence times for the liquid and solid phases are 24.8 and 55.6 seconds, respectively. This is because that the solids (glass) density is higher than the liquid (water) density.

The predicted RTD curves for the solids and liquid phases are shown in Fig. 2.9 under  $U_l = 15$  cm/s and  $G_s = 5$  kg/m<sup>2</sup>s. It is seen that the liquid and solids flow patterns are close to the plug flow similar to the case shown in Fig. 2.8 for  $U_l = 10$  cm/s. In addition, the average residence times for the liquid and solid phases are 17.7 and 30.8 seconds, respectively. Also, Figs. 2.8 and 2.9 demonstrate that the increase in the liquid superficial velocity results in the increase of the solids dispersion and the decrease of the dispersion of liquid stream.

In summary, the axisymmetric CFD model for the simulation of the liquid-solid turbulent flows in a riser is able to provide the detailed information, such as local phasic velocity and volume fraction, and resistance time distributions in the riser, which is useful for the riser design.

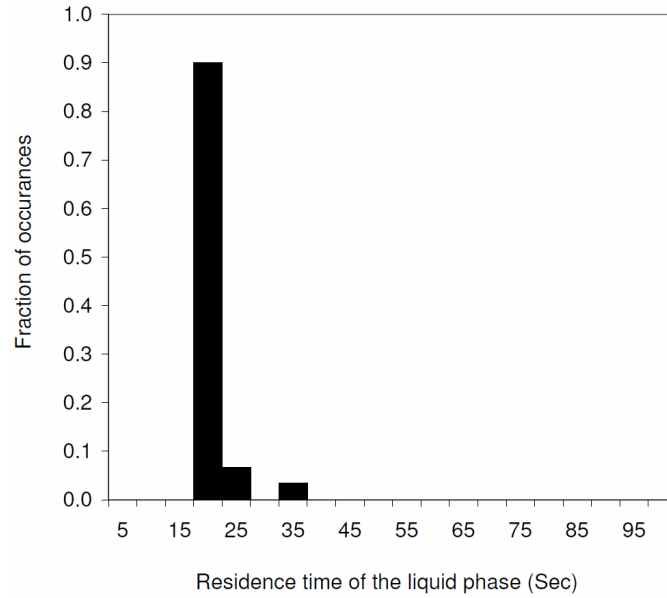


(a)

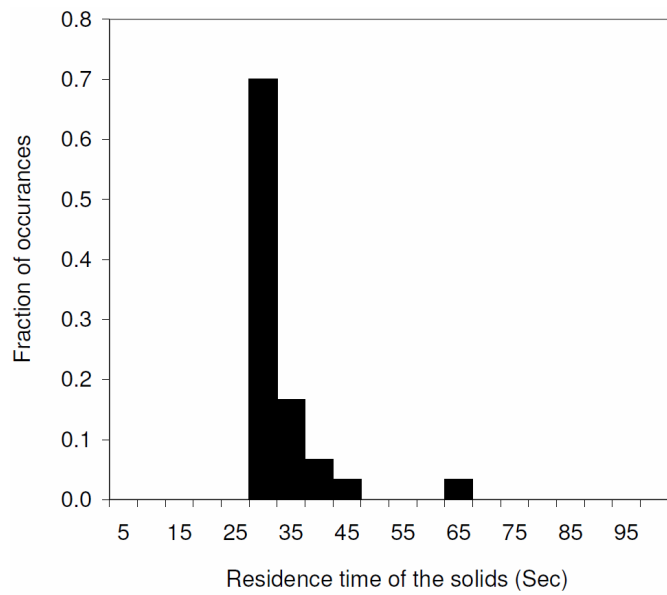


(b)

**Figure 2.8: The residence time distributions of (a) the liquid phase and (b) the solid phase at  $G_s=5 \text{ kg/m}^2\text{sec}$  and  $U_l=10 \text{ cm/s}$ .**



(a)



(b)

**Figure 2.9: The residence time distributions of (a) the liquid phase and (b) the solid phase at  $G_s=5 \text{ kg/m}^2\text{sec}$  and  $U_l=15 \text{ cm/s}$ .**

## 2.6 Conclusions

The CFD model was proposed to provide qualitative and quantitative pictures of the turbulent two phase flows in an LSCFB riser. Three different types of  $k-\epsilon$  multiphase



turbulence models were examined in this work and it was found that the dispersed  $k-\varepsilon$  turbulence model is more efficient than other ones because of the lower computational time and higher accuracy. Comparisons of the predicted liquid velocity profiles and solids holdup profiles are in a good agreement with the experimental data. It was found that the non-uniformity of liquid velocity distribution in the LSCFB is higher than that in a conventional liquid-solid fluidized bed. In addition, it was shown that the increase in the liquid superficial velocity decreases the average cross-sectional solids holdup under the same solids circulation rate in the LSCFB. Furthermore, in order to observe the global dispersion, the CFD model was adapted to predict the solids and liquid RTDs. This implies that the model can be used for the scale-up and design of the real industrial-scale reactors.

## References

- Atta, A., Razzak, S. A., Nigam, K. D. P., & Zhu, J. X. (2009). (Gas)-Liquid-Solid Circulating Fluidized Bed Reactors: Characteristics and Applications. *Ind. Eng. Chem. Res.*, 48, 7876–7892.
- Ding, J., & Gidaspow, D. (1990). A bubbling fluidization model using kinetic theory of granular flow. *AIChE Journal*, 36 (4), 523–538.
- Doroodchi, E., Galvin, K. P., & Fletcher, D. F. (2005). The influence of inclined plates on expansion behaviour of solid suspensions in a liquid fluidized bed-a computational fluid dynamics study. *Powder Technology*, 156, 1–7.
- Gidaspow, D. (1994). *Multiphase Flow and Fluidization: Continuum and Kinetic Theory Descriptions*. Boston: Academic Press.
- Johnson, P. C., & Jackson, R. (1987). Frictional-Collisional Constitutive Relations for Granular Materials with Application to Plane Shearing, Sheared in an Annular Cell. *J. Fluid Mech.*, 176, 67-93.
- Lettieri, P., Di Felice, R., Pacciani, R., & Owoyemi, O. (2006). CFD modelling of liquid fluidized beds in slugging mode. *Powder Technology*, 167, 94–103.
- Lun, C. K. K., Savage, S. B., Jeffrey, D. J., & Chepurniy, N. (1984). Kinetic theories for granular flow: inelastic particle in Couette flow and slightly inelastic particles in a general flow field. *J. Fluid Mechanics*, 140, 223–256.
- Razzak, S. A., Barghi, S., & Zhu, J. X. (2009). Application of electrical resistance tomography on liquid–solid two-phase flow characterization in an LSCFB riser. *Chemical Engineering Science* J., 64, 2851-2858.
- Roy, S., & Dudukovic, M. P. (2001). Flow Mapping and Modeling of Liquid-Solid Risers. *Ind. Eng. Chem. Res.*, 40, 5440-5454.

- Schaeffer, D. G. (1987). Instability in the evolution equations describing incompressible granular flow. *J. Differential Equations*, 66, 19–50.
- Shi, D. P., Luo, Z. H., & Zheng, Z. W. (2010). Numerical simulation of liquid-solid two-phase flow in a tubular loop polymerization reactor. *Powder Technology J.*, 198, 135-143.
- Sinclair, J. L., & Jackson, R. (1989). Gas-particle flow in a vertical pipe with particle-particle interactions. *AIChE Journal*, 35(9), 1473-1486.
- Syamlal, M., Rogers, W., & O'Brien, T. J. (1993). *MFIX Documentation: Theory Guide*. National Technical Information Service, vol. 1. DOE/METC-9411004, NTIS/DE9400087.VA: Springfield.
- Wen, C. Y., & Yu, Y. H. (1966). Mechanics of fluidization. *Chemical Engineering Progress Symposium Series*, 62, 100-111.
- Zheng, Y., & Zhu, J. X. (2003). Radial distribution of liquid velocity in a liquid-solids circulating fluidized bed. *Int J Chem Reactor Eng*, 1, 1-7.
- Zheng, Y., Zhu, J. X., Marwaha, N., & Bassi, A. S. (2002). Radial solid flow structure in a liquid-solid circulating fluidized bed. *Chem Eng J*, 88, 141–150.
- Zheng, Y., Zhu, J. X., Wen, J., Martin, S., Bassi, A. S., & Margaritis, A. (1999). The axial hydrodynamic behavior in a Liquid-Solid Circulating Fluidized Bed. *Can. J. Chem. Eng.*, 77, 284-290.

## Chapter 3

### 3. CFD modeling of continuous protein extraction process using liquid-solid circulating fluidized beds\*

#### 3.1 Introduction

The extraction of functional proteins from industrial broth has been of intensive interest during the recent years, due to concerns on limitations of the natural resources (Lan, 2001). Significant improvement in protein separation technology plays a crucial role in achieving the commercial success. The traditional procedure to extract proteins from biological broth has been using a series of individual separation steps. Different mechanisms have been used to achieve this purpose, such as centrifugation techniques, ultra-filtration, ion-exchange process, hydrophobic interaction chromatography, and a number of other processes of varying degree of selectivity (Lan et al. 2002).

The ion exchange process using the conventional fluidized bed has shown a potential for the protein extraction (Byers et al., 1997; Gordon et al., 1990; Higgins, 1969; Himsley, 1981). It has been found out that the conventional beds have some benefits such as the low and stable bed pressure drop and the direct application of unclarified whole broth feed.

As reviewed by Zhu et al. (2000), in addition to all advantages of the conventional fluidized beds, circulating fluidized beds (CFBs) have many unique features including continuous operation with adsorption and desorption carried out simultaneously, high throughput due to high liquid velocity in the riser, highly efficient liquid-solid contact, favorable mass and heat transfer, maintaining the nearly plug flow condition in the riser which reduced back-mixing of phases and integrated reactor and smaller processing volumes. To take advantage of the exceptional characteristics of CFBs, Lan et al. (2000) developed a liquid–solid circulating fluidized bed (LSCFB) ion-exchange system for

---

\* This manuscript has been accepted by Canadian Journal of Chemical Engineering for publication.

continuous extraction of protein. Generally speaking, an LSCFB is comprised of a riser, a downcomer, a liquid-solid separator and other auxiliary components. The downcomer is assigned for protein adsorption and the riser is designed as a stripper to desorb the protein and to regenerate the particles. Proteins are thus adsorbed onto the ion exchange particles in the downcomer and the loaded-particles are regenerated simultaneously in the riser in a continuous mode. The operating conditions in the two columns of an LSCFB system could be controlled independently with the liquid flow rate and the solids circulating rate between the two columns.

A number of models have been developed to describe the protein adsorption and desorption behaviors in packed beds, conventional fluidized beds and circulating fluidized beds with various types of approximations to the physical reality. Several steps are involved in the process of adsorption of proteins onto the adsorbent particles: (1) convective and diffusion mass transfer from the liquid phase to the adsorbent surface, (2) diffusion through the pore of the ion exchange particles and (3) the surface reactions. The surface adsorption reaction is sufficiently rapid compared to the first two steps and is not usually considered as a limiting step (Mazumder et al., 2009). Veeraraghavan et al. (1989) developed a model for adsorption of phenol onto granular activated carbon in a liquid-solid fluidized bed considering liquid and solid phase axial dispersion, film mass transfer resistance and pore diffusion. Wright and Galsser (2001) developed a similar model for the adsorption of proteins in a fluidized bed and studied the effect of operating parameters on the adsorption performance. Later on, Ping et al. (2005) and Junxian et al. (2005) modeled the protein adsorption in a conventional fluidized bed and they considered axial distribution of particles size and axial variations of bed voidage. Lan et al. (2000) developed a model for continuous protein recovery in LSCFB ion-exchange systems assuming the process is not surface reaction limited. However, detailed hydrodynamics of the LSCFB was not included in their model. Recently, Gaikwad et al. (2008) developed another model on adsorption in an LSCFB considering the film mass transfer resistance as the limiting step. Their model included only the adsorption in the downcomer whereas the protein desorption process was not considered. In order to simplify the physical reality, the detailed hydrodynamics of the LSCFB was not included in all above-mentioned models and they assumed that the distributions of the solid holdup

( $\epsilon_s$ ), solids velocity ( $U_s$ ) and liquid velocity ( $U_l$ ) are uniform throughout both the riser and the downcomer. In contrast, experimental data clearly demonstrated that both axial and radial distributions of hydrodynamic properties are not uniform along the riser of an LSCFB (Liang et al., 1997, Razzak et al., 2009). In recent decades, computational fluid dynamics (CFD) techniques have received many attentions in simulating the transport phenomena in fluidized bed reactor; however, most past studies focused on using CFD method for gas-solid fluidized bed reactors and less attention has been paid to the CFD modeling of the liquid-solid fluidized bed reactors (Shi, 2010).

The purpose of this study is to develop a sophisticated numerical model to simulate the protein extraction process using an LSCFB ion-exchange system. This model will take into account a more accurate study on the nature of this system including hydrodynamics, mass transfer and kinetics. The simulation of the desorption process in the LSCFD riser is based on Eulerian-Eulerian (E-E) approach incorporating the kinetic theory of granular flow. A two-dimensional axisymmetric CFD model is applied to capture the detailed information about the local values of volume fraction, velocity and protein concentration of both the liquid stream and the solid particles in the riser. In addition, the adsorption process in the LSCFB downcomer is simulated by a one-dimensional mathematical model using the adsorption kinetics correlations developed by Lan et al. (2000).

## 3.2 Experimental setup of the LSCFB system

In one of our earlier work, Lan et al. (2000) has conducted an experimental study on the protein extraction process. In that study, an LSCFB ion exchange system was designed and manufactured in a lab scale. This system was able to carry out protein extraction from model broth. The main components of this system will be explained in the following section, and also all materials and kinetics of ion exchange process will be summarized.

### 3.2.1 Apparatus

The schematic of the LSCFB ion exchange system used by Lan et al. (2000) is shown in Figure 3.1. The major components of the LSCFB extractor include a riser, a downcomer,

a liquid-solid separator, a top solids-return pipe, a bottom solids-return pipe, a top washing section, a bottom washing section, a riser distributor and a downcomer distributor. The riser is 3.0 m in height and 0.038 m in diameter, and the downcomer is 2.5 m in height and 0.120 m in diameter.

Two different types of liquid streams are used to fluidize the particles in the riser and downcomer. The liquid velocity in the riser is higher than the terminal velocity of the particles; therefore, the particles can be entrained up along the riser. However, the liquid velocity in the downcomer is less than the terminal velocity of the particles, so particles can flow down from the top of downcomer. As a result, the particles are able to circulate between the two columns.

The distributor for the downcomer is a tubular ring that is carefully designed in order to have a uniform liquid distribution while allowing the solids to flow down. The riser distributor divides the incoming stream into two substreams: the primary and auxiliary streams. The primary stream enters through a tubing of 1.1 cm in ID extending 5.1 cm into the riser. The outlet of the primary stream was located above the solids entrance at the bottom of the riser. Also, the auxiliary stream is introduced through a perforated plate at the bottom of the riser. The particles at the bottom are mobilized by the auxiliary stream, and then the particles are entrained up along the riser by the combination of the primary and auxiliary streams.

The dynamic seals between the riser and downcomer are achieved by maintaining the two solids return pipes in the moving packed-bed regime. The top wash section and the bottom wash section clean the particles before they entering the solids return pipes to avoid penetrating liquid solution from one column to another.

The solids circulation rate is controlled by a butterfly valve installed on the bottom solids return pipe. The solids circulation rate was measured by a device which is installed at the top on downcomer and made of a central vertical plate and two half butterfly valves.

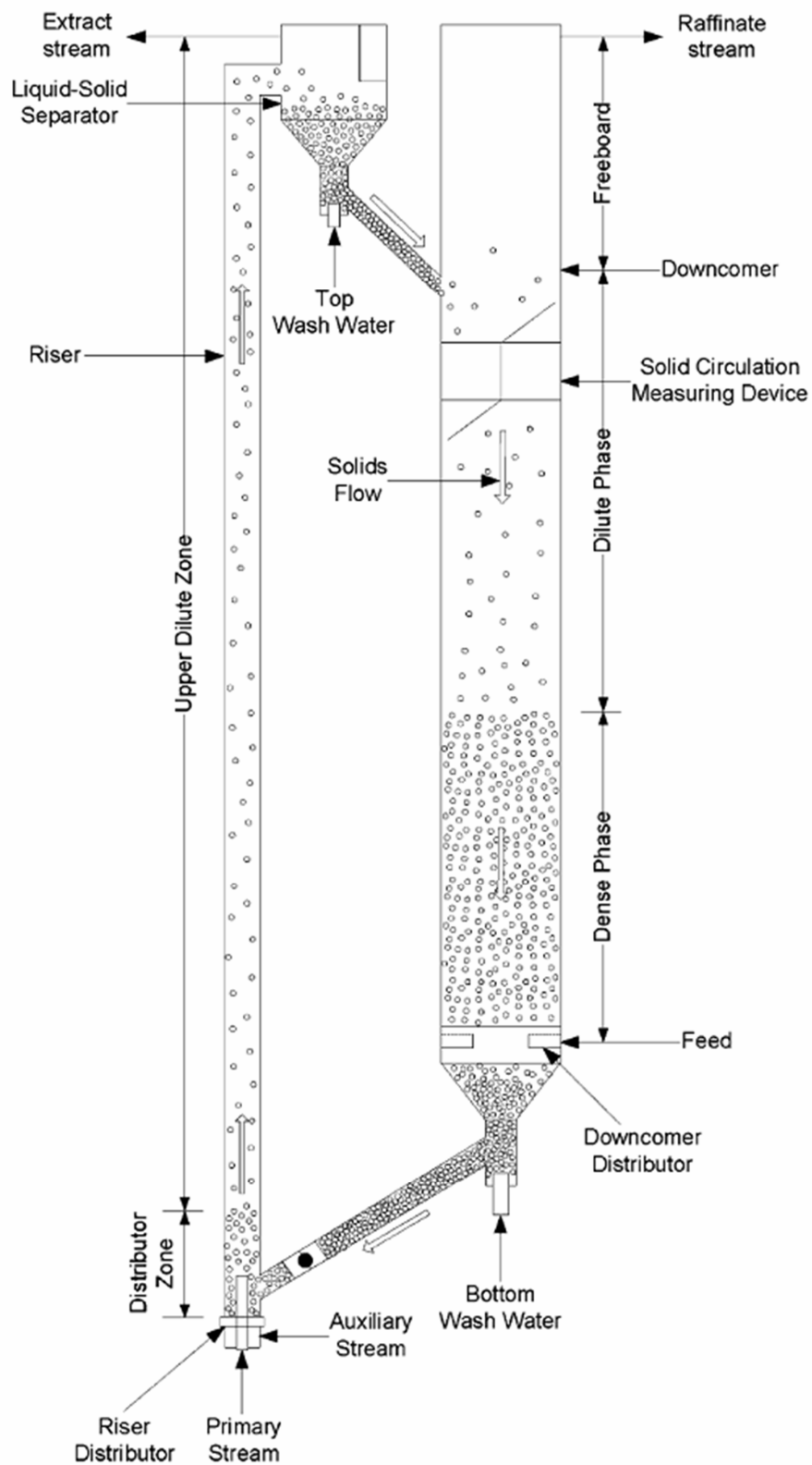


Figure 3.1: Schematic diagram of the LSCFB ion-exchange system Lan et al. (2000).



### 3.2.2 Materials

Bovine serum albumin (BSA) was used as model protein and continuous recovery of BSA solution in the LSCFB ion exchange system was conducted with the BSA solution as feed in the downcomer and 0.4 M NaCl solution as the extracting buffer in the riser. Diaion HPA25 particles were used as ion-exchange particles for all BSA adsorption-desorption studies. The properties of Diaion HPA25 particles are listed in Table 3.1.

**Table 3.1: Properties of Diaion HPA25 ion-exchange particles (Lan et al. 2002).**

Matrix	Polystyrene Žhighly porous.
Functional group	Quaternary alkylamine
Ionic form	$\text{Cl}^-$
Average diameter ( $d_p$ , mm)	0.32
apparent density, ( $\rho_w$ , $\text{kg/m}^3$ )	1080
Total exchange capacity $\text{Cl}^-$ , meq/mL)	0.6
Terminal velocity ( $U_t$ , mm/s)	4.5
Bed expansion index ( $n$ )	2.67
BSA adsorption capacity ( $q_m$ , $\text{kg/m}^3$ )	87.9

### 3.2.3 Kinetics of Ion Exchange mechanism in the LSCFB System

For a continuous ion-exchange process in the LSCFB, the BSA solution as the feed protein is entered from the bottom of the downcomer, while the ion exchange particles are introduced from the top solids return pipe into the top of the downcomer. Since liquid velocity in the downcomer is maintained lower than the terminal velocity of the ion-exchange particles, the ion-exchange particles move down countercurrent to the rising feed liquid. Because of the excellent contact between the particles and feed liquid in the downcomer, the BSA protein in the feed is adsorbed onto the ion exchange particles and then the deproteinized solution is discarded from the top of the downcomer. The loaded

particles are then transferred to the bottom of the riser through the bottom solids return pipe after washing.

The extracting buffer (0.4 M NaCl solution), the combination of the primary and auxiliary streams, is entered from the bottom of the riser. The superficial velocity of the extracting buffer ( $U_{lr}$ ) is kept higher than the terminal velocity of the ion exchange particles; therefore, the loaded particles are carried upward along the riser while the BSA protein is desorbed and the ion exchange particles are regenerated. Then, the regenerated particles are returned to the top of the downcomer through the top solids return pipe after washing.

### 3.3 Mathematical modeling

#### 3.3.1 CFD modeling of flow field and mass transfer in the Riser

Since the liquid phase velocity in the riser is higher than the terminal velocity of the ion exchange particles, the riser is operated under the circulating fluidization regime. The CFD model used in this study takes into account the effects of the hydrodynamics and mass transfer on the protein extractions in the riser.

Generally, there are two approaches to model two-phase flows: Eulerian-Lagrangian (E-L) approach and Eulerian-Eulerian (E-E) approach. In the E-L approach, the liquid phase is considered as a continuous phase and Navier–Stokes (N-S) equations are solved for it. The solid phase is treated as a discrete phase and each solid particle is tracked by solving the Lagrangian force balance equation. However, the main drawback of this approach is that a high computational cost is required to solve the dense two-phase flow. In the E-E approach, also well known as two-fluid model, each phase is treated as an interpenetrating continuum and the concept of phase volume fraction is introduced. The conservation equations of mass, momentum, and chemical species for both the particulate and the fluid phases are solved.

In the current work, the two phase flow in the riser of the LSCFB is modeled by E-E approach. The conservation of the mass, momentum and mass transfer between the

phases provide the governing equations for the liquid and solid phases. The governing equations for the solid phase have similar structure to those for the liquid phase. However, in order to close the pseudo N-S equation for the solid phase, the viscosity, pressure and stresses of the solid phase are modeled by the kinetic theory of granular phase (KTGP), which has been widely applied for particulate flows (Sinclair and Jackson, 1989; Gidaspow, 1994). In this theory, the mean square of the random particle velocity is defined as the granular temperature ( $\theta$ ). Thus the solids viscosity and the solids stress are a function of this granular temperature, which varies with time and position in a fluidized bed.

The relevant equations for liquid-solid flows based on the kinetic theory of granular flow are listed in Table 3.2. The granular bulk viscosity which describes the resistance of an emulsion to compression or expansion is determined by the equation proposed by Lun et al. (1984). The viscosity of the solid phase comes from three sources: inter-particle collision, friction and kinetic energy of particles. The correlation by Gidaspow et al. (1990) is used for the collisional viscosity. Frictional viscosity is calculated by the expression of Schaeffer (1987), with an angle of internal friction of  $30^\circ$ . The kinetic portion of the granular viscosity and the granular conductivity are both obtained by the relationships from Syamlal et al. (1993). The radial distribution function of Ding and Gidaspow (1990) takes into account the probability of particles colliding with each other. External body, lift and virtual mass forces are neglected in the momentum equations. The momentum exchange between the liquid and solid phases is described by empirical the drag laws of Wen and Yu (1966). Since the protein desorption from the ion exchange particles is processed in riser. The mass transfer of protein species from ion-exchange particles to the liquid phase needs to be considered. The protein mass transfer rate of the protein species in the riser is calculated by the equation of Lan et al. (2000).

### 3.3.2 Hydrodynamics and mass transfer simulation in downcomer

In order to maintain stable operation, the liquid velocity in the downcomer must be kept less than the particle terminal velocity. Therefore, three distinctive zones are observed in

**Table 3.2: Governing equations for liquid-solid flows in the riser**

Continuity equation	$\frac{\partial}{\partial t}(\alpha_q \rho_q) + \nabla \cdot (\alpha_q \rho_q \vec{v}_q) = 0, \quad \sum_q \alpha_q = 1.$	
Momentum equations	$\frac{\partial}{\partial t}(\alpha_l \rho_l \vec{v}_l) + \nabla \cdot (\alpha_l \rho_l \vec{v}_l^2) = -\alpha_l \nabla p + \nabla \cdot \bar{\bar{\tau}}_l + \alpha_l \rho_l \vec{g} + K_{sl}(\vec{v}_s - \vec{v}_l),$ $\frac{\partial}{\partial t}(\alpha_s \rho_s \vec{v}_s) + \nabla \cdot (\alpha_s \rho_s \vec{v}_s^2) = -\alpha_s \nabla p + \nabla p_s + \nabla \cdot \bar{\bar{\tau}}_s + \alpha_s \rho_s \vec{g} + K_{ls}(\vec{v}_l - \vec{v}_s),$ $\bar{\bar{\tau}}_q = \alpha_q \mu_q (\nabla \cdot \vec{v}_q + \nabla \cdot \vec{v}_q^T) + \alpha_q \left( \lambda_q - \frac{2}{3} \mu_q \right) \nabla \cdot \vec{v}_q \bar{\bar{I}}.$	
Liquid solid drag	$K_{sl} = \frac{3}{4} C_D \frac{\alpha_s \alpha_l \rho_l  \vec{v}_s - \vec{v}_l }{d_s} \alpha_l^{-2.65},$ $C_D = \frac{24}{\alpha_l \text{Re}_s} \left[ 1 + 0.15 (\alpha_l \text{Re}_s)^{0.687} \right], \quad \text{Re}_s = \frac{\rho_l d_s  \vec{v}_s - \vec{v}_l }{\mu_l}.$	(Wen and Yu, 1966)
Solids pressure	$P_s = \alpha_s \rho_s \Theta_s + 2 \rho_s (1 + e_{ss}) \alpha_s^2 g_{O,ss} \Theta_s$	(Lun et al., 1984)
Radial distribution function	$g_{O,ss} = \left[ 1 - \left( \frac{\alpha_s}{\alpha_{s,\max}} \right)^{1/3} \right]^{-1}$	(Ding and Gidaspow, 1990)
Solids shear stress	$\mu_s = \mu_{s,col} + \mu_{s,kin} + \mu_{s,fr}$ $\mu_{s,col} = \frac{4}{5} \alpha_s \rho_s d_s g_{O,ss} (1 + e_{ss}) \sqrt{\frac{\Theta_s}{\pi}}$ $\mu_{s,kin} = \frac{\alpha_s \rho_s d_s \sqrt{\Theta_s \pi}}{6(3 + e_{ss})} \left[ 1 + \frac{2}{5} (1 + e_{ss}) (3e_{ss} - 1) \alpha_s g_{O,ss} \right]$ $\mu_{s,fr} = \frac{\rho_s \sin \phi}{2 \sqrt{I_{2D}}}$	(Gidaspow et al., 1990) (Syamlal et al., 1993) (Schaeffer, 1987)
Bulk viscosity	$\lambda_s = \frac{4}{3} \alpha_s^2 \rho_s d_s g_{O,ss} (1 + e_{ss}) \sqrt{\frac{\Theta_s}{\pi}}$	(Lun et al., 1984)
Granular temperature	$\frac{3}{2} \left[ \frac{\partial}{\partial t} (\rho_s \alpha_s \Theta_s) + \nabla \cdot (\rho_s \alpha_s \vec{v}_s \Theta_s) \right] = (-p_s \bar{\bar{I}} + \bar{\bar{\tau}}_s) : \nabla \cdot \vec{v}_s + \nabla \cdot (k_{\Theta_s} \nabla \Theta_s) - \gamma_{\Theta_s} + \Phi_{ls}$	
Granular conductivity	$k_{\Theta_s} = \frac{15 d_s \rho_s \alpha_s \sqrt{\Theta_s \pi}}{4(41 - 33\eta)} \left[ 1 + \frac{12}{5} \eta^2 (4\eta - 3) \alpha_s g_{O,ss} + \frac{16}{15\pi} (41 - 33\eta) \eta \alpha_s g_{O,ss} \right]$ $\eta = \frac{1}{2} (1 + e_{ss})$	(Syamlal et al., 1993)
Collisional dissipation of energy	$\gamma_{\Theta_s} = \frac{12(1 - e_{ss}^2) g_{O,ss}}{d_s \sqrt{\pi}} \rho_s \alpha_s^2 \Theta_s^{3/2}$	(Lun et al., 1984)
Inter-phase Energy exchange	$\Phi_{ls} = -3 K_{ls} \Theta_s$	
Protein mass transfer equation	$\frac{\partial}{\partial t} (\alpha_q \rho_q Y_q^i) + \nabla \cdot (\alpha_q \rho_q \vec{v}_q Y_q^i) = D_{i,m} \nabla \cdot (\alpha_q \nabla Y_q^i) + \sum_{p=1}^2 (\dot{m}_{p^i q^j} - \dot{m}_{q^j p^i}),$ $\dot{m}_{s^i l^j} = -k_r \alpha_s \rho_s Y_s^i, \quad \dot{m}_{l^i s^j} = 0,$ $k_r = 0.045 \text{ (1/sec)}.$	(Lan et al., 2000)

the downcomer which have different solid holdups, the dense zone, the dilute zone, and the freeboard zone as shown in Figure 3.1.

It was observed that the solid holdup in the freeboard zone is zero and the solid holdup in the dilute zone is much lower than that in the dense zone. Therefore, the mass transfer of protein species from feed to ion exchange particle is neglected in the freeboard zone and dilute zone, and the mathematical model is only developed for the dense zone. Diaion HPA251 ion exchange particles are assumed to be uniform in size and spherical in shape. The riser and the downcomer are operated at steady state condition with the ion exchange particles continuously circulated between the two columns.

The dense zone in the downcomer operates as a conventional fluidized moving bed in which solids move downward and liquid moves upward. Thus, all hydrodynamic quantities such solids, liquid velocity and solid holdup in downcomer are assumed uniform. The bed voidage,  $\epsilon_d$ , can be described by an empirical correlation (Lan et al., 2000):

$$U_{ld} + U_{sd} \frac{\epsilon_d}{1 - \epsilon_d} = U_1 \epsilon_d^n \quad (1)$$

where,  $U_{ld}$  and  $U_{sd}$  are the superficial liquid and solids velocities, respectively,  $U_1$  is the superficial liquid velocity at the bed voidage  $\epsilon_d = 1$  and  $n$  is the bed expansion index.

The superficial solids velocity,  $U_{sd}$ , is given as:

$$U_{ld} = \frac{G_s}{\rho_s} \quad (2)$$

where  $G_s$  is the solids circulation rate between riser and down comer.

In order to derive the governing equations for the kinetics reactions in downcomer of the LSCFB ion exchange system, the following assumptions are considered: (a) The surface adsorption process is instantaneous and thus a local equilibrium is established at the particle surface between the protein concentration in the liquid–solid interface and the solid resin phase. The equilibrium is well represented by a Langmuir isotherm (Lan et al.,

2001); (b) The rate of adsorption is limited by the mass transfer resistance film surrounding an individual adsorbent particle and the intra-particle diffusional resistance; (c) The back mixing of the solids in the downcomer is negligible; and (d) The thermal effect is negligible, that is, the system operates at isothermal condition. Therefore, the protein transport in the liquid and solid phases can be described by following one-dimensional equations (Mazumder et al., 2009):

$$\varepsilon_d \frac{\partial C_d}{\partial t} + U_{ld} \frac{\partial C_d}{\partial Z} = \varepsilon_d D_{ax,l} \frac{\partial^2 C_d}{\partial Z^2} - K_L a (C_d - C_{eq})(1 - \varepsilon_d) \quad (3)$$

$$(1 - \varepsilon_d) \frac{\partial q_d}{\partial t} + U_{sd} \frac{\partial q_d}{\partial Z} = (1 - \varepsilon_d) D_{ax,s} \frac{\partial^2 q_d}{\partial Z^2} + K_L a (C_d - C_{eq})(1 - \varepsilon_d) \quad (4)$$

where,  $C_d$  and  $q_d$  are the protein concentration of the liquid phase and solid phase in the downcomer, respectively,  $Z$  is the axial distance from the bottom of the downcomer,  $D_{ax,l}$  and  $D_{ax,s}$  are axial dispersion coefficients of the liquid phase and solid phase, respectively,  $K_L$  is the lumped mass transfer rate coefficient,  $a$  is the specific surface area of the ion-exchange resins,  $C_{eq}$  is the liquid phase protein concentration at the liquid–solid interface which is in equilibrium with the solid phase. As mention before, the mass transfer rates of protein species in the freeboard and dilute zones are negligible.

Since the liquid velocity is very low, the fluidization in the downcomer can be considered as homogeneous. So, the effects of the liquid dispersion and solids back mixing are negligible. Again, the lumped mass transfer rate coefficient ( $K_L$ ) can be expressed as:

$$K_L = \psi k_f \quad (5)$$

where,  $k_f$  is the film mass transfer coefficient and  $\psi$  is a constant factor which includes the effect of intra-particle diffusion.

The equilibrium of the BSA adsorption on Diaion HPA251 ion exchange resin can be described by Langmuir Isotherm. Therefore, the equilibrium liquid phase protein concentration at the liquid–solid interface ( $C_{eq}$ ) can be expressed as:

$$C_{eq} = \frac{K_d q_d}{q_m - q_d} \quad (6)$$

where,  $q_m$  is the maximum adsorption capacity of the ion-exchange particles and  $K_d$  the dissociation constant. As the system always maintains a dynamic seal between the two columns, the feed solution cannot be mixed with the ion exchange particles in the bottom return pipe, thus, protein concentrations in the ion exchange particles are the same at both the bottom of the downcomer ( $q_{ed}$ ) and the inlet of the riser ( $q_{or}$ ).

### 3.3.3 Parameters of modeling

The mass transfer equations in the riser and downcomer include some coefficients which can be obtained by either individual experiments or available empirical correlations.

The correlation of Monkos (1996) is used to determine the viscosity and density of BSA solution. The film mass transfer coefficient ( $k_f$ ) in the downcomer is a function of solid holdup ( $\epsilon_{sd}$ ), the Schmidt number ( $Sc$ ) and particle Reynolds number ( $Re_p$ ). The film mass transfer coefficient is obtained by the correlation of Fan et al. (1960):

$$\begin{aligned} k_f &= \frac{D_m}{d_p} [2 + 1.03(\epsilon_{sd} Re_p)^{0.5} (Sc)^{0.33}], \\ Re_p &= \frac{d_p U_{slip} \rho}{\mu}, \\ Sc &= \frac{\mu}{\rho D_m} \end{aligned} \quad (7)$$

Where,  $U_{slip}$  is the superficial slip velocity between the two phases and  $D_m$  is the molecular diffusion coefficient of BSA.

The coefficient of intra-particle diffusion ( $\psi$ ) is tuned using available experimental results (Lan et al., 2000, 2002). The fine-tuning procedure is based on minimization of deviation between the experimental data and the model predictions. Maximum adsorption capacity of Diaion HPA25 ion-exchange particles ( $q_m$ ), dissociation coefficient ( $K_d$ ) and

the desorption rate constant in the riser ( $K_r$ ) were reported by Lan et al. (2000). These modeling parameters are listed in table 3.3.

**Table 3.3: model parameters (Lan et al., 2000)**

$K_d$ (kg/m <sup>3</sup> )	$q_m$ (kg/m <sup>3</sup> )	$K_r$ (s <sup>-1</sup> )	$\psi$
0.00907	87.9	0.045	0.15

### 3.3.4 Numerical methodology

Under each operating condition, the value of the bed voidage in the downcomer is obtained by solving Eq. 1. Then, by using the following boundary conditions, the mass transfer equations, Eqs. 3 and 4, which are the ordinary differential equation, are solved by a finite difference method:

$$C_d(Z=0) = C_{od} \quad \text{and} \quad q_d(Z=h_d) = q_{er}. \quad (8)$$

where  $C_{od}$  is the protein concentration in feed solution and  $q_{er}$  is the protein concentration in the regenerated ion-exchange particles which are coming from the exit of the riser. At the beginning of the circulation,  $q_{er}$  equals to zero. As a result, this mathematical model is able to predict the protein concentration in liquid and solid phase along the downcomer and also the protein concentration of loaded particles which are entrained to the bottom of the riser can be obtained.

The two phase flow in the riser is simulated with an axisymmetric model to reduce computational cost. The commercial software, ICEM CFD, Ansys 13.0, is used to create the riser geometry and then generate the mesh. The governing equations are then solved by the commercial CFD code FLUENT, Ansys 13.0 based on the laminar flow regime. The computational domain of the downcomer is shown in Figure 3.2(a) and the computational domain of riser is given in Figure 3.2(b). As it is shown, the inlet of primary stream of the liquid phase is named as ‘Inlet 1’ where there is no solid particle. Also, the ‘Inlet 2’ represents the inlet of both Auxiliary stream and solid particle phase, therefore the velocities of the liquid and solid phase, and solid holdup are set on this cross-section. No-slip and free-slip boundary conditions are imposed on the wall for



liquid and solid phases, respectively. The expressions of Johnson and Jackson (1987) are used to calculate the slip velocity and granular temperature of solid phase near the wall. Fully-developed flow condition is used for all flow quantities at the top of the riser. The symmetry conditions are imposed at the central axis of the column.

The convection terms and gradients in all transport equations are discretized by the second order upwind method and green-gauss cell based method, respectively. Then, the SIMPLE algorithm using a segregated solution technique is used to solve the pressure field and velocity field separately within an iteration cycle.

The mesh independence is examined using three different grids,  $20 \times 2000$ ,  $25 \times 2500$ ,  $30 \times 3000$  and  $35 \times 3500$ . The radial distributions of the solid holdup at the height of 2.5 m from these three grids are compared and the comparison indicates the  $30 \times 3000$  grid gives less than 0.5% variation in comparison to the finer grid. Therefore, this mesh can provide mesh-independent results. The time step independence test shows that 0.0004 sec time step can give the time step independent results.

As a result, protein concentration in the riser is determined in the first cycle of solids circulation between downcomer and riser. Because of unique design of the LSCFB, the solid phase protein concentration at the top of the riser ( $q_{er}$ ) is equal to the one at the top of downer ( $q_{od}$ ), so the value of  $q_{er}$  from the current riser simulation is used as  $q_{od}$  in the next downcomer simulation. While particles are entraining between these two columns, adsorption capacity of the downcomer and desorption capacity of the riser are establishing a kinetic equilibrium. Eventually, the LSCFB ion exchange system reaches a stable operation condition.

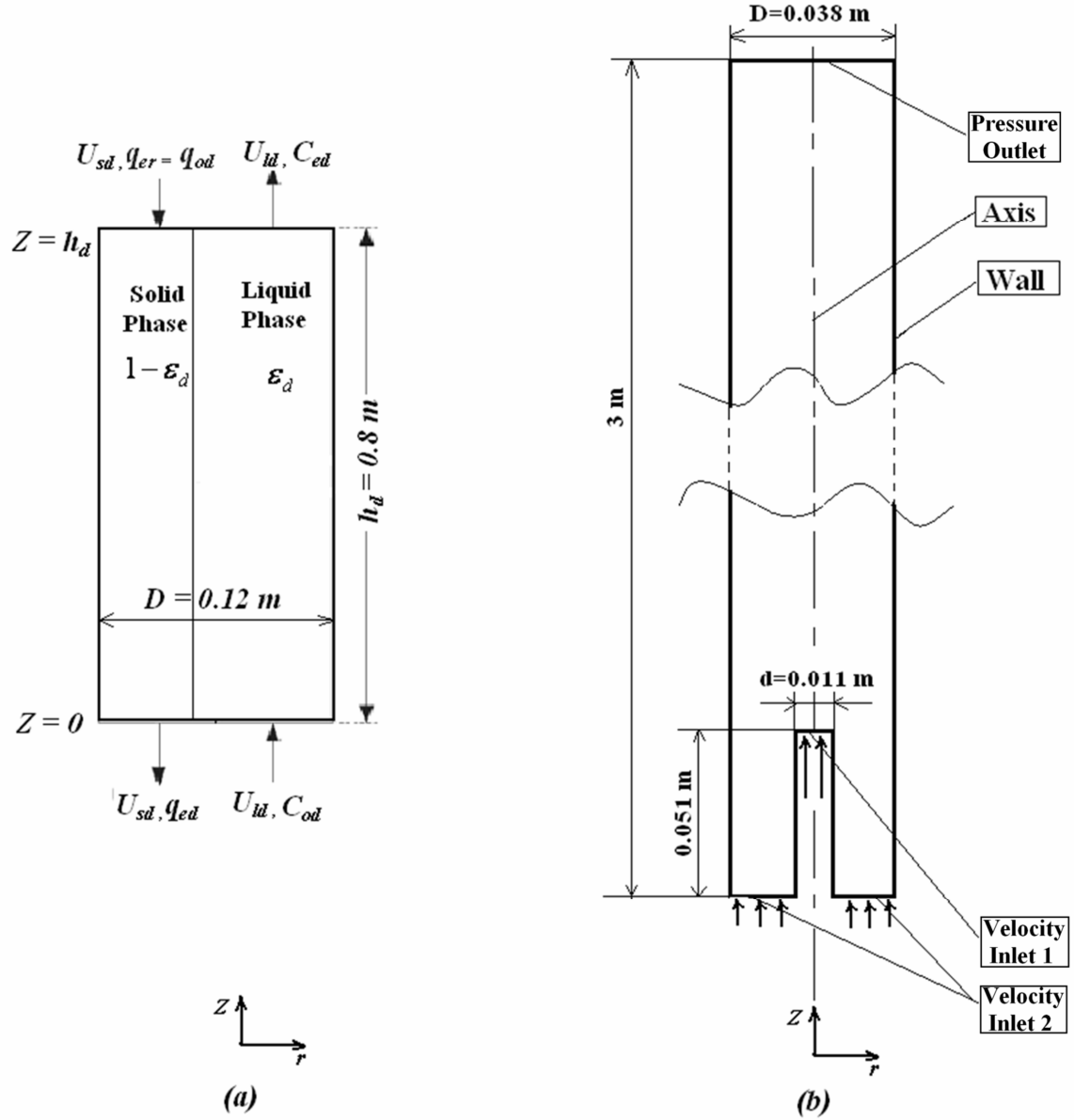


**Figure 3.2: Computational domain of in the downcomer and riser of the LSCFB. (a) Downcomer and (b) Riser.**

### 3.4 Results and Discussion

The numerical model presented in this study is able to predict the hydrodynamics and mass transfer characteristics of the ion exchange particles in the LSCFB. The numerical results are compared with available experimental data (Lan et al., 2000) to validate the

numerical model. Then, the effects of the operating conditions on the distribution of the protein concentration along the downcomer and the riser are investigated.

Furthermore, the protein production rate ( $P$ ) and the total efficiency of protein extraction process in the LSCFB ( $E$ ) are the two key performance parameters of the system which are defined by the following equations:

$$\text{Protein production rate } (P) = U_{lr} A_r C_{er} \quad (9)$$

$$\text{Total Efficiency } (E) = \frac{\text{Protein production rate}}{\text{Amount of protein in the feed}} = \frac{U_{lr} A_r C_{er}}{U_{ld} A_d C_{od}}$$

These parameters ( $E$  and  $P$ ) can be considered as the two objective functions to find out the optimal conditions for the protein extraction process using the LSCFB. The current numerical model will predict the two objectives under different operating conditions.

In this study, one of the stable operating conditions is selected as the reference point. The parameters at this reference point are  $C_{od}=2 \text{ (kg/m}^3\text{)}$ ,  $U_{ld}=0.0006 \text{ (m/s)}$ ,  $U_{lr}=0.0113 \text{ (m/s)}$  and  $G_s=1.24 \text{ (kg/m}^2\text{/s)}$ . The height of the dense zone in the downcomer is  $0.8 \text{ (m)}$  at the reference point.

### 3.4.1 Validation of the numerical model

In order to validate the present numerical model, the predicted results are compared with the experimental data (Lan et al., 2000). The protein concentration of liquid phase in the downcomer is shown in Figure 3.3 under different superficial liquid velocities in the downcomer ( $U_{ld}$ ). In this simulation, the rest of operating conditions are set at the reference point.

As it is seen that the liquid phase protein concentration in the downcomer ( $C_d$ ) decreases along the column as the protein is adsorbed onto the ion-exchanger resin. There is a good agreement between the numerical results and experimental data, especially at the outlet of the downcomer, although the liquid dispersion, solids back mixing and non-uniformity of velocity field are not taken in account in the numerical model.

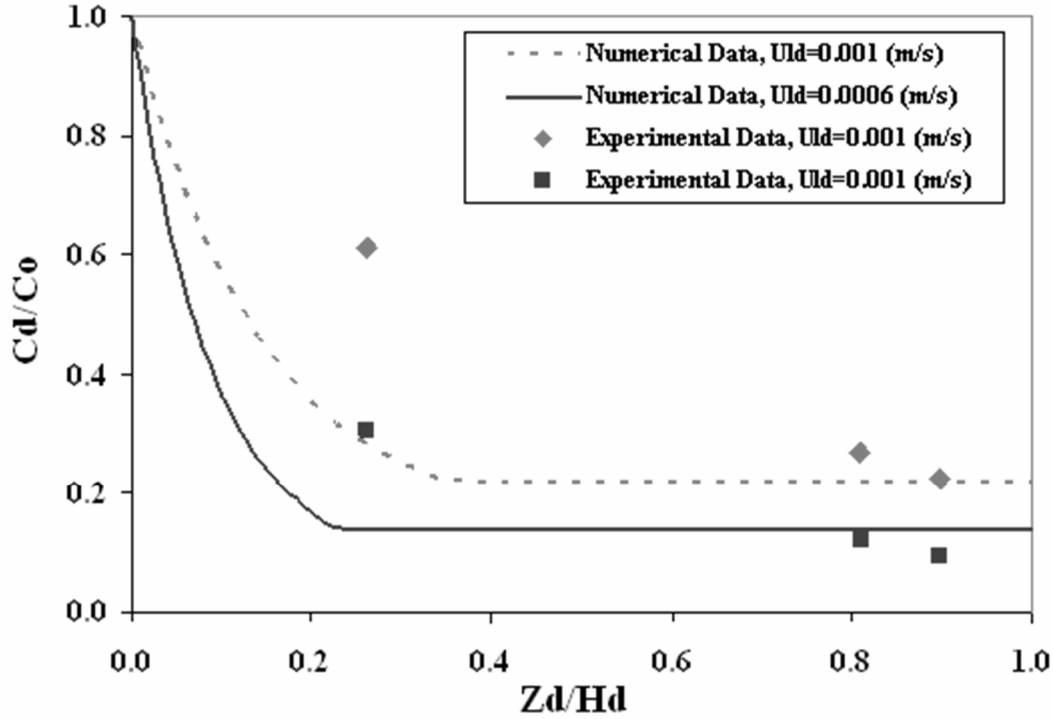


**Figure 3.3: Comparison of the liquid protein concentration along the downcomer at different superficial liquid velocities ( $U_{ld}$ ) in the downcomer at  $C_{od}=2 \text{ kg/m}^3$ ,  $G_s=1.24 \text{ kg/m}^2/\text{s}$ ,  $U_{lr}=0.0113 \text{ m/s}$  (Experimental data by Lan et al. (2000, 2002a)).**

Figure 3.4 shows the liquid phase protein concentration along the riser at different superficial liquid velocities in the riser ( $U_{lr}$ ). In this simulation, the rest of the operating conditions are set at the reference point. The protein concentration of the liquid phase in the riser ( $C_r$ ) increases along the column as the protein of the ion-exchanger resin is desorbed by the extracting solution. This plot also exhibits a reasonable agreement between the experimental data and numerical results, especially at the top of the riser. The average difference between the CFD results and experimental data is about 17.8 %.

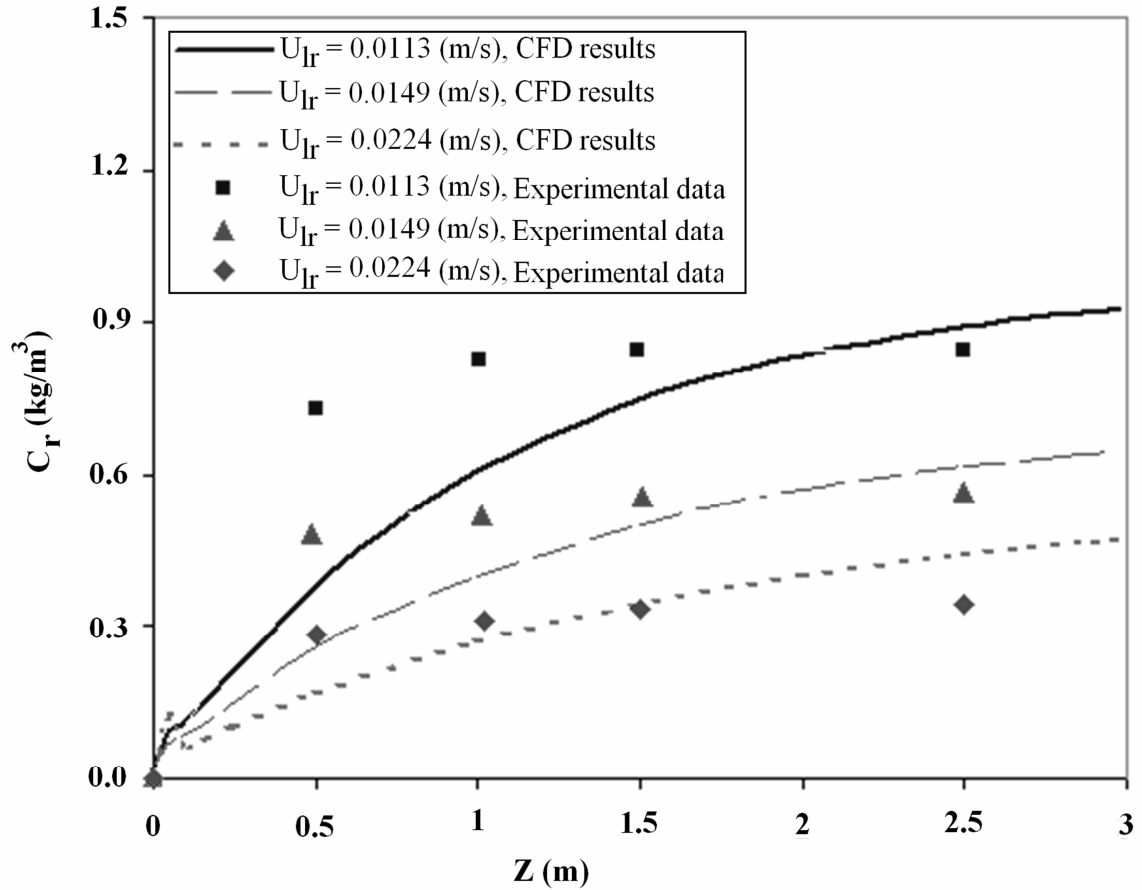


**Figure 3.4: Comparison of the liquid protein concentration along the riser at different superficial liquid velocities ( $U_{lr}$ ) in the riser at  $C_{od}=2 \text{ kg/m}^3$ ,  $G_s=1.24 \text{ kg/m}^2/\text{s}$ ,  $U_{ld}=0.006 \text{ m/s}$  (Experimental data by Lan et al. (2000, 2002a)).**

The reaction rate constant in the riser ( $k_r$ ) can be one of the main reasons for the deviation between the experimental data and numerical results, because  $k_r$  is assumed to be constant in the current model, which should be a function of the local solid holdup. The protein concentration of the liquid phase in the riser ( $C_r$ ) is illustrated by a contour in Figure 3.5.

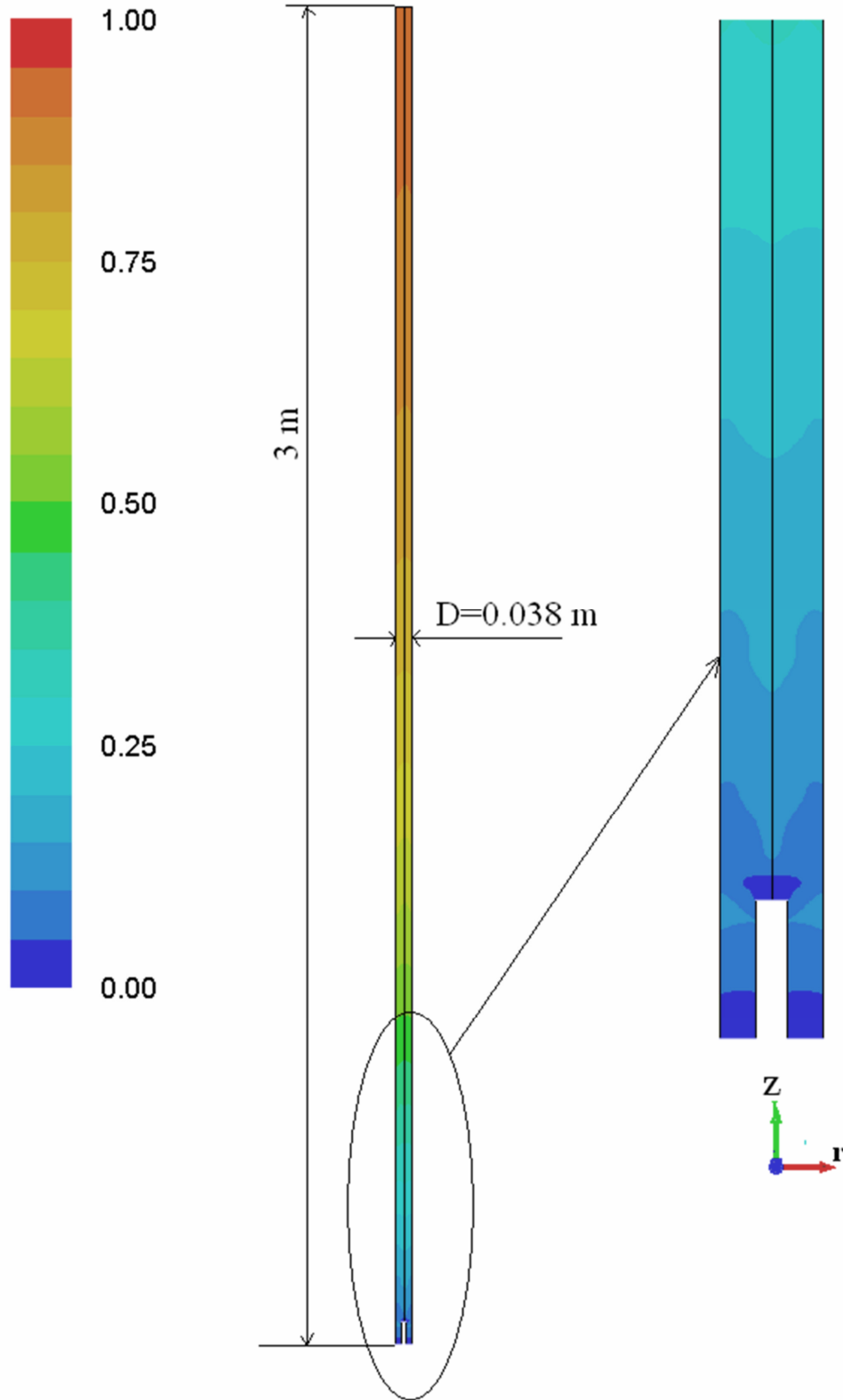
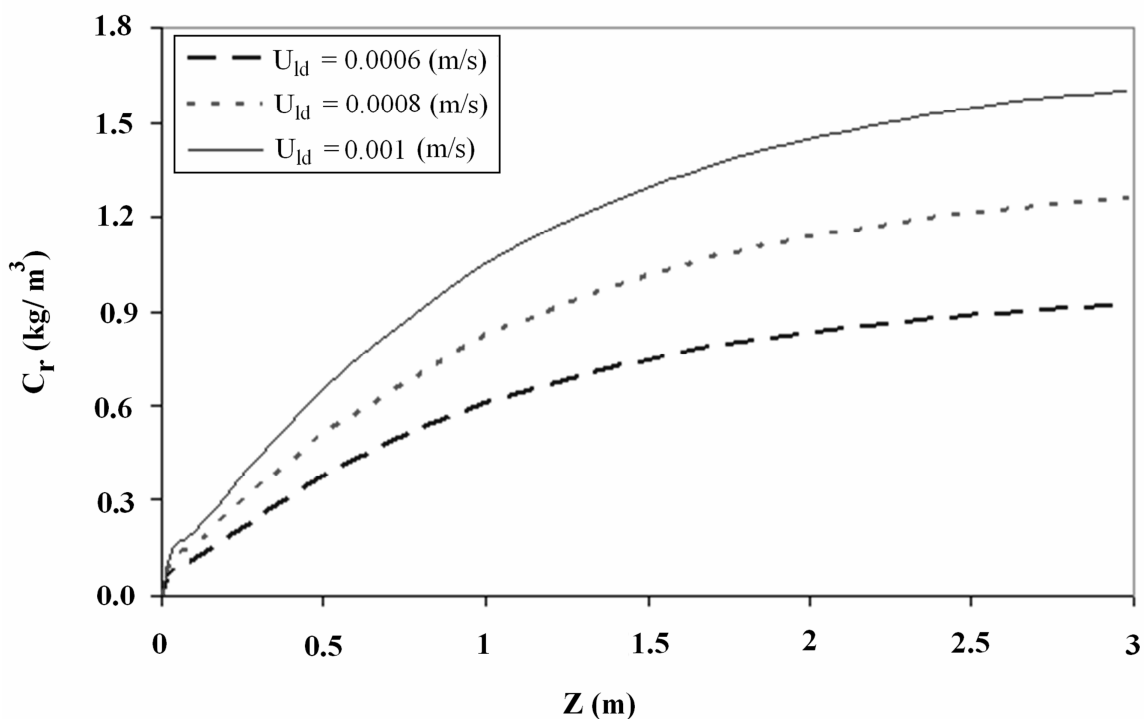


Figure 3.5: Contour of the protein concentration of the liquid in the riser,  $C_r$  ( $\text{kg/m}^3$ ).

### 3.4.2 Effect of the liquid velocity in the downcomer

The liquid velocity in downcomer ( $U_{ld}$ ) has significant effect on the performance of the ion exchange LSCFB. They could be identified in many aspects. First of all, the increase in  $U_{ld}$  will decrease the resident time of liquid phase. Therefore, it leads to less time for the adsorption process and as a result, the protein concentration in the raffinate stream will increase. Secondly, it influences the bed voidage in the downcomer based on Eq. (1). The increase in  $U_{ld}$  will increase the bed voidage. On the other hands, under a constant solids circulation rate ( $G_s$ ), the volume flow rate of the feed increases with the increase in  $U_{ld}$  and it changes the mass balance on the BSA in the downcomer.

The liquid phase protein concentration profile along the riser is plotted in Figure 3.6 at different  $U_{ld}$  while keeping other operating conditions the same as those at the reference point.



**Figure 3.6: Variation of the liquid protein concentration along the riser at different superficial liquid velocity in downcomer,  $U_{ld}$  ( $C_{od}=2 \text{ kg/m}^3$ ,  $G_s=1.24 \text{ kg/m}^2/\text{s}$ ,  $U_{lr}=0.0113 \text{ m/s}$ ).**

Figure 3.6 shows that with the increase in  $U_{ld}$ , the liquid phase protein concentration ( $C_r$ ) increases at the outlet of the ion extracting stream. As the protein loading rate in the downcomer increases when  $U_{ld}$  increases, the ion exchange particles carry over higher amount of protein to the riser which result in higher desorption rate in the riser.

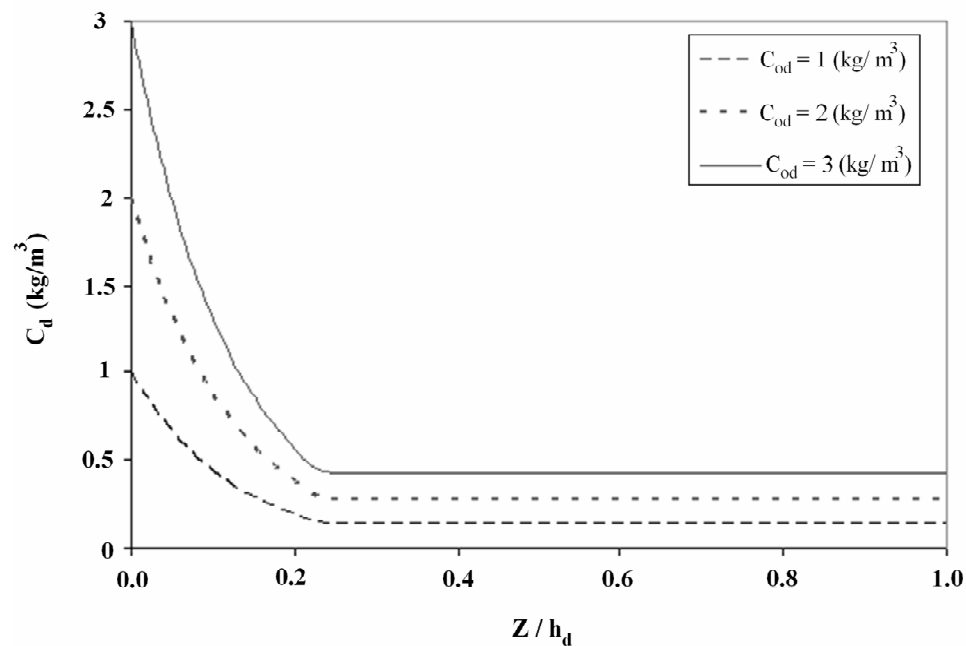
### 3.4.3 Effect of the liquid velocity in the riser

The liquid velocity in the riser ( $U_{lr}$ ) has a significant effect on the operation of an LSCFB ion exchange system as shown in Figure 3.4. It can be seen from Figure 3.4 that the protein concentration of the raffinate ( $C_{er}$ ) decreases at the outlet of the riser with the increase in  $U_{lr}$ . It causes the reduction of solid phase residence time in the riser and the decrease in the desorption capacity. That is why the protein concentration of the liquid phase ( $C_r$ ) decreases with the increase in  $U_{lr}$ .

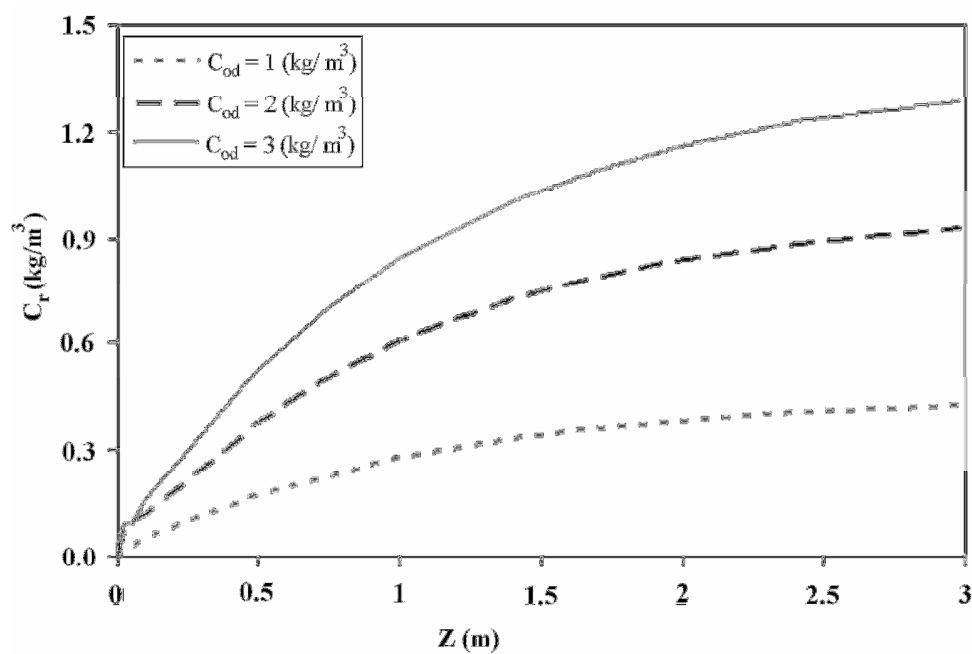
### 3.4.4 Effect of the feed concentration

The protein concentration in the feed can have a dominant role on the performance of LSCFB ion exchange systems. Figure 3.7 shows the profile of the liquid protein concentration in both riser and downcomer at different feed protein concentration, while other operating conditions remain at the reference point. It can be seen in Fig. 3.7 (a) that the protein concentration of the liquid phase at  $Z/h_d=1.0$  is increasing with the increase in the feed protein concentration. As a result, the increase in  $C_{od}$  causes that a higher amount of BSA is discharged from the outlet of the raffinate stream. The distribution of the average protein concentration in the liquid phase of the riser ( $C_r$ ) is illustrated under various feed protein concentration ( $C_{od}$ ) in Fig. 3.7(b). It indicates that the protein concentration at the outlet of the riser ( $C_{er}$ ) increases with the increase in  $C_{od}$ . As the loading rate of the protein increases in the downcomer due to higher  $C_{od}$ , the protein concentration of the loaded particles which are introduced to the bottom of riser, increases; therefore, the desorption capacity and  $C_{er}$  are higher in the riser.





(a)



(b)

**Figure 3.7: Influence of the feed protein concentration ( $C_{od}$ ) on the protein concentration of the liquid phase at  $G_s=1.24 \text{ kg/m}^2/\text{s}$ ,  $U_{ld}=0.0006 \text{ m/s}$ , and  $U_{lr}=0.0113 \text{ m/s}$ . (a) downcomer, (b) riser**

### 3.4.5 Evaluation of the system efficiency and protein production rate

Increasing the system efficiency and production are two dominate objectives of each ion exchange LSCFB system. The protein production rate ( $P$ ) and the total efficiency of protein extraction process in an LSCFB ( $E$ ) can be calculated by Eq. (9). The predicted values of these two objective functions can be used to perform an optimization study on the protein extraction system. The values of the protein production rate ( $P$ ) and system efficiency ( $E$ ) are summarized in Table 3.4 under different operating conditions.

**Table 3.4: Protein production rate and system efficiency under different operating conditions**

$U_{lr}$ (m/sec)	$G_s$ (kg/m <sup>2</sup> sec)	$C_{od}$ (kg/m <sup>3</sup> )	$U_{ld}$ (m/s)	Protein Production Rate (kg/hr)	System Efficiency (%)
Effect of $U_{lr}$					
0.0113	1.24	2	0.0006	0.0422	86
0.0149	1.24	2	0.0006	0.0393	80
0.0224	1.24	2	0.0006	0.0319	65
Effect of $U_{ld}$					
0.0113	1.24	2	0.0006	0.0422	86
0.0113	1.24	2	0.0008	0.0539	83
0.0113	1.24	2	0.001	0.0634	78
Effect of $C_{od}$					
0.0113	1.24	1	0.0006	0.0214	87
0.0113	1.24	2	0.0006	0.0422	86
0.0113	1.24	3	0.0006	0.059	80

Table 3.4 shows that both the protein production rate and system efficiency decrease with the increase in  $U_{lr}$ , because it reduces the protein adsorption and desorption capacity in the downcomer and riser, respectively. Also, it is observed that the protein production rate is enhanced when  $U_{ld}$  increases due to higher protein loading rate. However, the total

efficiency of the LSCFB ion exchange system has an opposite trend compared to the protein production rate, i.e. it decreases with the increase of  $U_{ld}$ . Generally, the production rate goes up with the increase of  $C_{od}$  because of higher loading rate. However, the overall system efficiency decreases with the increase of  $C_{od}$  due to the limited BSA capacity.

### 3.5 Conclusions

A CFD model to simulate the protein extraction process in the LSCFB ion exchange system has been presented. This model took into account both adsorption and desorption processes. The simulation of the desorption process in the LSCFB riser was based on Eulerian-Eulerian (E-E) approach incorporating the kinetic theory of granular flow. In addition, the adsorption process in the LSCFB downcomer was formulized by a one-dimensional mathematical model using the adsorption kinetics correlations developed before. The numerical results were validated favorably with reported experimental data.

The adsorption and the desorption behavior were studied under various operating parameters to better understand the performance of the system. The model could predict the protein production rate and the overall system efficiency which can be considered two objective functions for the optimization study on the protein extraction process. In general, it was found that both the rate of protein production and the total system efficiency decrease with the increase in the superficial liquid velocity in the riser. In contrast, with the increase in the feed flow rate and the feed protein concentration, the rate of protein production increases, but the overall system efficiency decreases.

## References

- Byers, C. H., Sisson, W. G., Snyder, T. S., Beleski, R. J., Nayak, U. P., & Francis, T. L. (1997). *Zirconium and hafnium separation in sulfate solution using continuous ion exchange chromatography*. U.S. Patent No. 5,618,502.
- Ding, J., & Gidaspow, D. A. (1990). A bubbling fluidization model using kinetic theory of granular flow. *AIChE J.*, 36, 523–538.
- Fan, L. T., Yang, Y. C., & Wen, C. Y. (1960). Mass transfer in semifluidized beds for solid-liquid system. *AIChE J.*, 6(3), 482–487.
- Gaikwad, A., Kale, S., & Lali, A. (2008). Modeling of counter-current adsorption in continuous liquid-solid circulating fluidized bed adsorption chromatography. *Chem Eng Sci.*, 63, 1062–1071.
- Gidaspow, D. (1994). *Multiphase Flow and Fluidization: Continuum and Kinetic Theory Descriptions*. Boston: Academic Press.
- Gordon, N. F., Tsujimura, H., & Cooney, C. L. (1990). Optimization and simulation of continuous affinity recycle extraction. *Bioseparation*, 1, 9–21.
- Higgins, I. R. (1969). Continuous ion exchange of process water. *Chemical Engineering Progress*, 65, 59–62.
- Himsley, A. (1981). *Continuous countercurrent ion exchange process*. U.S. Patent No. 4,279,755.
- Johnson, P. C., & Jackson, R. (1987). Frictional-Collisional Constitutive Relations for Granular Materials with Application to Plane Shearing, Sheared in an Annular Cell. *J. Fluid Mech.*, 176, 67-93.
- Junxian, Y., Dong, Q. L., & Shan, J. Y. (2005). Predictive modeling of protein adsorption along the bed height by taking into account the axial nonuniform liquid dispersion and particle classification in expanded beds. *J Chromatogr A*, 1095, 16–26.

Lan, Q. D., Zhu, J. X., Bassi, A. S., Margaritis, A., Zheng, Y., & Rowe, G. E. (2000). Continuous Protein Recovery Using a Liquid- Solid Circulating Fluidized Bed Ion Exchange System: Modeling and Experimental Studies. *Can. J. Chem. Eng.*, 78, 858–866.

Lan, Q. D. (2001). *Development of Continuous Liquid-Solid Circulating Fluidized Bed Ion Exchange System and its Application in Protein Purification* (Ph.D. Thesis). University of Western Ontario, Canada.

Lan, Q., Bassi, A. S., Zhu, J. X., & Margaritis, A. (2001). A modified Langmuir model for the prediction of the effects of ionic strength on the equilibrium characteristics of protein adsorption onto ion exchange/affinity adsorbents, *Chemical Engineering Journal*, 81, 179-186.

Lan, Q. D., Zhu, J. X., Bassi, A.S., & Margaritis, A. (2002). Continuous protein recovery with a liquid-solid circulating fluidized bed ion exchanger. *AIChE J.*, 48, 252–261.

Liang, W. G., Zhang, S. L., Zhu, J. X., Yu, Z. Q., Jin, Y., & Wang, Z. W. (1997). Flow characteristics of the liquid-solid circulating fluidized bed. *Powder Tech.*, 90, 95–102.

Lun, C. K. K., Savage, S. B., Jeffrey, D. J., & Chepurniy, N. (1984). Kinetic theories for granular flow: inelastic particle in Couette flow and slightly inelastic particles in a general flow field. *J. Fluid Mechanics*, 140, 223–256.

Mazumder, J., Zhu, J., Bassi, A. S., Ray, & A. K. (2009). Modeling and simulation of liquid–solid circulating fluidized bed ion exchange system for continuous protein recovery. *Biotechnology and Bioengineering*, 104, 111-126.

Monkos, K. (1996). Viscosity of bovine serum albumin aqueous solution as a function of temperature and concentration. *Int J Biol Macromol*, 18, 61–68.

Ping, L., Guohua, X., & Alirio, E. R. (2005). Experimental and modeling study of protein adsorption in expanded bed. *AIChE J.*, 51, 2965–2977.

Razzak, S. A., Barghi, S., & Zhu, J. X. (2009). Application of electrical resistance tomography on liquid-solid two-phase flow characterization in an LSCFB riser. *Chem Eng Sci*, 64, 2851–2858.

Schaeffer, D. G. 1987. Instability in the evolution equations describing incompressible granular flow. *J. Differential Equations*, 66, 19–50.

Shi, D. P., Luo, Z. H., & Zheng, Z. W. 2010. Numerical simulation of liquid-solid two-phase flow in a tubular loop polymerization reactor. *Pow Tech J.*, 198, 135-143.

Sinclair, J. L., & Jackson, R. (1989). Gas-Particle Flow in a Vertical Pipe with Particle-Particle Interactions. *AIChE J.*, 35, 1473-1486.

Syamlal, M., Rogers, W., & O'Brien, T. J. (1993). *MFIX Documentation: Theory Guide*. National Technical Information Service., vol. 1. DOE/METC-9411004, NTIS/DE9400087. VA : Springfield,.

Veeraraghavan, S., Fan, L. T., & Mathews, A. P. (1989). Modeling adsorption in liquid-solid fluidized beds. *Chem Eng Sci*, 44, 2333–2344.

Wen, C. Y., & Yu, Y. H. (1966). Mechanics of fluidization. *Chemical Engineering Progress Symposium Series*, 62, 100-111.

Wright, P. R., & Galsser, B.J. (2001). Modelling mass transfer and hydrodynamics in fluidized-bed adsorption of proteins. *AIChE J*, 47, 474–488.

Zhu, J. X., Zheng, Y., Karamanev, D. G., & Bassi, A. S. (2000). (Gas-) Liquid-Solid Circulating Fluidized Beds and Their Potential Applications to Bioreactor Engineering, *Can. J. Chem. Eng.*, 78, 82–94.

## Chapter 4

### 4 Numerical Simulation of Counter-Current Flow Field in the Downcomer of a Liquid-Solid Circulating Fluidized Bed\*

#### 4.1 Introduction

The extraction of functional solids materials from industrial broth has received high attentions during the recent years due to concerns on limitations of the natural resources (Lan, 2001). The continuous ion exchange process using the conventional fluidized is one of the major extraction equipment which has been used extensively (Byers et al., 1997; Gordon et al., 1990; Higgins, 1969; Himsley, 1981). Although the conventional fluidized beds have some benefits such as the low and stable bed pressure drop and the direct application of unclarified broth feed, the continuous transportation of a large number of particles between vessels becomes a challenging issue (Gaikwad et al., 2008). Because of the unique features of the liquid–solid circulating fluidized bed (LSCFB) including continuous operation in vessels, high throughput due to high liquid velocity in the riser, high efficient liquid-solid contact, integrated reactor and smaller processing volumes, Zhu et al. (2000) proposed LSCFB system as a potential candidate for the continuous extraction process. A typical LSCFB is comprised of a riser, a downcomer, a liquid-solid separator and other auxiliary components. Also, liquid-solid flow pattern is co-current in the riser and counter-current in the downcomer.

To take advantage of the exceptional characteristics of LSCFBs, Lan et al. (2000, 2002) reported a liquid–solid circulating fluidized bed (LSCFB) ion-exchange system for continuous extraction of protein. In addition to modeling the riser, they also developed a semi-empirical correlation to predict the solids holdup in the downcomer. The correlation was derived from Richardson and Zaki equation (Richardson and Zaki, 1954; Kwauk, 1992). Further, they studied the effects of operating conditions on the overall efficiency

---

\* This manuscript has been submitted to Particuology Journal for publication.

of the protein extraction process. Feng et al. (2003) carried out the cesium separation using a continuous ion exchange circulating fluidized bed.

Control and optimization of the extraction process using ion exchange LSCFB require a comprehensive study on the hydrodynamics in the riser and downcomer. In the last decade, computational fluid dynamics (CFD) techniques have received more attentions in simulating the transport phenomena in liquid-solid fluidized bed reactors; however, there is only a few works in the literature on the behavior of the two-phase flows in a downcomer. In addition, because of the counter-current contact of two phases, the flow field in the downcomer is more complex. As far as we know, there has been no CFD study on the liquid-solid counter-current flow in the literature. Din et al. (2010) developed a CFD model to simulate a liquid-liquid counter-current flow in the pulsed sieve plate extraction column. The model was based on Eulerian–Eulerian approach with standard multiphase  $k-\epsilon$  turbulence model. A pulse generation model was incorporated to simulate the effect of pulses in the system. By Comparison with experimental data, the CFD results shows 27.83% of the error.

The purpose of this study is to develop a sophisticated CFD model to simulate the liquid-solid flow field in the LSCFB downcomer. This model is based on Eulerian-Eulerian approach incorporating the kinetic theory of granular flow. The proposed model is used to examine the effect of operating condition on hydrodynamic characteristics and to obtain the residence time distribution (RTD) of solid particles using a Pulse technique.

## 4.2 Configuration of the LSCFB ion-exchange system

The LSCFB ion exchange system used in this study was developed by Lan et al. (2000), where an experimental study on hydrodynamics and kinetics of the protein extraction process in this LSCFB ion exchange system was conducted. In that study, a lab scale system was designed and manufactured. The schematic diagram of the LSCFB ion exchange system used by Lan et al. (2000) is shown in Fig. 4.1. It is comprised of a riser, a downcomer, a liquid-solid separator, a top solids-return pipe, a bottom solids-return pipe, a top washing section, a bottom washing section, a riser distributor and a



downcomer distributor. The riser is 3.0 m in height and 0.038 m in diameter, and the downcomer is 2.5 m in height and 0.120 m in diameter.

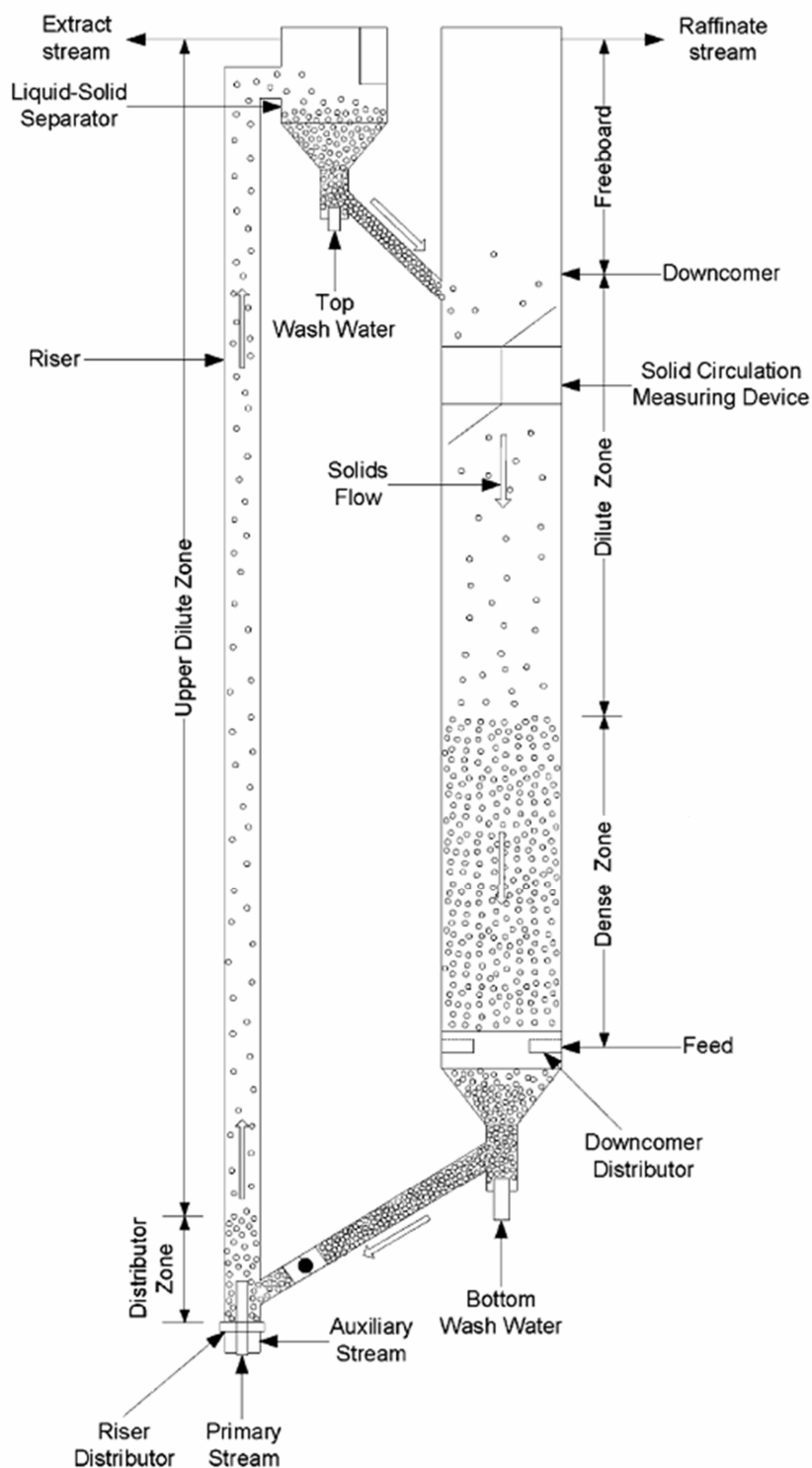


Figure 4.1: Schematic diagram of the LSCFB ion-exchange system Lan et al. (2000).

In the downcomer, Bovine serum albumin (BSA) solution was used as a liquid feed and Diaion HPA25 particles were used as solid ion-exchange particles ( $d_p=0.32\text{ mm}$ ,  $\rho_w=1.08\text{ gr/mL}$  and  $U_i=4.5\text{ mm/s}$ ).

The liquid feed stream is introduced into the bottom of the downcomer through distributor and ion-exchange particles are simultaneously entered into downcomer through top solids entrance. The liquid velocity in the downcomer is less than the terminal velocity of the particles; therefore, particles can flow down from the top of downcomer and the flow pattern of the two phases is counter-current. Since the feed distributor is designed like a tubular ring, it can provide a uniform liquid distribution while allowing the solids to flow down.

### 4.3 Mathematical modeling

There are two CFD approaches available to model liquid-solid flows: Eulerian-Lagrangian (E-L) approach and Eulerian-Eulerian (E-E) approach. In the E-L approach, the liquid phase is considered as a continuous phase and Navier–Stokes (N-S) equations are solved for it. The solid phase is treated as a discrete phase and each solid particle is tracked by solving the Lagrangian force balance equation. However, the main drawback of this approach is that a high computational cost is required to solve the dense two-phase flow.

In the E-E approach, also well known as two-fluid model, each phase is treated as an interpenetrating continuum and the concept of phasic volume fraction is used. The conservation of the mass, momentum and energy provide the governing equations for the liquid and solid phases. The governing equations for the solid phase have similar structure to those for the liquid phase. However, in order to close the pseudo N-S equation for the solid phase, the viscosity, pressure and stresses of the solid phase are modeled by the kinetic theory of granular phase (KTGP), which has been widely applied for particulate flows (Sinclair and Jackson, 1989; Gidaspow, 1994). In this theory, the mean square of the random particle velocity is defined as granular temperature ( $\theta$ ) and the solids viscosity, pressure and stress are functions of the granular temperature, which varies with time and position in a fluidized bed.

### 4.3.1 Governing equations

In this work, a CFD model is developed to simulate the counter-current flow field in the downcomer of an LSCFB. The model is based on the E–E approach incorporating the kinetic theory of granular phase. The relevant equations are listed in Table 4.1. The granular bulk viscosity ( $\lambda_s$ ) which describes the resistance of an emulsion to compression or expansion is determined by the equation proposed by Lun et al. (1984). The viscosity of the solid phase ( $\mu_s$ ) is generated by three sources: inter-particle collision, friction and kinetic energy of particles. The correlation by Gidaspow et al. (1994) is used for the collisional viscosity ( $\mu_{s,col}$ ). Frictional viscosity ( $\mu_{s,fl}$ ) is calculated by the expression of Schaeffer (1987), with an angle of internal friction ( $\Phi$ ) of  $30^\circ$ . The kinetic portion of the granular viscosity ( $\mu_{s,kin}$ ) and the granular conductivity ( $k_{\theta s}$ ) are both obtained by the relationships from Syamlal et al. (1993). The solid pressure ( $p_s$ ) is estimated by the correlation developed by Lun et al. (1984).

External body, lift and virtual mass forces are neglected in the momentum equations. The coefficient of the momentum exchange between the liquid and solid phases ( $K_{sl}$ ) is described by the empirical drag correlation of Wen and Yu (1966).

### 4.3.2 Boundary conditions

In order to solve governing equations, a set of appropriate boundary conditions are defined on the computational domain which is illustrated in Fig. 4.2. As it is seen, the specified velocity boundary conditions are imposed at the inlet for both solids and liquid streams. Also, the specified velocity boundary condition is used on the outlet of the solids. The no-slip and free-slip boundary conditions are defined on the wall for liquid and solid phases, respectively.

**Table 4.1: Governing equations for liquid-solid flows**

Continuity equation	$\frac{\partial}{\partial t}(\alpha_q \rho_q) + \nabla \cdot (\alpha_q \rho_q \vec{v}_q) = 0, \quad \sum_q \alpha_q = 1.$	
Momentum equations	$\frac{\partial}{\partial t}(\alpha_l \rho_l \vec{v}_l) + \nabla \cdot (\alpha_l \rho_l \vec{v}_l^2) = -\alpha_l \nabla p + \nabla \cdot \bar{\bar{\tau}}_l + \alpha_l \rho_l \vec{g} + K_{sl}(\vec{v}_s - \vec{v}_l),$ $\frac{\partial}{\partial t}(\alpha_s \rho_s \vec{v}_s) + \nabla \cdot (\alpha_s \rho_s \vec{v}_s^2) = -\alpha_s \nabla p + \nabla p_s + \nabla \cdot \bar{\bar{\tau}}_s + \alpha_s \rho_s \vec{g} + K_{ls}(\vec{v}_l - \vec{v}_s),$ $\bar{\bar{\tau}}_q = \alpha_q \mu_q (\nabla \cdot \vec{v}_q + \nabla \cdot \vec{v}_q^T) + \alpha_q \left( \lambda_q - \frac{2}{3} \mu_q \right) \nabla \cdot \vec{v}_q \bar{\bar{I}}.$	
Liquid-solid drag	$K_{sl} = \frac{3}{4} C_D \frac{\alpha_s \alpha_l \rho_l  \vec{v}_s - \vec{v}_l }{d_s} \alpha_l^{-2.65},$ $C_D = \frac{24}{\alpha_l \text{Re}_s} \left[ 1 + 0.15 (\alpha_l \text{Re}_s)^{0.687} \right],$ $\text{Re}_s = \frac{\rho_l d_s  \vec{v}_s - \vec{v}_l }{\mu_l}.$	(Wen and Yu, 1966)
Solids pressure	$P_s = \alpha_s \rho_s \Theta_s + 2 \rho_s (1 + e_{ss}) \alpha_s^2 g_{0,ss} \Theta_s$	(Lun et al., 1984)
Radial distribution function	$g_{0,ss} = \left[ 1 - \left( \frac{\alpha_s}{\alpha_{s,\max}} \right)^{1/3} \right]^{-1}$	(Ding and Gidaspow, 1990)
Solids shear stress	$\mu_s = \mu_{s,col} + \mu_{s,kin} + \mu_{s,fr}$ $\mu_{s,col} = \frac{4}{5} \alpha_s \rho_s d_s g_{0,ss} (1 + e_{ss}) \sqrt{\frac{\Theta_s}{\pi}}$ $\mu_{s,kin} = \frac{\alpha_s \rho_s d_s \sqrt{\Theta_s \pi}}{6(3 + e_{ss})} \left[ 1 + \frac{2}{5} (1 + e_{ss}) (3e_{ss} - 1) \alpha_s g_{0,ss} \right]$ $\mu_{s,fr} = \frac{p_s \sin \phi}{2 \sqrt{I_{2D}}}$	(Gidaspow et al., 1994) (Syamlal et al., 1993) (Schaeffer, 1987)
Bulk viscosity	$\lambda_s = \frac{4}{3} \alpha_s^2 \rho_s d_s g_{0,ss} (1 + e_{ss}) \sqrt{\frac{\Theta_s}{\pi}}$	(Lun et al., 1984)
Granular temperature	$\frac{3}{2} \left[ \frac{\partial}{\partial t} (\rho_s \alpha_s \Theta_s) + \nabla \cdot (\rho_s \alpha_s \vec{v}_s \Theta_s) \right] = (-p_s \bar{\bar{I}} + \bar{\bar{\tau}}_s) : \nabla \cdot \vec{v}_s + \nabla \cdot (k_{\Theta_s} \nabla \Theta_s) - \gamma_{\Theta_s} + \Phi_{ls}$	
Granular conductivity	$k_{\Theta_s} = \frac{15 d_s \rho_s \alpha_s \sqrt{\Theta_s \pi}}{4(41 - 33\eta)} \left[ 1 + \frac{12}{5} \eta^2 (4\eta - 3) \alpha_s g_{0,ss} + \frac{16}{15\pi} (41 - 33\eta) \eta \alpha_s g_{0,ss} \right]$ $\eta = \frac{1}{2} (1 + e_{ss})$	(Syamlal et al., 1993)
Collisional dissipation of energy	$\gamma_{\Theta_s} = \frac{12(1 - e_{ss}^2) g_{0,ss}}{d_s \sqrt{\pi}} \rho_s \alpha_s^2 \Theta_s^{3/2}$	(Lun et al., 1984)
Inter-phase Energy exchange	$\Phi_{ls} = -3 K_{ls} \Theta_s$	

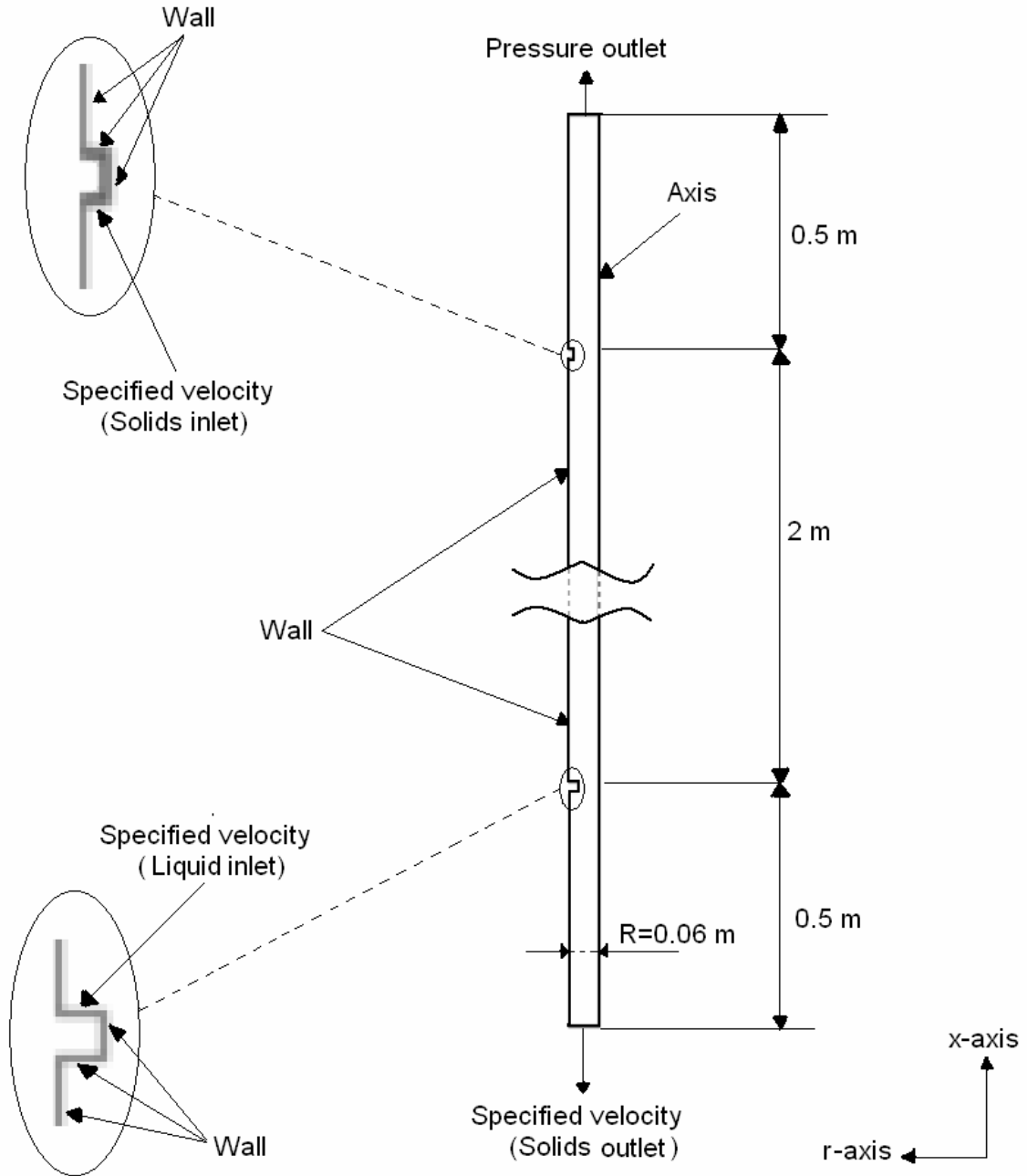


**Figure 4.2: Schematic diagram of the computational domain to simulate the liquid-solid flow in the downcomer of the LSCFB**

The granular temperature of the solid phase near the wall is calculated based on the correlation by Johnson and Jackson (1987):

$$q_{w,\theta_s} + \frac{\pi \rho_p u_{slip}^2 \psi \sqrt{\theta_s}}{2\sqrt{3} \left( \frac{\alpha_{s,max}}{\alpha_s} - \frac{\alpha_{s,max}^{2/3}}{\alpha_s^{2/3}} \right)} - \frac{\sqrt{3} \pi \rho_p (1 - e_{sw}^2) \theta_s^{3/2}}{4 \left( \frac{\alpha_{s,max}}{\alpha_s} - \frac{\alpha_{s,max}^{2/3}}{\alpha_s^{2/3}} \right)} = 0. \quad (1)$$

where  $u_{slip}$  and  $q_{w,\theta_s}$  are the slip velocity and the flux of fluctuation energy within the solids flow approaching the wall. The fully-developed flow condition is imposed for all flow quantities at the top outlet of the downcomer.

#### 4.4 Numerical methodology

The flow in the downcomer is assumed axisymmetric. The geometry of the computational domain and mesh grid are created by using the commercial software, ICEM CFD, ANSYS 14.0. The governing equations are then solved by the commercial CFD code, FLUENT, ANSYS 14.0. The convection terms and gradients in all transport equations are discretized by the second order upwind method and green-gauss cell based method, respectively. The SIMPLE algorithm using a segregated solution technique is used to solve the pressure field and velocity field. The initial bed height and initial solids holdup are given as 1.2 m and 0.6, respectively. The mesh independence is examined using three different grids, 15×750, 20×1000 and 26×1350. The axial distributions of the cross-sectional solids holdup obtained by these three grids are compared. The result from 20×1000 grid deviates less than 0.5% from the one using the finer mesh. Therefore, this mesh is used in the rest of simulations in this study. The time step independence test shows that the time step of 0.005 sec can satisfy the time step independency.

#### 4.5 Results and Discussion

The CFD model developed in this study is used to predict the liquid-solids two-phase flow field in the downcomer of the LSCFB. The accuracy of the numerical simulation is examined by comparing the numerical results with available experimental data (Lan et al., 2000). Also, the effects of the liquid superficial velocity in the downcomer ( $U_{ld}$ ) and solids circulation rate ( $G_s$ ) on the hydrodynamic characteristics in the downcomer of the LSCFB are investigated. The solids holdup distribution in the downcomer is illustrated by a contour in Fig. 4.3.

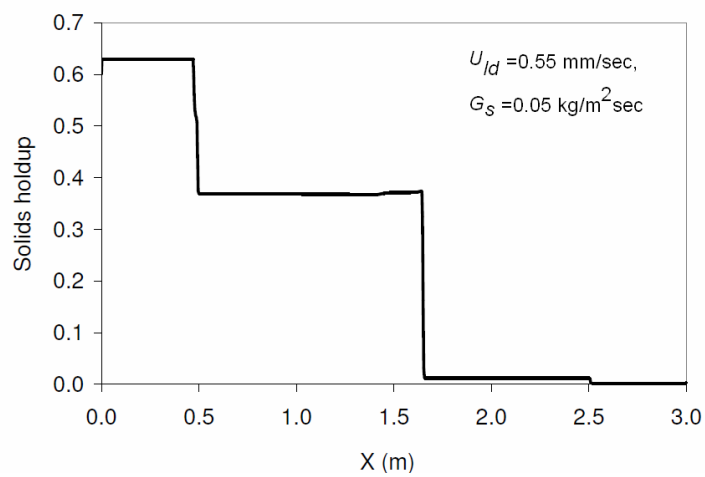
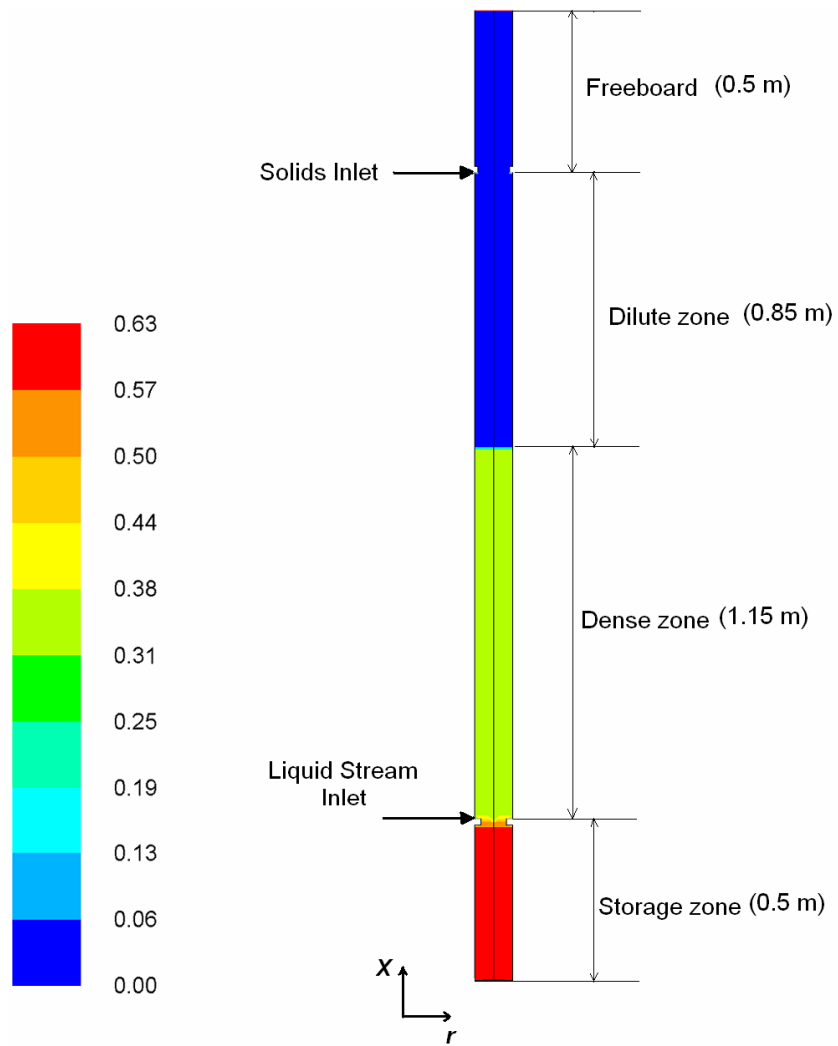


**Figure 4.3: Predicted solids holdup distribution in the downcomer at  $U_{ld} = 0.55$  mm/sec and  $G_s = 0.05$  kg/m<sup>2</sup>sec.**

This simulation was performed at  $U_{ld} = 0.55$  mm/sec and  $G_s = 0.05$  kg/m<sup>2</sup>sec. In order to maintain stable operation, the liquid velocity in the downcomer must be kept less than the particle terminal velocity. Therefore, four distinctive zones are observed in the downcomer which have different solids holdup, the storage zone, the dense zone, the dilute zone, and the freeboard zone as shown in Fig. 4.3.

It illustrates that the solid holdup in the freeboard zone is zero and the solid holdup in the dilute zone is much lower than that in the dense and storage zones, and the particles are packed in the bottom of downcomer (the storage zone) and solids holdup in this zone is higher than other zones in the downcomer. It is also seen that the expansion of the bed equals 0.45 m ((1.15+0.5)-1.2).

#### 4.5.1 Validations of the numerical model

In order to validate the proposed numerical model, simulations are performed under three different superficial liquid velocities ( $U_{ld}$ ) for the downcomer. The comparison between the numerical results and experimental data for the average solids holdup in the dense zone of the downcomer ( $\alpha_{sd}$ ) is shown in Fig. 4.4 under  $G_s = 1.06$  kg/m<sup>2</sup>sec, which shows the predictions are in an acceptable agreement with the experimental data.



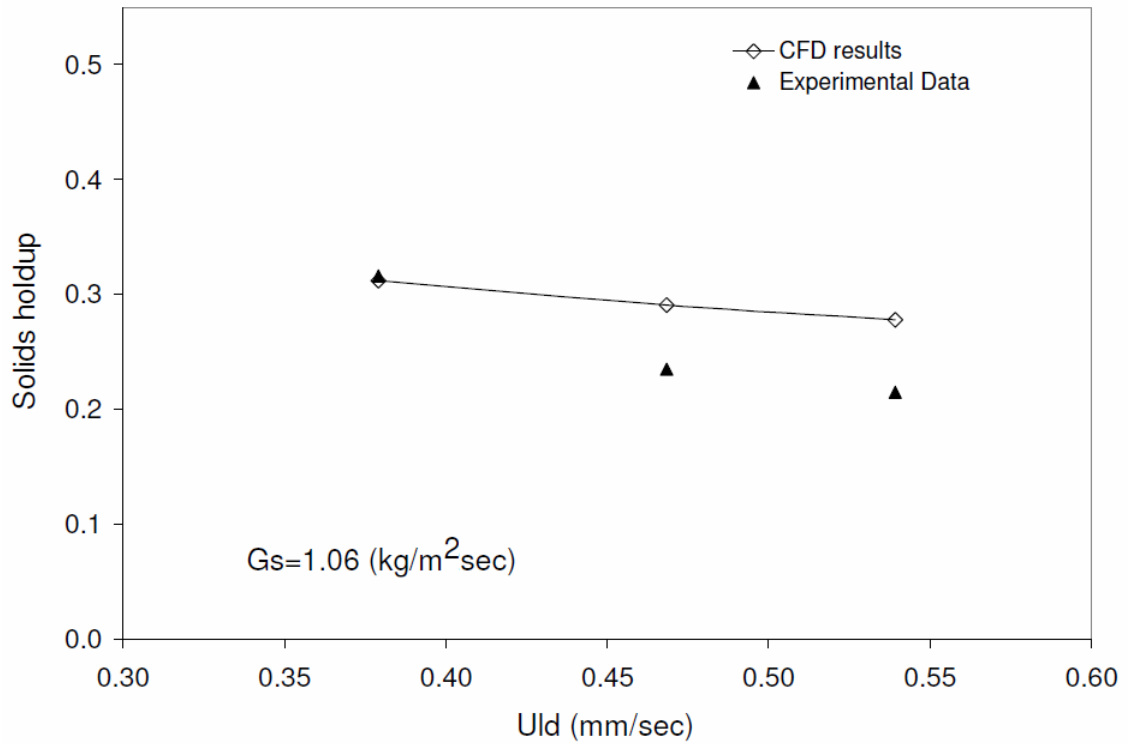


**Figure 4.4: Comparison of numerical and experimental results for the average solids holdup in the dense zone of the downcomer (Experimental data by Lan et al. (2000)).**

#### 4.5.2 Effect of superficial liquid velocity on solids holdup

To investigate the influence of the superficial liquid velocity in the downcomer on the hydrodynamic quantities, the simulations are performed under three different superficial liquid velocities and  $G_s=0.05 \text{ kg/m}^2\text{sec}$ . In Fig. 4.5, the predicted solids holdup in the dense zone of the downcomer ( $\alpha_{sd}$ ) is plotted with respect to the superficial liquid velocity.

It is illustrated that  $\alpha_{sd}$  decreases with an increase in the superficial liquid velocity in the downcomer. This result is in agreement with those previously obtained from the modified Richardson and Zaki equation (Lan et al., 2000).

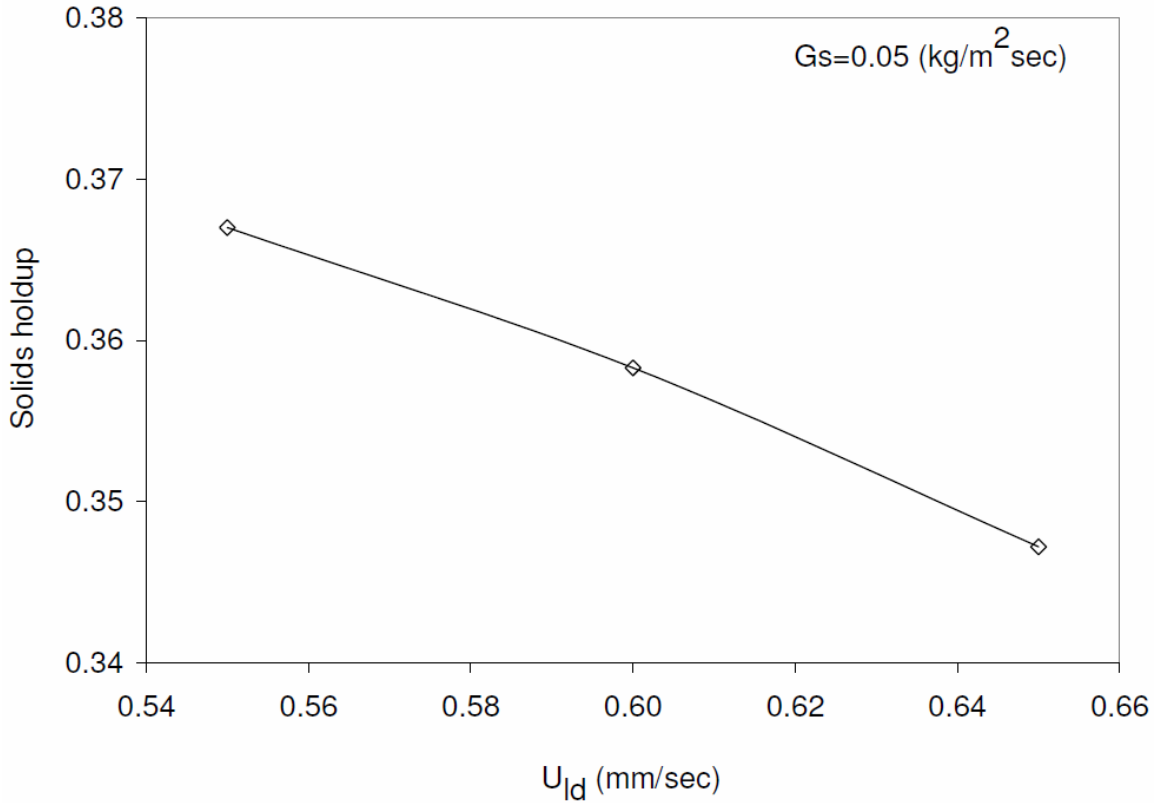


**Figure 4.5: Variation of the solids holdup in the dense zone of the downcomer ( $\alpha_{sd}$ ) at different superficial liquid velocity**

### 4.5.3 Effect of solids circulation rate on solids holdup

Fig. 4.6 shows the numerical results for the radial distributions of the solids holdup in the dense zone of the downcomer ( $\alpha_{sd}$ ) at  $U_{ld} = 0.6$  mm/sec under different solids circulation rates. It is clearly seen that the increase in the solids circulation rate results in a decrease in the solids holdup in the dense zone of the downcomer ( $\alpha_{sd}$ ) for the same superficial liquid velocity. The main reason of this trend is that the increase in the solids circulation rate increases the relative velocities between two phases.

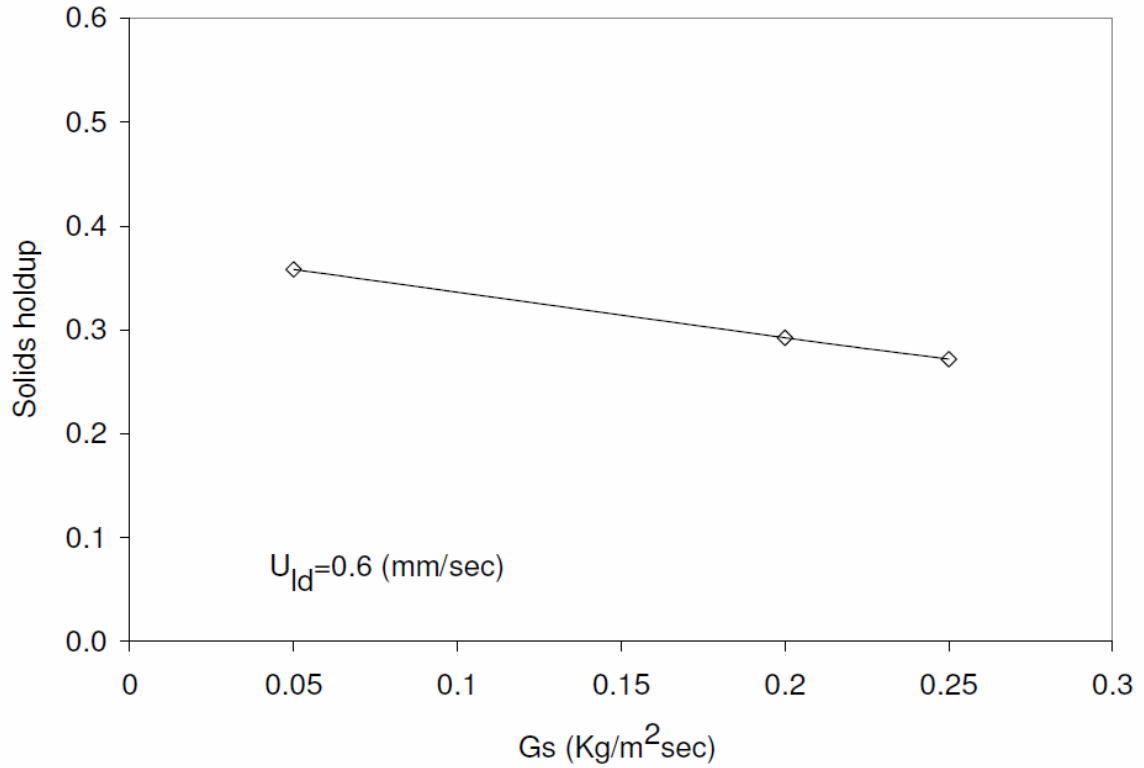


**Figure 4.6: Variation of the solids holdup in the dense zone of the downcomer ( $\alpha_{sd}$ ) at different solids circulation rates**

#### 4.5.4 Radial distribution of the solids holdup

The radial distribution of the solids holdup in the downcomer is plotted in Fig 4.7. It shows the numerical results under two different superficial liquid velocities,  $G_s=0.05$  kg/m<sup>2</sup>sec and at  $X=1.5$  m. It is seen that the radial distribution of the solids holdup is uniform in the dense zone of the downcomer and it is consistent with the nature of the liquid-solid particulate flow (Couderc, 1985).

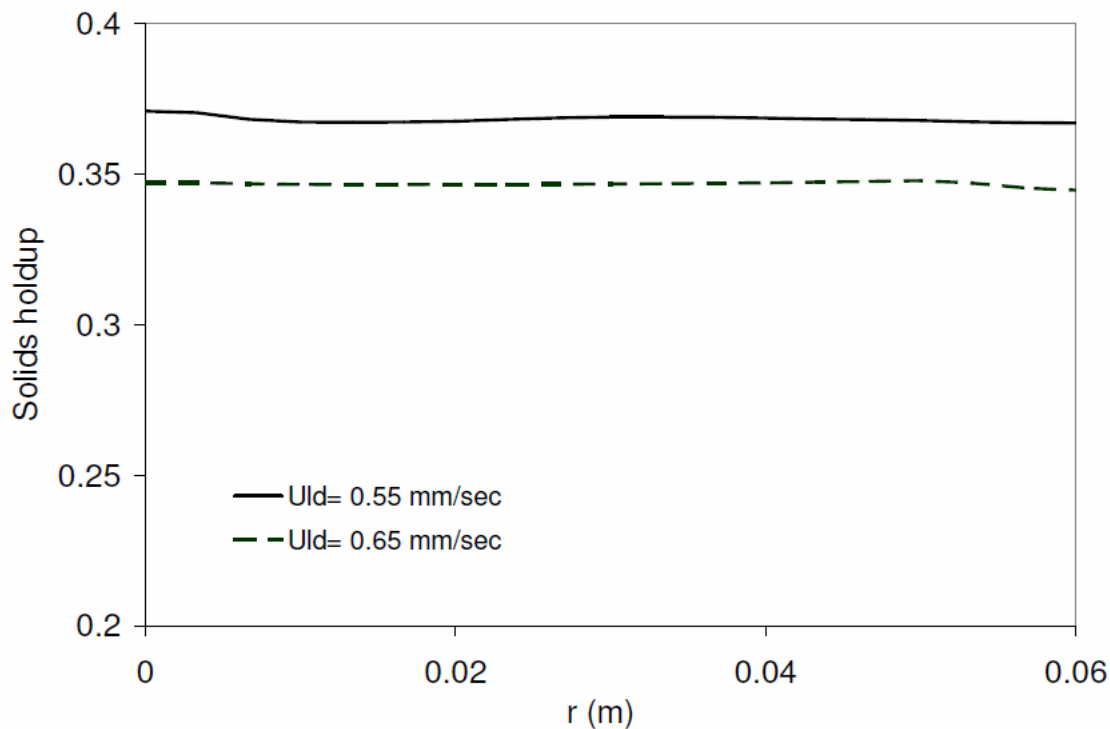


**Figure 4.7: Radial distribution of the solids holdup in the dense zone of the downcomer at  $G_s=0.05 \text{ kg/m}^2\text{sec}$  and  $x=1.5 \text{ m}$**

#### 4.5.5 Effect of superficial liquid velocity on the dispersion of the solid particles

The residence time distribution (RTD) of the solid particles, illustrating the solids dispersion, can be determined by using the results of E-E model and applying the pulse technique (FLUENT User's Guide, 2013). After the calculations of the E-E model reach a steady-state, tracers with the same physical properties of the solid particles are defined and injected at the inlet boundary of the solid phase based on the pulse technique. By solving the Lagrangian equations for each tracer, their location versus time are tracked and the RTD of solid phase are predicted. However, because only the final steady-state flow field has been used, the micro-mixing effects are neglected in this mathematical technique.

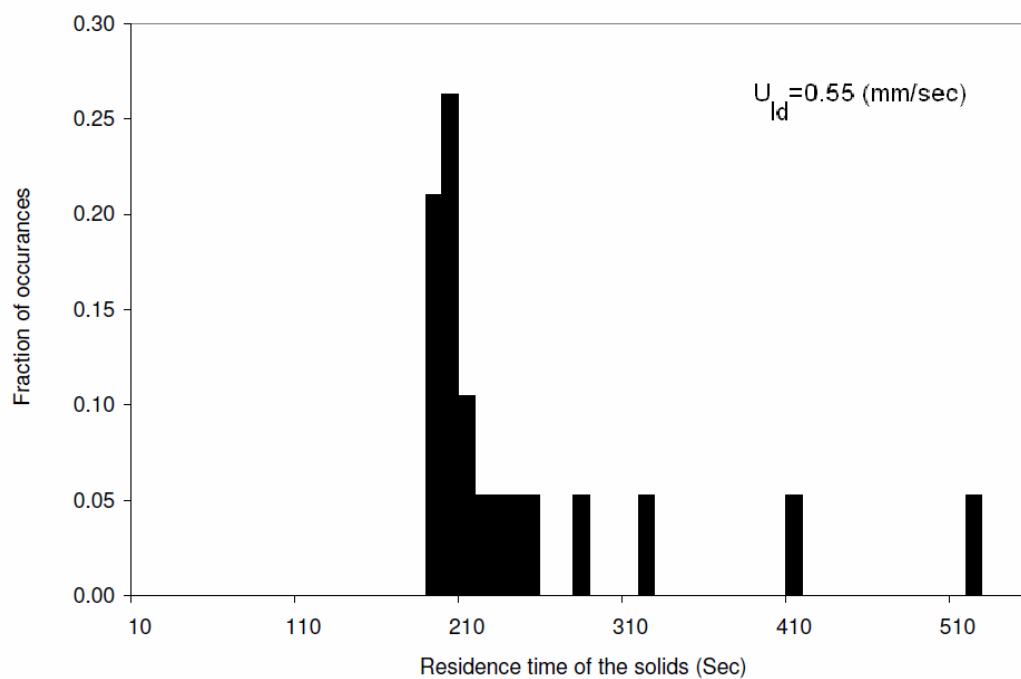
Fig. 4.8 shows the predicted RTD curves of the solid phase at  $G_s=0.05 \text{ kg/m}^2\text{s}$  and under two different superficial liquid velocities. It is seen that the solids flow pattern at

$U_{ld}=0.65$  mm/sec are closer to the plug flow than the one at  $U_{ld}=0.55$  mm/sec. it indicates that the increase in the superficial liquid velocity results in the decrease of the solids dispersion in the downcomer of the LSCFB.

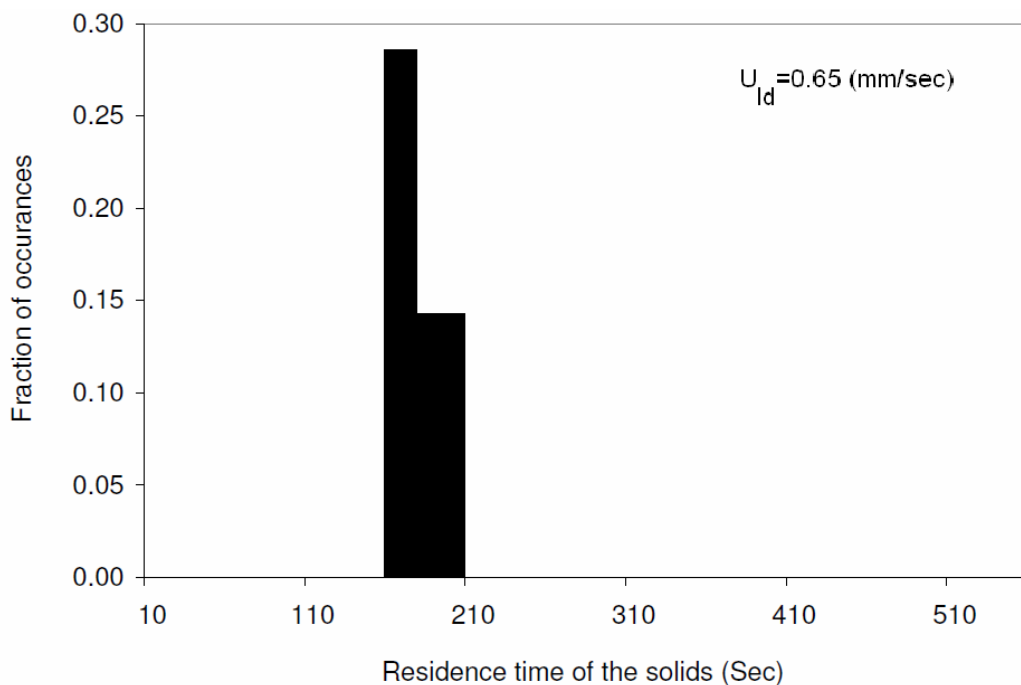
## 4.6 Conclusions

A CFD model was developed to simulate the counter-current two phase flows in the downcomer of an LSCFB. The model was based on Eulerian-Eulerian (E-E) approach incorporating the kinetic theory of granular flow. The numerical results were validated favorably with reported experimental data. The hydrodynamic characteristics of the flow were studied under various operating parameters to better understand the system.

It was found that the bed expansion of the particles in the downcomer is directly affected by the superficial liquid velocity in the downcomer ( $U_{ld}$ ) and solids circulation rate ( $G_s$ ). The solids holdup in the dense zone of the downcomer ( $\alpha_{sd}$ ) decreases with the increase in either  $U_{ld}$  or  $G_s$ . It was also found that the radial distribution of solids holdup is very uniform. In addition, in order to study the influence of  $U_{ld}$  on the solids dispersion, the CFD model was adapted to predict the solids RTDs. It was illustrated that the increase in the  $U_{ld}$  decreases the solids dispersion in the downcomer. As a result, the model can be used as a robust tool for the scale-up and design of the real industrial-scale counter-current reactors.



(a)



(b)

**Figure 4.8: The residence time distributions of the solid phase at  $G_s=0.05$  kg/m<sup>2</sup>sec and (a)  $U_{ld}=0.55$  mm/sec, (b)  $U_{ld}=0.65$  mm/sec**

## Reference

- Byers, C. H., Sisson, W. G., Snyder, T. S., Beleski, R. J., Nayak, U. P., & Francis, T. L. (1997). *Zirconium and hafnium separation in sulfate solution using continuous ion exchange chromatography*. U.S. Patent No. 5,618,502.
- Couderc, J. P. (1985). Incipient Fluidization and Particulate Systems, In J. F. Davidson, R. Clift, & D. Harrison (2nd ed.), *Fluidization* (pp. 1-46). London: Academic Press.
- Din, G. U., Chughtai, I. R., Inayat, M. H., Khan, I. H., & Qazi, N. K. (2010) Modeling of a two-phase countercurrent pulsed sieve plate extraction column-A hybrid CFD and radiotracer RTD analysis approach. *Separation and Purification Technology*, 73, 302–309
- Ding, J., & Gidaspow, D. (1990). A bubbling fluidization model using kinetic theory of granular flow. *AIChE J.*, 36, 523–538.
- Gaikwad, A., Kale, S., & Lali, A. (2008). Modeling of counter-current adsorption in continuous liquid-solid circulating fluidized bed adsorption chromatography. *Chem Eng Sci.*, 63, 1062–1071.
- Gidaspow, D. (1994). *Multiphase Flow and Fluidization: Continuum and Kinetic Theory Descriptions*. Boston: Academic Press.
- Gordon, N. F., Tsujimura, H., & Cooney, C. L. (1990). Optimization and simulation of continuous affinity recycle extraction. *Bioseparation*, 1, 9–21.
- Higgins, I. R. (1969). Continuous ion exchange of process water. *Chemical Engineering Progress*, 65, 59–62.
- Himsley, A. (1981). Continuous countercurrent ion exchange process. U.S. Patent No. 4,279,755.
- Johnson, P. C., & Jackson, R. (1987) Frictional-Collisional Constitutive Relations for Granular Materials with Application to Plane Shearing. *J. Fluid Mech.*, 176, 67-93.

- Kwauk, M. (1992). *Fluidization: Idealized and Bubbleless, with Applications*. Beijing and New York: Science Press.
- Lan, Q. D., Zhu, J. X., Bassi, A. S., & Margaritis, A. (2002). Continuous protein recovery with a liquid-solid circulating fluidized bed ion exchanger. *AIChE J.*, 48, 252–261.
- Lan, Q. D., Zhu, J. X., Bassi, A. S., Margaritis, A., Zheng, Y., & Rowe, G. E. (2000). Continuous Protein Recovery Using a Liquid- Solid Circulating Fluidized Bed Ion Exchange System: Modeling and Experimental Studies. *Can. J. Chem. Eng.*, 78, 858–866.
- Lun, C. K. K., Savage, S. B., Jeffrey, D. J., & Chepurniy, N. (1984) Kinetic theories for granular flow: inelastic particle in Couette flow and slightly inelastic particles in a general flow field. *J. Fluid Mech.*, 140, 223–256.
- Richardson, J. F. & Zaki, W. N. (1954). Sedimentation and Fluidization, *Trans. Inst. Chem. Eng.*, 32, 35-53.
- Schaeffer, D. G. (1987) Instability in the evolution equations describing incompressible granular flow. *J. Diff. Eqs.*, 66, 19–50.
- Sinclair, J. L., & Jackson, R. (1989). Gas-particle flow in a vertical pipe with particle-particle interactions. *AIChE J.*, 35, 1473-1486.
- Syamlal, M., Rogers, W., & O'Brien, T. J. (1993). MFIX Documentation: Theory Guide. National Technical Information Service, vol. 1, DOE/METC-9411004, NTIS/DE9400087, Springfield, VA.
- Wen, C. Y., & Yu, Y. H. (1966). Mechanics of fluidization, *Chem. Eng. Progress Symposium Series*. 62, 100-111.
- Zhu, J. X., Zheng, Y., Karamanev, D. G., & Bassi, A. S. (2000). (Gas-) Liquid-Solid Circulating Fluidized Beds and Their Potential Applications to Bioreactor Engineering. *Can. J. Chem. Eng.*, 78, 82–94.



## Chapter 5

### 5 Conclusions

In this study, novel CFD models were developed to describe the detailed hydrodynamics of the liquid-solid flow in the LSCFB riser and downcomer. A comprehensive model was also proposed to simulate the protein extraction process using the LSCFB ion exchange system.

The hydrodynamics of the turbulent liquid-solid flow in the LSCFB riser was modeled by developing a CFD model (chapter 2). The model was based on Eulerian-Eulerian (E-E) approach incorporating the kinetic theory of granular flow. Three different types of  $k$ - $\varepsilon$  multiphase turbulence models were examined in this work and it was found that the dispersed  $k$ - $\varepsilon$  turbulence model is more efficient than other ones because of the lower computational time and higher accuracy. Numerical predictions of the local liquid velocity and solids holdup are in a good agreement with the experimental data. It was found that the non-uniformity of liquid velocity distribution in the LSCFB is higher than that in a conventional liquid-solid fluidized bed. In addition, it was shown that the increase in the superficial liquid velocity decreases the average cross-sectional solids holdup in the LSCFB. Furthermore, in order to observe the global dispersion, the CFD model was adapted to predict the solids and liquid RTDs.

The kinetics of the protein extraction process in the LSCFB ion exchange system was simulated by a comprehensive numerical model incorporating the CFD model of the hydrodynamics in LSCFB riser (chapter 3). This model took into account both adsorption and desorption processes. The simulation of the desorption process in the LSCFB riser was carried out by a CFD model based on E-E approach incorporating the kinetic theory of granular flow. In addition, the adsorption process in the LSCFB downcomer was formulated by a one-dimensional mathematical model using the adsorption kinetics correlations developed before. The numerical results were validated favorably with the reported experimental data. In addition, the model could predict the protein production rate and the overall system efficiency which can be considered two objective functions

for the optimization study on the protein extraction process. In general, it was found that both the rate of protein production and the total system efficiency decrease with the increase in the superficial liquid velocity in the riser. In contrast, with the increase in the feed flow rate and the feed protein concentration, the rate of protein production increases, but the overall system efficiency decreases.

The hydrodynamics of the counter-current liquid-solid flow in the downcomer of the LSCFB was simulated by a comprehensive CFD model (chapter 4). The model was based on E-E approach incorporating the kinetic theory of granular flow. The numerical predictions of the hydrodynamic characteristics were validated favorably with our earlier experimental data. Numerical studies on the flow field under various operating parameters show that the bed expansion of the particles in the downcomer is directly affected by the superficial liquid velocity in downcomer ( $U_{ld}$ ) and solids circulation rate ( $G_s$ ). The solids holdup in the dense zone of the downcomer ( $\alpha_{sd}$ ) decreases with the increase in either  $U_{ld}$  or  $G_s$ . It was also illustrated that the radial distribution of the solids holdup is uniform in the downcomer. In addition, the residence time distributions of the solid particles were determined by a pulse technique and it was found out that the solids dispersion decreases with increase in the superficial liquid velocity.

In conclusion, it is demonstrated that the proposed CFD models can be a reliable tool for the scale-up and design of industrial LSCFB reactors for diverse applications, such as protein extraction process, wastewater treatment, petroleum and metallurgical industries.

## Curriculum Vitae

<b>Name:</b>	Abbas Dadashi
<b>Post-secondary Education and Degrees:</b>	<p>Tehran Polytechnic Tehran, Iran 2002-2006 B.Sc.</p> <p>Tehran Polytechnic Tehran, Iran 2006-2009 M.Sc.</p> <p>The University of Western Ontario London, Ontario, Canada 2010-2013 M.E.Sc.</p>
<b>Honours and Awards:</b>	<p>Graduate Research Scholarship, The University of Western Ontario, 2010-2013</p> <p>Graduate Teaching Scholarship, The University of Western Ontario 2011-2013</p>
<b>Related Work Experience</b>	<p>Teaching Assistant The University of Western Ontario 2011-2013</p>

### Publications:

Dadashi, A., Zhu, J., & Zhang, C. (2013). CFD Modeling of Continuous Protein Extraction Process Using Liquid-Solid Circulating Fluidized Beds. *Canadian Journal of Chemical Engineering*, 2013.

Dadashi, A., Zhu, J., & Zhang, C. (2013). A Computational Fluid Dynamics Study on the Flow Field in a Liquid-Solid Circulating Fluidized Bed Riser. *Power Tech.*, 2013 (Submitted)

Dadashi, A., Zhang, C., & Zhu, J. (2013). Numerical Simulation of Counter-Current Flow Field in the Downcomer of a Liquid-Solid Circulating Fluidized Bed, *Particuology Journal*, 2013 (Submitted)